UNIVERSIDAD COMPLUTENSE DE MADRID

FACULTAD DE CIENCIAS MATEMÁTICAS

Departamento de Matemática Aplicada

MODELOS MATEMÁTICOS DE DESARROLLO VASCULAR (MATHEMATICAL MODELS OF VASCULAR DEVELOPMENT)

MEMORIA PARA OPTAR AL GRADO DE DOCTOR
PRESENTADA POR

Álvaro Köhn Luque

Bajo la dirección de los doctores
Miguel Ángel Herrero García
José María Pérez Pomares

Madrid, 2012

UNIVERSIDAD COMPLUTENSE DE MADRID

FACULTAD DE CIENCIAS MATEMÁTICAS

Departamento de Matemática Aplicada

Modelos Matemáticos de Desarrollo Vascular

(Mathematical Models of Vascular Development)

Memoria para optar al grado de doctor
presentada por

Álvaro Köhn Luque

bajo la dirección de

Dr. Miguel Ángel Herrero García

Dr. José María Pérez Pomares

Madrid, Abril de 2012

¡Lo que sabemos entre todos!
¡Oh, eso es lo que no sabe nadie!

Antonio Machado, Juan de Mairena 1936

Acknowledgements

I am very grateful to all those who in one way or another made this PhD work possible. One of the pleasures of finally finishing is this opportunity to thank them.

To begin with, I am deeply indebted with my two advisors, Professor Miguel A. Herrero and Dr. José María Pérez Pomares. Their guidance, advice and care were indispensable factors in my accomplishments. Since the very first time I met Dr. Pérez Pomares, I have very much appreciated his detailed explanations and constructive discussions about vascular development. My continued visits to his laboratory were always a pleasure and an invaluable opportunity to learn and discuss about the great experimental work developed there. It has also been a real honour to spend the last years of my life close to Prof. Herrero. His kind support and guidance have been of great value. I feel extraordinary grateful for all the knowledge and enthusiasm he has passed on to me. His endless wisdom about many aspects of science and life has certainly had a remarkable influence on me.

Besides my advisors, a number of scientists directly collaborated with me. I am extremely grateful to Walter de Back for his essential contributions in simulation results and the corresponding analysis. Moreover, our extensive discussions were a continuous source of ideas and motivation. My sincere thanks to Jörn Starruß for his excellent computational support. I owe my most sincere gratitude to Takashi Miura and his students, Kenji Yoshimura and Yoshimi Yamaguchi from Kyoto University who performed the in vitro experimental work in Chapter 3. I also thank Andrea Mattiotti from Pérez Pomares lab for his key contributions in the in vivo experimental work in Chapter 2.

I acknowledge the initial support provided by Professors Carlos Parés and Juan Soler that turned out to be essential to start my PhD. I also acknowledge the support of Professors Luigi Preziosi and Hans Meinhardt that lead me to obtain a PhD grant from the Spanish Ministry of Education.

Professors Andreas Deutsch and Philip Maini have been very generous hosts to me during the several months I spent at Technische Universität Dresden and University of Oxford, respectively. I am very grateful for their guidance and advice. Their discussions about my work have been very helpful. I also thank all the people I met in their labs that made me feel part of them.

My sincere thanks are due to the official referees of this dissertation, Prof. Nicola Bellomo, Prof. Hans Meinhardt and Dr. Gerardo Oleaga, for their detailed and kind reports on my work.

My gratitude is also extended to a number of excellent teachers that I had during my studies at the Universities of Málaga, Granada, Madrid, Dresden and Oxford. In particular, I wish to thank José M. Arrieta, Andreas Beyer, Lutz Brush, Ana Carpio Rodríguez, Alberto Castellón Serrano, Manuel Castro Díaz, María Angustias Cañadas Pinedo, Jesús Ildefonso Díaz, Radek Erban, Daniel Girela Alvarez, David Gómez-Ullate, Manuel Gutierrez López, Miguel A. Herrero, Amable Liñan, María Lorente Domínguez, Julian López Gómez, Juanjo Lopez Velázquez, Fabricio Macià, Jorge Macías Sánchez, Philip K. Maini, Santiago Marín Malave, Francisco Javier Martín Reyes, Aniceto Murillo, Gerardo Oleaga, Pedro Ortega Salvador, Francisco Palma Molina, Carlos Parés Madroñal, Alfredo Pinelli, Angel Manuel Ramos del Olmo, Aníbal Rodríguez Bernal, Luis Vázquez Martínez, Ignacio Villanueva and Antonio Viruel.

During my PhD I met many interesting scientist all over the world that made my way smooth and enjoyable. I wish to extend my warmest thanks to Tomás Alarcón (Barcelona), Alexander Anderson (Tampa), David Basanta (Tampa), Leonid Berlyand (State College), Katrin Böttger (Dresden), Yin Cai (Heidelberg), Juan Calvo (Granada), Antonio Capuccio (Paris), David Casero (Los Angeles), Osvaldo Chara (Dresden), Arnaud Chauvière (Albuquerque), Ornella Cominetti (Oxford), Jill Gallaher (Tampa), Pilar Guerrero (Barcelona), Haralambros Hatzikirou aka Babis (Braunschweig), Juan Carlos Lopez Alfonso (Madrid), Juanma Melchor (Granada), Oleksandr Misits (State College), Mayasu Mimura (Tokyo), Philip Murray (Oxford), Pablo Padilla (Mexico D.F.), Monika Piotrowska (Warsaw), Marianito Rodrigo (Wollongong), Fabian Rost (Dresden), Shawn Ryan (State College), Esperanza Santamaría (Madrid), Jacob Scott (Oxford), Nadia Smith (Madrid), María Pilar Velasco Cebrián (Madrid), Lisa Willis (London), Xiaoming Zheng (Michigan), Roland Zimm (Dresden), Ksenia Zlobina (Moscow), etc.

Last but not least, I thank the support and patience of my whole family and friends.

Publications

The work presented in this dissertation has led to a series of publications. They are listed here for reference.

- **Herrero M.A., Köhn A. and Pérez-Pomares J.M.,** *Modelling vascular morphogenesis: current views on blood vessels development*, Mathematical Models and Methods in Applied Sciences, vol. 19, Suppl 1 (2009) 1483-1537.
- **Köhn-Luque A., de Back W., Starruß J., Mattiotti A., Deutsch A., Pérez-Pomares J.M. and Herrero M.A.** *Embryonic Vascular Patterning by Matrix-Mediated Paracrine Signalling: A Mathematical Model Study*, PLoS ONE, 6(9) (2011) e24175. doi:10.1371/journal.pone.0024175
- **Köhn-Luque A., de Back W., Yamaguchi Y., Yoshimura K., Herrero M.A. and Miura T.** *Periendothelial accumulation of exogenous VEGF guides in vitro vasculogenesis.* (2012) Submitted.
- **Köhn-Luque A., Mattiotti A., de Back W., Deutsch A., Herrero M.A. and Pérez-Pomares J.M.** *Retinoic acid-mediated low angioblasts proliferation is required for early avian embryonic vasculogenesis.* (2012) In preparation.

Summary

The use of Mathematics to understand relevant problems in Biology dates back at least as far the seminal works of D. Bernoulli on the efficacy of vaccination against smallpox (1760) and L. Euler on the flow of blood in arteries (1775). Since then, the field of Mathematical Biology has undergone extraordinary growth and a great deal of fascinating challenges have arisen. One of such challenges is that of unravelling morphogenesis (the emergence of biological shape) by means of mathematical methods, a problem that has important precedents in the influencial works of D. W. Thompson (1917), A. Turing (1952) and H. Meinhardt (1972).

The present dissertation is devoted to mathematical modelling and simulation of a specific problem in early vascular morphogenesis, a process that constitutes the initial step in the generation of the vascular system in vertebrates. More precisely, a combined mathematical, computational and experimental approach is used to get new insights into key molecular and cellular mechanisms underlying the self-assembly of new blood vessels. The thesis is divided in three main sections: Preliminaries (Chapter 1), Research Work (Chapters 2 and 3) and Perspectives and Conclusions (Chapters 4 and 5). An overview of the field together with an introduction to the main problem is presented in Chapter 1, where the main literature on the subject is reviewed from a critical point of view. In Chapter 2, a new mechanism and a new hybrid mathematical model for early vascular patterning in the embryo are proposed and examined. The study of the proposed model raises a number of new biological hypotheses, many of which are beyond the current experimental reach. In some particular cases, however, they have been validated in a controlled situation using simplified *in vitro* assays, as shown in Chapter 3. While doing so, relevant quantitative information related with the kinetic and diffusive properties of a key molecule in vascular development (VEGF) was also obtained. Chapter 4 is devoted to future perspectives in the field under consideration. In particular, two ongoing projects that are extensions of the work here considered are outlined. Finally, the main conclusions of this study are gathered in Chapter 5.

In summary, the mathematical and computational methods developed in this study, when combined with suitable experimental techniques, provide information of a relevant problem in vascular morphogenesis that was not previously known. Moreover, the proposed theoretical framework can be used not only to propose new hypotheses but also to assist in the design of accurate and feasible biological experiments to test them.

Resumen

El uso de las Matemáticas para comprender problemas relevantes en Biología se remonta al menos a los trabajos pioneros de D. Bernoulli sobre la eficacia de la vacuna contra la viruela (1760) y L. Euler sobre el flujo sanguíneo en arterias (1775). Desde entonces, el campo de la Biomatemática ha experimentado un extraordinario desarrollo, a lo largo del cual han surgido una gran cantidad de desafíos fascinantes. Uno de ellos es el de esclarecer la morfogénesis (la emergencia de las formas biológicas) haciendo uso de métodos matemáticos, una cuestión que ha sido abordada, entre otros, en los influyentes trabajos de D.W. Thompson (1917), A. Turing (1952) y H. Meinhardt (1972).

La memoria que ahora se presenta se ocupa de la modelización y simulación matemática de un problema específico de la morfogénesis vascular temprana, un proceso que constituye el primer paso en la formación del sistema vascular de los vertebrados. Concretamente, en este estudio se presenta una combinación de métodos matemáticos, computacionales y experimentales que permiten obtener nuevos avances en los mecanismos moleculares y celulares fundamentales que subyacen al proceso de autoorganización de la red vascular. La tesis se divide en tres secciones principales: Preliminares (Capítulo 1), Trabajo de Investigación (Capítulos 2 y 3) y Perspectivas y Conclusiones (Capítulos 4 y 5). En el Capítulo 1 se presenta una visión general del campo junto con una introducción al problema principal. Además se revisa la bibliografía sobre la materia desde un punto de vista crítico. En el Capítulo 2 se propone y examina un nuevo mecanismo y un nuevo modelo matemático de tipo híbrido para explicar la formación del patrón vascular considerado. El estudio del modelo matemático propuesto plantea una serie de hipótesis biológicas nuevas, la mayoría de las cuales se encuentran más allá del alcance experimental. No obstante, algunas de estas hipótesis se pueden validar en casos particulares. Esto se muestra en el Capítulo 3 haciendo uso de una situación controlada y simplificada consistente en un cultivo celular *in vitro*. En ese proceso también se ha obtenido información cuantitativa sobre las propiedades cinéticas y difusivas de una molécula fundamental en el desarrollo vascular (VEGF). El Capítulo 4 está dedicado a perspectivas de trabajo futuro en

el campo considerado. En particular, se detallan dos proyectos en curso consistentes en extensiones de los modelos matemáticos aquí considerados. Por último, el Capítulo 5 recoge las principales conclusiones de este estudio.

En resumen, los métodos matemáticos y computacionales que se han desarrollado en esta tesis, combinados con técnicas experimentales apropiadas, proporcionan información sobre un problema relevante de la morfogénesis vascular que no era conocida previamente. Además, el marco teórico propuesto puede usarse tanto para proponer nuevas hipótesis biológicas, como para contribuir al diseño de experimentos biológicos precisos y viables que permitan evaluarlas.

Contents

Part I

Preliminaries

Chapter 1

Modelling vascular morphogenesis: current views on blood vessels development

Contents

1.1 Introduction

The question of ascertaining how embryos develop from a single cell (the fertilized egg) until transforming into a complex multicellular structure is known to have attracted the attention of mankind since the earliest recorded scientific thought. Aristotle, for instance, observed that such developmental process (that he termed epigenesis) should be a sequential one, whereby animal parts "form one after another ... similarly to the knitting of a net" [11]. Concerning the internal

rules that should govern such a process, he regarded them to be as those ruling "... automatic mechanisms, whose pieces can be set in motion by some external action, and then transmit that motion to the nearest ones..." [11].

As a matter of fact, the formation of any complex body follows a structural building plan that did stabilize throughout the course of evolution. The similitude of that process with architectural design is a natural one. It is to be noted, however, that while the plans of a building are laid out well before construction begins, the building plans of an embryo are dynamical and self-regulating. In other words, it is the ordered activation of each structure through time which determines the building block that has to be formed next, and where such piece has to be located.

The astonishing regularity followed by embryonic development strongly suggests that such process obeys to precise deterministic laws. On the other hand, it is widely acknowledged that Mathematics provides the most precise toolkit to deal with quantitative matters which is available as yet. It is thus natural to wonder whether mathematical models could be derived so that they could describe embryonic development as Newton's and Kepler's laws account for the motion of objects in the solar system. Far as such long-ranging goal might be, during the last century many researchers have attempted to develop mathematical models to explain biological structures and processes (see for instance, Refs. [41, 60, 74, 88, 101, 138, 142]). When doing so, a number of assumptions had to be made, and many approaches have been discussed. For instance, the importance of optimal design (or variational) problems in prescribing the actual form of organs was already highlighted in Ref. [138], whereas the role of molecular reactions, that can be accurately described by systems of differential equations, has gained momentum over the last years [119, 145].

However, when trying to study developmental processes, mathematical models have often stepped into a formidable stumbling block: complexity. Indeed, Mathematics shows its full power when dealing with archetypical, simplified problems which have been stripped bare of details, to retain only a few features considered as essential ones. It is commonly assumed, however, that Biology is bound to face highly complex structures, which are endowed with emerging properties. By this we mean that the latter appear as a consequence of the complex interplay of the elements involved in the system and cease to be observed if attention is focused only in parts or constituents of the whole structure.

A possible way to confront the complexity issue may come through the concept of modularity, which has become pervasive in contemporary Developmental Biology (see Ref. [130]). According to it, many biological processes can be thought

of as consisting of a set of building pieces or modules, connected between them by means of suitable interfaces. Such modules operate in an integrated way but any of them has a degree of insensitivity to context, so that they can perform similar functions in different biological situations. These features, which in a way make modules similar to electronic circuits, hint at the possibility of representing them by means of comparatively simple mathematical models, mutually interconnected in a hierarchical manner.

Another difficulty inherent in the modelling process is related with the presence of model parameters. When dealing with developmental processes, the set of parameters is usually large, and typically, most of them are not known *a priori*. Moreover, it is often the case that the model is too complicated to allow for exact solution or analytical treatment, even when ignoring many essential aspects of the system under consideration. Our current computing power, however, makes it possible to perform numerical simulations of quite complex models as long as suitable estimates for model parameters are provided. The numerical approach therefore focuses on certain trajectories related with the specific problem under consideration and allows for quantitative, precise comparison with experimental data. When doing so, a natural way to obtain an overview over all possible behaviours of the systems is to explore the parameter space though large-scale simulations and perform sensitivy analysis for those that are of particular interest.

When dealing with these matters, mathematicians need often to bridge boundaries among disciplines. Specific biological knowlegde is essential for selecting the questions and problems to deal with as well as to consider a minimal set of suitable variables and parameters to build up models. Sometimes, it is also important to understand a wide variety of experimental techniques that are used to obtain experimental data. For instance, some of the techniques developed to estimate model parameters make use of mathematical tools but are often deeply based on physical and biochemical theories. Also, computational skills are crucial to implement numerical methods and run simulations, for which high performance computers are sometimes needed. Computing is also essential to acquire quantitative information from experiments by means of image processing techniques or to compare simulated and experimental data, a key task during the modelling process.

In this work I make use of the conceptual tools described above with the aim of gaining insight into a particular problem in embryonic vascular morphogenesis, the process that give rise to the vascular system of vertebrates. To begin with, this background chapter introduces the problem and reviews the existing literature on it from a critical point of view. More precisely, an overview of my

current understanding of the way in which the formation of the vascular system in vertebrates occurs is presented in Section 1.2. Particular attention is paid to describe the structure and function of blood vessels, the detail of what is known about their embryonic origin and the cellular mechanisms by which they develop. Section 1.3 reviews the main mathematical models that have been introduced to describe particular aspects of the process under consideration. The focus here is laid on models that were proposed to explain the patterning of the early vasculature. Those include continuous models that make use of nonlinear partial differential equations, as well as discrete and hybrid ones that account for the position and shape of biological cells individually. Finally, a number of conclusions are gathered in Section 1.4.

1.2 The formation of the vascular system in vertebrates

The simplest three-dimensional structures which develop in the early embryo are tubes. Cylindrical hollow tissue arrangements are quite common during embryonic development [2, 25, 27]. Such tubes appear through quite different morphogenetic mechanisms and can be used as scaffolds for the development of more complex structures. One of the best-known examples of biological tubes is that of blood vessels, which constitute the main subject of the present dissertation.

1.2.1 A variety of blood vessels: structure and function

Circulatory systems are present in many living beings. In the words of Aristotle: "...the system of blood vessels in the body may be compared to that of water courses which are constructed in gardens: they start from one source, or spring, and branch off into numerous channels, and then into still more, and so on progressively, so as to carry a supply to every part of the garden ..." [10].

Vessel networks in animals are responsible for sustaining metabolism and should guarantee physiological homeostasis, that is, the equilibrium of organic physiology. An apparent requisite for the appearance of vascular structures, both in embryonic development and throughout evolution, is the progressive decrease of the body surface/volume ratio as the animal grows. This increase in size implies that diffusion, a slow mass transfer process [28], is no longer an efficient physical mechanism to distribute oxygen. Under these conditions the uptake of nutrients and elimination of metabolic waste soon becomes a serious limitation. The raising of vascular-like structures is an answer of Nature to these problems [20, 39, 81].

Vertebrate blood vessels are different from those found in many invertebrate animals. In particular, the former are the only ones continuously lined by a thin layer consisting of specific vascular cells, the endothelium. Moreover, vertebrate blood vessel systems are closed vascular beds with no uncontrolled leakage of blood into the surrounding tissues.

There is a variety of blood vessels among vertebrates, see Figure 1.1. Of these, the arterial, capillary and venous types are the most relevant ones. Vertebrate arteries have thick elastic and multilayered walls. Large mature arteries are made up of three concentric tissue layers: i) an outer *tunica adventitia* constituted of fibroblasts, ii) a *tunica media* including smooth muscle and elastic fibers, iii) and a *tunica intima*, formed by the innermost endothelium and the underlying elastic fibers. Arteries are capable of peristaltic pumping, they approximately contain a 35-40 % of the total body blood volume and act as a buffering system for the oscillations of pressure in the circulatory flow [39].

Arteries connect the heart to an intricate network of capillaries through arterioles and metarterioles. Under normal conditions, the potential blood content of all the capillaries of an individual is estimated to be a 15 % of all the body blood. However, since metarterioles normally end in a pre-capillary sphincter that controls the local flow of blood in the capillary bed, only a half of this potential blood volume (around 7 %) is actually contained by capillaries at a given

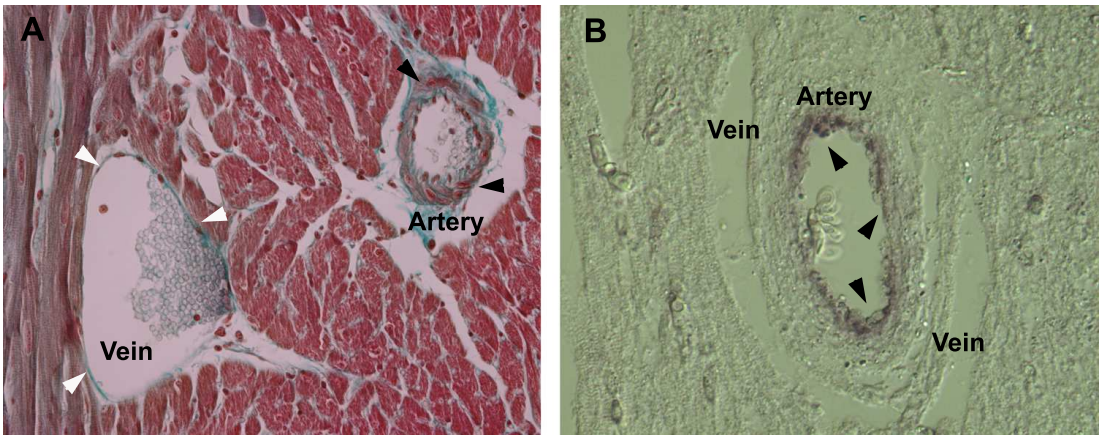

Figure 1.1: **A variety of blood vessels**. **A.** Embryonic coronary arterio-venous pairs illustrate differences between arteries and veins. The former have a more complex vessel wall (black arrowheads) and a smaller diameter. The latter display a wide diameter, but the vessel wall is thinner (white arrowheads). **B.** Arterial endothelium has a specific molecular profile as compared to venous endothelium. The dark precipitate on the endothelium of this transversal section of an artery (arrowheads) denotes the expression of the ephrinB2 gene (mRNA in situ hybridization). Note that the venous endothelium is negative for the staining.

time. Capillaries are the smallest vessels of the body and are in charge of the delivery of oxygen and nutrients at the cellular level. They are composed of endothelial tubes of small diameter (around 5-10 microns) discontinuously covered by pericytes, a characteristic supporting cell type for endothelial cells. Pericytes present focal contacts with endothelial cells and modulate blood vessel development, maturation and remodelling. Pericytes are related to smooth muscle cells (SMCs) and many authors favour the idea that they could represent a cell subtype ontogenetically and functionally placed between fibroblasts and smooth muscle cells [64].

Veins provide the return pathway for the blood circulating from capillaries to the heart. Veins have a great inner diameter and normally present a less complex wall than arteries. At least a 50 % of the total volume of blood of vertebrates is to be found in veins, which can act as a reservoir of blood to sustain arterial pressure in case of haemorrhage [39, 86].

1.2.2 Embryonic origin of blood vessel cell progenitors: the angioblastic and endothelial cell types

Angioblasts are the vascular progenitors of endothelial cells, the specific epithelial cell type that lines the inner surface of vertebrate blood vessels, see Figure 1.2. Angioblasts have been characterized as originally isolated mesenchymal-like cells of mesodermal origin displaying an early expression of vascular markers like the transcription factor SCL/TAL-1 or the type II receptor for the Vascular Endothelial Growth Factor (VEGF) VEGFR-2/Flk-1/KDR [36, 68, 122]. VEGF is the paradigm of growth factors promoting blood vessel formation. It has been shown to control a variety of endothelial cell processes, including cell survival, migration and proliferation. Both angioblasts and VEGF are regarded as primary elements in most of the mathematical models attempting to explain early vascular morphogenesis. As a matter of fact, it is well known that VEGF signalling is critical for the coalescence and integration of angioblasts into a primitive vasculature. However, the precise role of VEGF in this process remains unclear [115, 122, 144]. VEGF is a glycoprotein that is primarily produced by the embryonic endoderm and some embryonic mesodermal cells, but there is no evidence that angioblasts produce a significant amount of it. Accordingly, VEGF is regarded here as having essentially a paracrine effect on adjacent angioblasts. This observation plays a fundamental role in this study as detailed below.

Maturation of angioblasts into endothelial cells implies the progressive increase in expression of signalling molecules related to cell-cell adhesion like

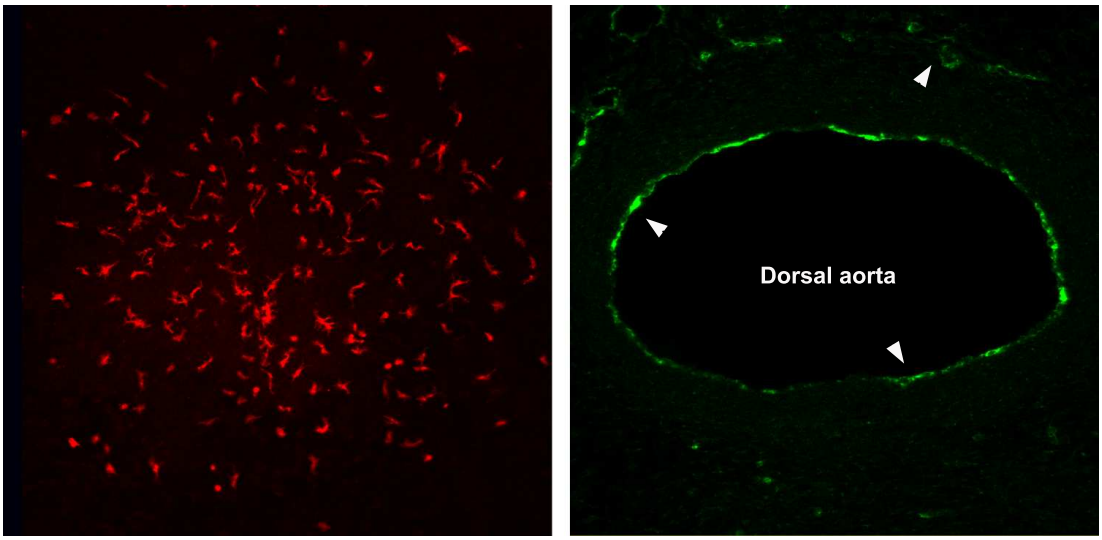

Figure 1.2: **From angioblasts to blood vessels**. **A.** Vascular progenitors (angioblasts, red dots) are free mesenchymal cells that can be cultured on 2D or 3D (as the image shows) *in vitro* assays. In this illustration, quail embryonic angioblasts have been localized after QH1 staining (red). **B.** Endothelial cells form the inner layer of forming vessels like the dorsal aorta. Endothelial cells express the type II receptor for VEGF (VEGFR-2) (green, arrowheads)

PECAM/CD31 and VE-Cadherin, leading to the formation of a coherent epithelial tissue known as endothelium [122]. Accordingly, endothelial cells should be regarded as a part of a complex histological unit, the endothelium. Mature adult endothelial cells secrete von Willebrand factor (vWF), a glycoprotein that acts as a carrier of factor VIII (a key ingredient of the coagulation process) and accumulates in Weibel-Palade bodies (WPb). Transmission Electron Microscopy studies reveal that the presence of WPb, caveolae, a reduced cytoplasm, and a nucleus with an elliptical section are the prototypic structural features of endothelial cells [17]. However, not all endothelial cells are equal. From a structural point of view, blood-brain barrier endothelial cells display tight cell-to-cell junctions that make of this endothelium a highly selective one, whereas liver sinusoidal and renal glomerular endothelia present fenestrations that transform it into a permeable tissue. Furthermore, the endothelium of big vessels (*macroendothelium*) has been shown to be different to that of small vessels like capillaries (*microendothelium*). At the molecular level, microendothelial cells tend to show a diffuse cytoplasmic distribution of vWF, lacking the characteristic WPb of macroendothelium; in this regard microendothelial cells resemble embryonic endothelial cells. Finally, the expression of extracellular matrix (ECM) molecules, matrix metalloproteinases (MMPs) and lectin-binding properties are also different between microvascular and macrovascular endothelial cells [1, 32, 66, 72, 80].

The molecular and cellular mechanisms that control the determination and

differentiation of angioblasts are still subject to controversy. An important question that remains without answer is whether all embryonic endothelial cells of an individual originate from a common original pool of angioblasts differentiated soon after gastrulation [12], or if different waves of angioblastic differentiation take place from the mesoderm as the embryo forms [36, 110, 132]. If we accept the first hypothesis, then most of the endothelial cells of any vertebrate should derive from a primordial source of angioblasts by a continuous and sustained proliferation along embryogenesis. Furthermore, under this premise, angioblasts should be able to actively migrate as the embryo grows (for more details, see Section 1.2.3 below). On the contrary, the second hypothesis favours the view that a high proliferation of angioblasts is not necessary to initiate vascular morphogenesis, since the process would be dependent on *de novo* local differentiation of angioblasts *in situ*.

The discussion on the proliferation of the angioblastic/endothelial cell type is crucial to understand early embryonic vascular development. It is commonly accepted that endothelial cells have a low proliferation rate in the adult, and a high one in the embryo [121]. However, the reported proliferation rates of *in vivo* angioblasts [19,78,97] are not high and, as a matter of fact, the strong pro-mitotic effect of well-known growth factors for endothelial cells like VEGF is characteristic of *in vitro*-cultured adult endothelial cells [4, 70] but has not specifically been reported for cultured angioblasts. Most interestingly, addition of exogenous VEGF to developing embryos (often used at supra-physiological levels *in vivo* as well as in *in vitro* settings) seems to produce vascular dysmorphogenesis by endothelial hyperfusion rather than increased cell numbers, so that the formed vessels are abnormal, displaying a wider lumen and a sinusoidal shape [35]. Finally, several studies have demonstrated that isolated embryonic angioblasts display a low cell proliferation [18, 53] as well as that a strict control of the proliferation of angioblasts and immature endothelial cells is essential to proper vascular development and remodelling [78]. For all these reasons, it has been suggested that proliferation is not a primary factor accounting for early blood vessel development.

1.2.3 Morphogenetic mechanisms of vascular development

Vertebrate blood vessels can form through very different cellular mechanisms. The earliest outline of the adult circulatory system appears very soon in development after a morphogenetic process named vasculogenesis. This phenomenon, which takes place before the onset of blood flow, involves the coalescence of isolated endothelial cell progenitors of mesodermal origin (angioblasts) to form

tubular endothelial structures of different calibre [49,114,120,122,123]. Therefore, the first vascular structures that appear in any individual form by vasculogenesis, which is the predominant vascular development mode in the early embryo. Primitive embryonic vascular networks continue growing by angiogenesis, an alternative mechanism of vessel growth based on the invasive sprouting or division of pre-existing blood vessels [40, 42, 58, 120]. Quite logically, angiogenesis, that will become the main normal and pathologic mechanism of blood vessel growth and remodelling throughout adulthood, depends on embryonic vasculogenesis to ever take place.

Vasculogenesis is a paradigmatic kind of mesodermal tube formation [61]. As pointed out in the previous section, a first fundamental step in this process is the onset of the endothelial cell lineage (angioblasts). Once such population is established within the mesenchymal component of the mesoderm, the next morphological event is the assembly and patterning of those cells into vascular networks. In this process, that takes place in a thin planar surface of the mesoderm, primary unicellular units (angioblasts) associate into secondary multicellular vascular units (vascular chords, blood islands) that will in turn fuse giving rise to planar blood vessel networks [122, 123]. During the assembly and fusion process, angioblasts progressively differentiate into endothelial cells and at the same time the formation of the vascular lumen occurs. The vasculogenic stage ends when vessels undergo maturation and initiate remodelling, which involves both angiogenic growth and vessel pruning.

Cellular characteristics of angiogenesis are different to those observed throughout vasculogenesis. Development of new vessels by angiogenesis involves the activation of quiescent (not dividing and not able to migrate) endothelium. Angiogenic endothelium is locally mobilized, loosing cell adhesion, gaining a disorganized aspect and producing characteristic filopodial projections at the front of the growing endothelium. In parallel, angiogenic endothelium proliferates and initiates an active degradation of the endothelial basal membrane and the surrounding extracellular matrix [16, 148]. As a result vessel sprouts are form that invade the surronding tissue guided by gradients of angiogenic signals, including VEGF [44]. Specific endothelial cells at the tip of growing vessel sprouts are called tip cells, whereas other endothelial cells that stay behind tip cells and maintain the integrity and perfusion of growing vessels are called stalk cells. The dynamic molecular and cellular mechanism that govern tip cell selection during sprouting angiogenesis have been partially elucidated [40]. During vasculogenesis, however, it remains largely unclear whether such phenotypic cell specialization exist. Also, the function of VEGF as a chemoattractant during angiogenesis (forming gradients that guide growing sprouts) is better understod than in vasculogenesis,

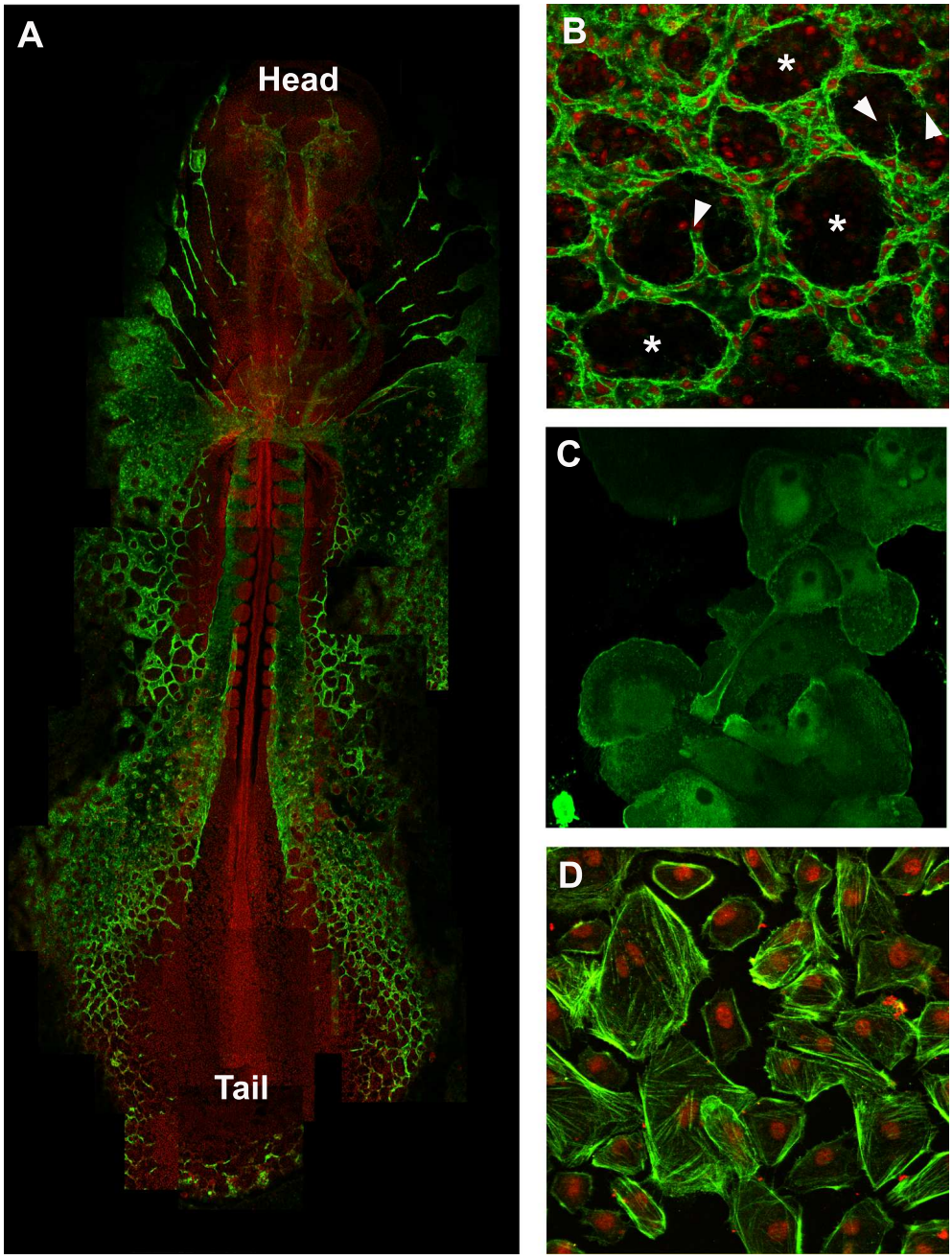

Figure 1.3: **Components of the embryonic vascular system**. **A.** The whole vascular tree of a quail embryo (36 hours of incubation) is shown. The endothelium has been counterstained with the quail specific vascular marker QH1 (green). **B.** A detail of the posterior vasculature shown in A is presented. Early vascular structures are arranged forming networks that display polygonal-like holes (asterisks). Arrowheads mark the appearance of endothelial sprouts in the developing vasculature. **C.** Mouse endothelial cells growing on plastic. The cell membrane of the cells expresses variable levels of the cell-cell adhesion molecule VE-cadherin (green) which allows for the formation of a characteristic cobblestone-like monolayered epithelium. **D.** Mouse vascular smooth muscle cells (green, α-smooth muscle actin-positive) in culture. The visceral musculature (non-striated) is a major component of the blood vessel wall (*medial layer*).

where VEGF signals from the endoderm are believed to more uniformly impinge on angioblasts.

Another important controversy in the understanding of the first steps of vasculogenesis is that of the much discussed migratory properties of angioblasts or, in other words, the ontogenetic relation existing between angioblasts and the locations where vascular formation takes place. In a classic paper, Poole and Coffin [26] classified vasculogenic events into two categories. In type I vasculogenesis, angioblasts would differentiate *in situ* and form a vessel in the same place where they first appeared as true vascular progenitors. On the contrary, type II vasculogenesis takes place when angioblasts differentiate far from the point where they will eventually form blood vessels. It is evident that type I implies a reduced migration of angioblasts whereas type II vasculogenesis relies on long-distance angioblast migration. Cardinal and vitelline veins as well as the primary vascular networks of visceral organs like the lungs, kidneys, spleen, heart (endocardium and coronary vessels), liver, pancreas and other elements of the digestive system form by type I vasculogenesis [8, 26, 69, 109, 110, 132, 141]. On the other hand, the nervous system becomes vascularized after the migration of angioblastic populations (type II vasculogenesis). These angioblasts first pre-organize themselves through vasculogenesis in a perineural vascular plexus that then undergoes an extensive angiogenesis [103, 104]. This may reflect the close relation that exists between the endoderm and the origin of angioblasts, so that the embryonic mesodermal territories can be divided into two main regions, a ventral visceral (splanchnic) one, which produces high numbers of angioblasts that tend to form blood vessels *in situ*, and a dorsal somatic one, where angioblast differentiation is enormously reduced. This latter situation results in angioblast recruiting from other locations. As described above, motility and migration of angioblasts is a pivotal aspect of early vascular development and must thus be taken into account when mathematical modelling of vascular development is performed.

Quite remarkably, early drafts of vascular structures show a characteristic patterning that is most evident during embryonic vasculogenesis, see Figure 1.3. Angioblasts are known to arrange in space forming planar networks displaying polygonal profiles even before expressing molecules that reveal their full commitment into the endothelial lineage [36, 37]. However, the signals and local cues that regulate the appearance of this pattern remain unclear. It has been widely discussed as whether a pre-patterning could exist for early vascular structures, i.e. if intrinsic properties of the primary (undifferentiated) mesodermal or endodermal tissues can account for the characteristic organization of primitive vascular networks. There is every indication that genetically predetermined cues play a crucial role in the patterning process, as for instance by determining precise

spatio-temporal expression of provascular growth factors. On the other hand, it is known that early vascular patterns vary substantially at the cellular scale between different embryos of the same species. Also, transplantation experiments between embryos of different species proved adaptation and integration of cells from tissue grafts to the new environment. This suggests a different mechanism where a dynamical, self-regulated activity of vascular precursors would influence the pattern in response to local environmental cues. Also, recent studies suggest that the collective, protrusive activity (sprouting) of embryonic endothelial cells and the interaction with a dynamic ECM is enough to create early vascular patterning [30,31]. A suitable mathematical formulation and its subsequent analysis seems particularly suited to shed light on that issue. Also, the appearance of geometrical vascular structures with characteristic forms and sizes calls at once for mathematical modelling.

1.3 Mathematical models of vascular networks formation

Mathematical modelling allows us to explore different biological hypothesis even beyond our experimental reach. At the same time it provides quantitative, precise ways of comparing predictions and experimental observations. In this section a number of mathematical models that have been proposed to explain particular aspects of early vascular patterning are discussed. Specifically, a number of models that keep track of the exchange of chemical signals, which goes along with (and to a large extent is a cause of) the unfolding of the vascular pattern, are analyzed. Some of those models explicitly account for cells, either through continuous densities or tracking them individually. Also, some mechanical and multiscale aspects involved in vascular patterning will be discussed.

It is important to note that although vascular networks are composed of tubes, which are three dimensional structures, the models of vasculogenesis to be discussed in this dissertation just account for two spatial dimensions. As a matter of fact, both in embryonic vasculogenesis and in the *in vitro* cultures of endothelial cells that will be considered here, the patterning process takes place in a thin and planar surface. As cell movements in the vertical direction are very small compared with the size of the simulated structures, a third spatial dimension is neglected. Also, the models presented here do not take into accout the formation of endothelial tubes, a process that runs in parallel to the patterning one.

1.3.1 Reaction-diffusion systems: the activator-inhibitor paradigm

Reaction-Diffusion (RD) systems are mathematical models which provide a description of processes whose major players at the microscopic level are i) random movement of molecules, and ii) chemical reactions between them (see Ref. [56] for a review). Some systems of Partial Differential Equations (PDEs) of this type have been proposed to explain the formation of vascular structures [73, 87, 90]. These models assume the existence of signalling molecules that are characterized by well-defined kinetic properties, such as their diffusion rate and half-life time. They are of a continuous nature, in the sense that chemical molecules are regarded as points moving in a surrounding space and are represented in the model by means of continuous density functions. To this day, they continue to be most widely used to describe pattern formation in Biology.

A basic building block for this sort of systems are the so-called Activator-Inhibitor (AI) models. These have been formulated in terms of linear systems [142] as well as by means of nonlinear ones [45]. The latter setting has proved to encode a richer dynamics than the former one. For instance, in reference [45] it was observed that crucial conditions for stable pattern formation are local self-enhancement and long-range inhibition. More precisely, their AI system describes the dynamics arising from the interplay of two substances. One of them (the activator), $a(x,t)$, is autocatalytic, and at the same time produces an antagonist (the inhibitor), $h(x,t)$. The inhibitor counteracts the activator, and diffuses faster than a does into the surrounding medium. In its simplest version, the model takes this form:

$$\begin{cases} \frac{\partial a}{\partial t} = D_a \Delta a + \frac{ca^2}{h} - \mu a, \\ \frac{\partial h}{\partial t} = D_h \Delta h + ca^2 - \nu h, \end{cases} \tag{1.1}$$

where D_a, c, μ, D_h, ν are positive constants and $\Delta f = \sum_{k=1}^{n} \frac{\partial^2 f}{\partial x_k^2}$ for $n = 1, 2, 3$. It has been shown by mathematical analysis and numerical simulations that random fluctuations on the ability to perform the reaction and/or the initial concentrations of the substances are sufficient for pattern initiation and stabilization within certain parameters sets [88, 101]; see Figure 1.4. An alternative for the antagonistic reaction consists of the depletion of a substrate s, which is required during the activator production, giving rise to the so-called activator-substrate model. Here, the substrate must also diffuse faster than the activator, to allow for the formation of the corresponding patterns [88].

The complexity of the patterns obtained from RD systems can be further increased if several such models are combined in a hierarchical, or modular, way, as

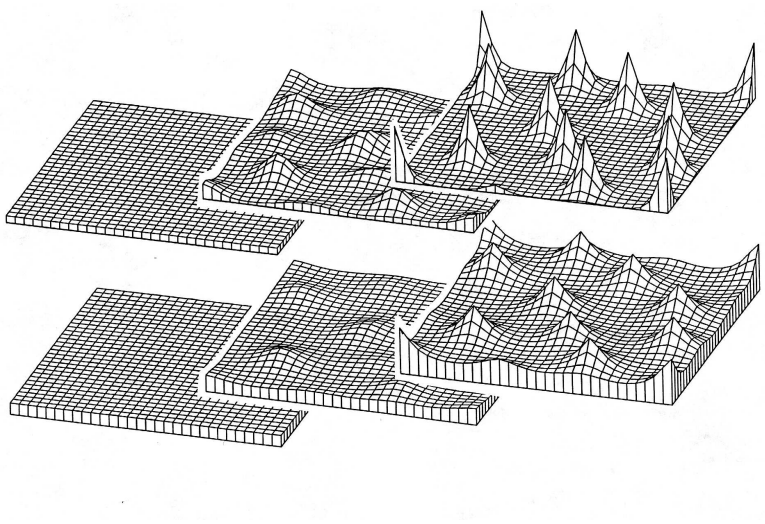

Figure 1.4: **Activator-Inhibitor model**. A typical pattern produced by the activator-inhibitor model (1.1) in two spatial dimensions. Initial, intermediate and final activator (top) and inhibitor (bottom) distributions are shown. Reprinted with permission by Prof. H. Meinhardt.

described below. Moreover, cell differentiation can be accounted for by assuming that, i) at an appropriate stage, the cells that are building a biological structure make use of position-dependent signals to change their state of determination, and ii) cells may maintain this acquired determination when the evoking signal vanishes, provided that the external cue is strong enough, and will remain in their previous stage otherwise. Such behaviour is usually termed as bistability. A simple example of a switching system that describes a bistable process is given by:

$$\frac{\partial y}{\partial t} = \rho \frac{y^2}{1 + ky^2} - \mu y + \sigma^{ext},$$

where ρ, k and μ are positive constants and σ^{ext} describes a external signal. Note that for suitable choices of the previous parameters, the function:

$$f(u) = \rho \frac{u^2}{1 + ku^2} - \mu u + \sigma^{ext},$$

behaves as indicated in Figure 1.5.

1.3.2 Reaction-diffusion models for the generation of network patterns

As observed in Section 1.2, reticular and filamentary structures are often encountered during vasculogenesis. A theoretical model that describes the development of a two-dimensional network consisting of filamentary structures was proposed

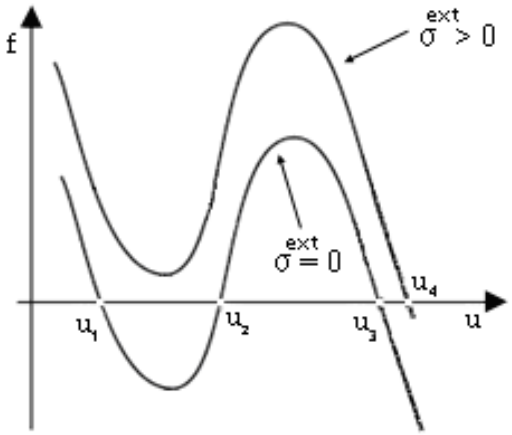

Figure 1.5: **Bistability**. Kinetic curves corresponding to $f(u)$ for different values of σ^{ext}. a) A typical bistable system, with two stable equilibria $y = u_1$, $y = u_3$ separated by an unstable one $y = u_2$. b) A graph of $f(u)$ for $\sigma^{ext} > 0$. Note that two of the former equilibria have disappeared.

in [87]. Its basic assumptions are: i) Filaments grow as a consequence of the action of an AI system, which generates a local signal for networks filaments elongation. ii) When these signals are above a certain threshold, the exposed cells irreversibly differentiate into members of the filament system. iii) To account for the invasion of a region not supplied by filaments, all cells are supposed to produce a growth factor that attracts the net and is consumed by the differentiated cells belonging to it. Keeping these ideas in mind, Meinhardt wrote the following system of PDEs:

$$\begin{cases} \frac{\partial a}{\partial t} &= D_a \Delta a + \frac{a^2 s}{h} + \rho_0 y, \\ \frac{\partial h}{\partial t} &= D_h \Delta h + a^2 s - \nu h + \rho_0 y, \\ \frac{\partial s}{\partial t} &= D_s \Delta s + c_0 - \lambda s - \varepsilon s y, \\ \frac{\partial y}{\partial t} &= \frac{y^2}{1+ky^2} - ey + da. \end{cases} \tag{1.2}$$

Here $a = a(x_1, x_2, t)$ (respectively, $h = h(x_1, x_2, t)$) denotes the concentration of a chemical which is termed as activator (respectively, inhibitor), $s = s(x_1, x_2, t)$ is the growth factor concentration, and $y = y(x_1, x_2, t)$ denotes a variable that accounts for cell differentiation. Such model can describe interesting features, some of which closely resemble those of actual biological networks: bifurcations and lateral branches can be formed, the density of filaments can be regulated according to local tissue demand, the outgrowth of a filament can be oriented towards a target area, and a damaged net can be repaired [87–90]. Moreover, the role played in the model by the growth factor s fits in some aspects with known

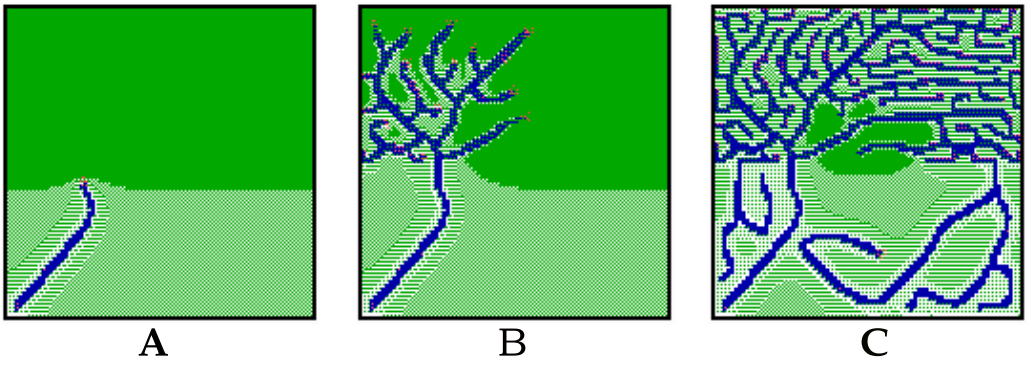

Figure 1.6: **Filamentary networks**. A simulation of system (1.2) is shown. **A.** Initially, a filamentary structure (blue) goes from the left bottom corner of the field to the top, where a high growth factor production is assumed (dark green). **B.** The filaments start branching in the middle top of the field. As high inhibition is assumed in the centre of the panel, no branches enter this area. **C.** The final configuration shows high-density networks in the middle top, while no or few filaments are formed in the centre and bottom sides of the panel. Note also that reconnections between different branches do not take place. Adapted from http://www.eb.tuebingen.mpg.de/departments/former-departments/h-meinhardt .

VEGF properties. For instance, it is well known that diffusible forms of VEGF are released by tissues attracting new vessels [79]. This can be mimicked by a suitable production term c_0 in the third equation of (1.2). Furthermore, tip cell activation depends on VEGF [44], as assumed in the model (see the term $\frac{a^2 s}{h}$ therein). Another remarkable fact accounted by the previous system (more than thirty years before its discovery) is that for tip cell selection to occur, a lateral-inhibition mechanism should be working. Indeed, experiments in angiogenesis have shown that lateral-inhibition is mediated by cell-to-cell contact throught the Notch-Delta pathway [40, 135]. Interestingly, recent experiments also suggest that stalk cells release VEGF inhibitors to the extracellular medium, thereby providing local guidance to the emerging vessel sprouts led by a tip cell [23]. This last mechanism, that was not included in the original model, is likely to have an impact on the simulated network patterns. It is important to note that the network patterns generated during the early stages of blood vessel development display differences with respect to the ones provided by the previous model. For instance, (1.2) does not favour vessel merging (anastomosis), see Figure 1.6, which is however observed in high vascular-density areas during active vasculogenesis or angiogenesis processes. Note also that, in this case, cell differentiation occurs *in situ*, and cell migration is not included in the model.

We next recall an alternative RD mechanism based in different hypotheses:

namely, that there are signals involved in the determination of avascular areas and others that establish the pattern where the cells should set up the structure, but cells as such are not explicitly taken into account. More precisely, in reference [73] a reticular structure is obtained from the interaction of four substances. The corresponding dynamics are described by means of two different, coupled AI systems. A first pair of equations for an activator and a substrate (a, s) gives rise to a distribution of patches, whereas the second AI system (b, h) generates stripes around previous patches. The corresponding equations are:

$$\begin{cases} \frac{\partial a}{\partial t} &= D_a \Delta a + \rho_a \left(\frac{s a^2}{1+k_a b^2} - a \right) + \sigma_a, \\ \frac{\partial s}{\partial t} &= D_s \Delta s - \rho_s \left(\frac{s a^2}{1+k_a b^2} \right) + \sigma_s, \\ \frac{\partial b}{\partial t} &= D_b \Delta b + \rho_b \left(\frac{s^2}{1+k_b a b^2} \left(\frac{b^2}{h} + \sigma_b \right) - b \right), \\ \frac{\partial h}{\partial t} &= D_h \Delta h + \rho_h \left(b^2 - h \right). \end{cases} \tag{1.3}$$

The coupling is done in a hierarchical way, so that the (a, s) system triggers the (b, h) one. The concentration of the activator a (avascular areas activator) acts in the third equation of (1.3) modulating the saturation value of the activator b (vascular areas activator). Therefore, in regions with high a concentration, the system (b, h) loses significance, while in areas of low a concentration the second system is able to generate stripes. Moreover, the term $\rho_b s^2$ in the third equation of (1.3) favours the stripes formation at high substrate s concentration regions, at the maximum distance from the patches. The final result is a reticulated structure similar to the polygonal vascular networks observed in vivo; see Figures 1.3 and 1.7. It has been pointed out in References [73] and [90] that such a pattern has size-regulating properties, since it keeps the size of avascular areas nearly constant even if the domain is growing. Nevertheless, identification of possible molecular agents playing an active role in the prepatterning of avascular areas (or *lacunae* as these are usually termed) remains an open question.

It is worth noticing that, while numerical simulations of the previous and similar systems are comparatively easy to perform, the mathematical analysis of activator-inhibitor and related systems (as for instance that describing the unfolding of a planar vascular net presented before [87]) is still far from being complete in the case of two and three space dimensions (see Refs. [125] and [9]). From a biological point of view, the identification of the chemicals actually involved is a difficult task. Quickly diffusing inhibitors are particularly elusive. In fact, what theory requires is that for an activator, the diffusion coefficient should be rather small, whereas the diffusion rate of an inhibitor should be much larger. As a matter of fact, the well-known Einstein-Smoluchowski theoretical formula for the

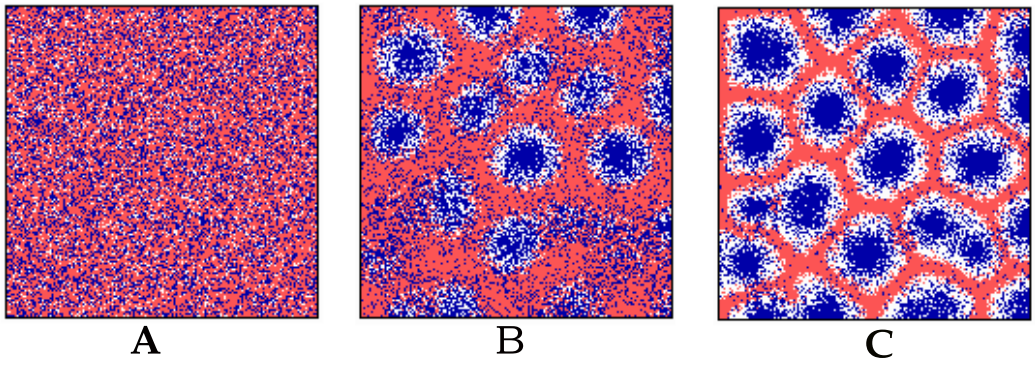

Figure 1.7: **Reticular networks**. A simulation of system (1.3) is shown. **A.** Initially, homogeneous concentration of the chemicals is assumed. **B.** An intermediate step of the simulation where patches of the avascular areas activator (blue) and stripes of vascular areas activator (red) are already present. **C.** The final configuration shows a distribution of similar size patches and a homogeneous reticulated structure. Adapted from http://www.eb.tuebingen.mpg.de/departments/former-departments/h-meinhardt .

diffusion coefficient D of molecules of a solute in a dilute solution (cf. Ref. [28]) gives:

$$D = \frac{k_B T}{6\pi r \eta},$$

where k_B is the Boltzmann constant, T is the absolute temperature, η is the viscosity of the solvent the solute molecules diffuse in, and r is the radius of the solute molecule. This would imply that, under our previous assumptions, the inhibitor should be a very small molecule. Actually, a diffusivity ten times higher would correspond to a radius ten times smaller. It may be possible that more complex kinetic schemes are needed for characterizing negative feedback loops as those encoded in the activator-inhibitor model recalled above. Also, an impaired diffusivity might result from a comparatively high affinity of the diffusing molecules with other particles. Related to this, it has been suggested very recently that in some systems the same molecules could have a dual role, functioning as activators and also as inhibitors after being re-processed, a procedure that involves, among other things, a change in their diffusivity [91].

1.3.3 More general continuous approaches

In the following paragraphs I will describe some continuous models that have been proposed to explain the generation of *in vitro* vascular networks, and that besides reation and diffusion, incorporate additional mechanisms.

A chemotaxis model. A chemotaxis model was introduced in references [43, 131] and later refined and analysed in references [5,75,77,139]. The authors aim at reproducing the observed dynamics in *in vitro* cultures of Human Umbilical Vascular Endothelial Cells (HUVECs) in a thin layer of Matrigel (a hydrated matrix with proteins that favours vascular development). In these cultures, structures with polygonal network shape emerge, similar to the ones observed *in vivo*. The networks formed in Matrigel can be seen as a series of nodes connected by cords. An interesting feature to highlight is that the average length of the cords is approximately constant (around 200 microns) if the initial number of cultured cells is in a range between one hundred and two hundred by mm^2. When the initial number is less than a hundred by mm^2 no connected structures are formed, while for high cellular densities a continuous pattern with big holes unfolds, which the authors call Swiss cheese pattern. The dependence of the network structure on the initial number of cells has been related by the authors to what is known in physics as a percolative transition [52, 133].

The quantitative model to be recalled below intends to account just for the initial behaviour of the culture. For its formulation the following assumptions are made: i) since the culture thickness is very small and the formed network is practically flat, it is supposed that the system can be studied in two space dimensions; ii) the cell population can be described by a continuous distribution of density $\rho(x, y, t)$ an velocity $\vec{v}(x, y, t)$ on each point (x, y) of the Matrigel surface and at every time t; iii) the cellular population in the early developmental stages can be modelled as a fluid of non-directly interacting particles; iv) no proliferation or cell death is taken into account; v) cells are accelerated by gradients of a diffusible substance (chemoattractant), whose concentration is described by $c(x, y, t)$; and vi) it is supposed that the chemoattractant is released by the cells themselves (below, we will refer to this hypothesis as autocrine chemotaxis hypothesis), diffuses and is degraded according to known diffusivity and half-life parameters. From these assumptions, using simple balance laws, the authors derive the following model:

$$\begin{cases} \frac{\partial \rho}{\partial t} + div\,(\rho \vec{v}) = 0, \\ \frac{\partial \vec{v}}{\partial t} + \vec{v} \cdot \nabla \vec{v} = \beta \nabla c, \\ \frac{\partial c}{\partial t} = D \Delta c + \alpha \rho - \frac{c}{\tau}. \end{cases} \tag{1.4}$$

While the first equation in (1.4) is a cell mass conservation equation, the second one corresponds to the hypothesis that cells are accelerated by chemical gradients; β measures the intensity of the chemotactic pull. The authors interpret the convective term in the second equation of (1.4) as accounting for cell persistence [5,131]. According to the third equation of (1.4), the chemoattractant

is released by cells at a rate α, diffuses freely in the medium (D is its diffusion coefficient) where is also degraded; τ is related with the half-life time for this substance. If we suppose that the diffusion is a faster process than the formation of the pattern (fast diffusion approximation), it is possible to drop the time derivative term in the third equation of (1.4), which then reads:

$$\left(-D\Delta + \frac{1}{\tau}\right) c = \alpha\rho.$$

This last can be formally solved for c:

$$c = \frac{\alpha}{D}\left(\frac{1}{\tau D} - \Delta\right)^{-1} \rho.$$

Replacing then c in the second equation of (1.4), we arrive at:

$$\begin{cases} \frac{\partial \rho}{\partial t} + div\left(\rho\vec{v}\right) = 0, \\ \frac{\partial \vec{v}}{\partial t} + \vec{v}\cdot\nabla\vec{v} = \frac{\alpha\beta}{D}\nabla\left(\left(\xi^{-2} - \Delta\right)^{-1}\rho\right), \end{cases}$$

where $\xi = \sqrt{\tau D}$ is a characteristic length scale that represents the effective range of interaction mediated by the assumed chemoattractant [131]. The initial condition for cell density is imposed in the form of a set of n randomly distributed bell-shaped bumps having a width of the order of the average cell diameter. Under a suitable choice of the parameters, a remarkable correspondence between simulations and experiments is reported, both in the dynamics and in the final pattern [5, 131]; see Figure 1.8. Some striking results are: i) If the chemoattractant is identified as VEGF, the characteristic lengths predicted by the model are said to be of the same order of magnitude as the ones observed in the cultures; ii) The model displays a percolative transition (for details on this concept see reference [52]) in terms of the initial number of endothelial cells.

In Reference [5], additional features are taken into account: a dissipative interaction with the substratum, non isotropic conditions for the chemoattractant, and a pressure term to take into account a limited compressibility of cellular matter. The presence of the pressure term in the model is critical, as it avoids the blow-up of solutions typical of many chemotaxis models [55, 76, 108]. Pressure becomes relevant in the presence of high densities, i.e. in the proximity of formed structures, and contributes to their regularization. In this way cell overcrowding is prevented. On the other hand (see Ref. [75]) a linear stability analysis suggests that chemotaxis is the key destabilising force in the mathematical model considered, while pressure is the main stabilizing one.

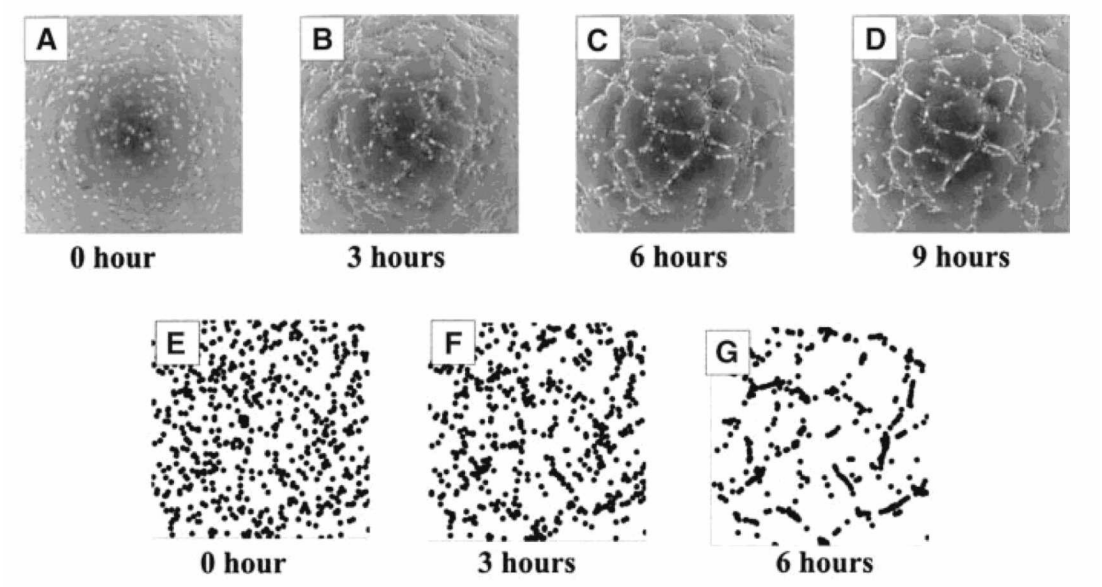

Figure 1.8: **Chemotaxis model**. Comparison between simulations and *in vitro* cultures. **(A-D)** Human microvascular ECs were plated on Matrigel and the time course of network formation recorded by time-lapse videomicroscopy. **(E-G)** Position of cell centroids obtained by model (1.4) using the same number of cells and physical values of the relevant parameters as in panels A-D. Reprinted by permission from Macmillan Publishers Ltd: The EMBO Journal (Ref. [131]), copyright (2003).

The aforementioned models mimic certain aspects of vascular development, but they contain some hypotheses that have not been fully substantiated from a biological point of view. Specifically, they assume that cell chemotaxis is induced by VEGF, which is produced and released by the cells themselves. Nevertheless, it is well known that most endothelial cells express VEGF receptors (as VEGFR2), but it is not clear whether they are normally able to produce VEGF (to be discussed in detail in Chapters 2 and 3). Another possibility is that other growth factors not considered in the model (or even not characterized yet) could play the same role which is therein conferred to VEGF.

An important remark is that it is usually observed in simulations that the reticulated structures that are formed are not stable (though they may last for comparatively large times), and they become undone as time passes. Nevertheless, it is possible to stabilize them by taking into account mechanical interactions between the cells and the substratum through a two-layer model [139].

A mechanical model. Mechanical aspects of pattern formation in vasculogenesis, a subject that deserves attention in itself, can be found in [6, 82, 83, 101, 102, 140], and references therein. Here, I just briefly review a mechanical model

mechanism proposed in [82] to account for *in vitro* cultures of HUVECs in Matrigel as the ones described before. The model is based on the Murray-Oster mechanochemical modelling framework developed in references [99, 100]. It attempts to capture the key interactions between mechanical forces generated by HUVEC cells and Matrigel. The main assumptions are as follows. Local changes in cell density occur mainly as a result of: i) a passive motion (or convection) due to the attachment of the cells on the moving matrix; and ii) a strain-biased random motion along areas of aligned matrix fibers. As in the *in vitro* cultures the matrix domain is much larger than the thickness of the matrix, it is approximated as a two-dimensional material. By considering only small strains, the matrix can be modelled as a linear viscoelastic material. The model accounts for three different type of forces: i) the cell-exerted traction; ii) the viscoelastic forces of the matrix material that are resisting the deformation caused by the cells; and iii) a drag force due to matrix-dish contact. Bearing in mind these assumptions, the following model was derived:

$$\begin{cases} \frac{\partial n}{\partial t} = -\nabla \cdot (n \frac{\partial \boldsymbol{u}}{\partial t}) + \nabla \cdot \nabla (\boldsymbol{D}(\boldsymbol{\epsilon}) n) \\ -\nabla \cdot \sigma_{cells} - \nabla \cdot \sigma_{matrix} = F_{drag} \end{cases} \tag{1.5}$$

where n is cell density, $\boldsymbol{u}$ is the vector displacement of the matrix and $\boldsymbol{\epsilon} = \frac{1}{2}(\nabla \boldsymbol{u} + \nabla \boldsymbol{u}^T)$ is the strain tensor. The form of $\boldsymbol{D}(\boldsymbol{\epsilon})$ depends on the specific assumption about how cells perform their random movements in a strained field, reviewed in Reference [101]. The symbols σ_{cells} and σ_{matrix} correspond to the stress tensor in the matrix due to cell traction and the viscoelastic stress tensor in the matrix, respectively. F_{drag} is the force due to the interaction of the matrix with the dish. More details about the specific assumptions to model the stress tensors and the drag force can also be found in Reference [101]. The first equation in (1.5) is a balance equation for the cell mass, while the second one is a force balance equation for the mixture of cells and matrix. The model mechanism was analyzed in [82, 101] using analytical and numerical methods . Some striking results are: i) Formation of network patterns is possible through just a purely mechanical process (see Figure 1.9); ii) Random motility of cells is not necessary for the formation of the pattern, provided that the seeding density was sufficiently large; iii) The sizes of the holes in simulated networks depends on matrix thickness as observed in experiments.

Previous studies on mechanical effects indicate that mechanics influences vascular patterning in *in vitro* cultures [22, 140]. The mechanical theory might even explain why different cell types also form characteristic networks [34, 105]. However, a pure mechanical scenario contradicts certain experimental observations

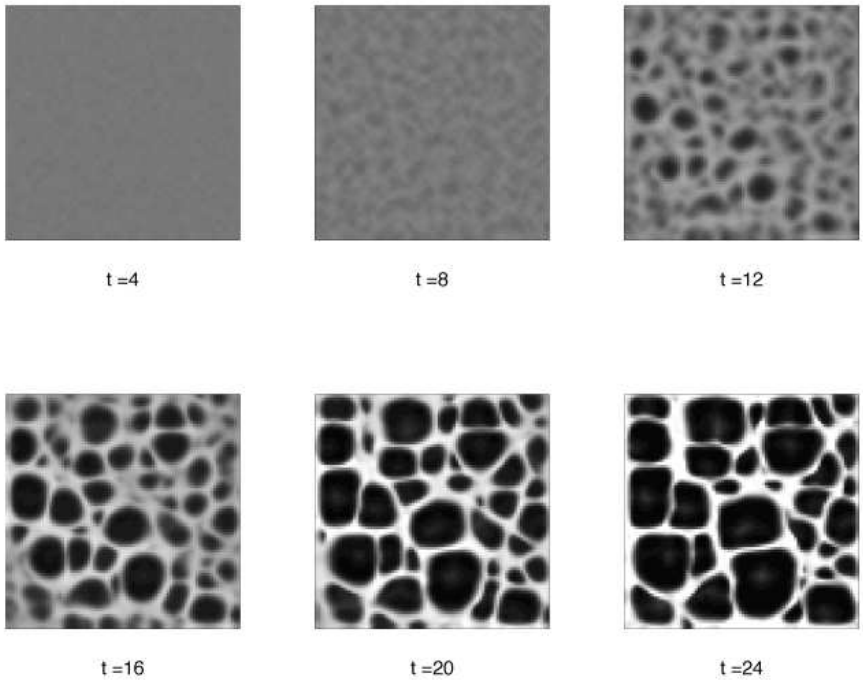

Figure 1.9: **Mechanical model**. Numerical simulations of system (1.5). Initially cells are approximately uniform, but slowly areas of higher cell densities form (white) which exert traction onto the matrix and generate areas devoid of cells (black). Figure from [83].

during embryonic vascular patterning. For instance, it is at conflict with the observation of cell sprouts *in vivo* not growing towards each other [127]. Moreover, it does not explain why growth factors as VEGF are crucial both *in vitro* and *in vivo*.

Kinetic theory of active particles. Another subject that deserves to be explored is the possible use of the kinetic theory of active particles in the study of the topics herein considered. The aforementioned theory can be roughly described as an extension of the classical kinetic theory, where macroscopic evolution equations (including RD equations in some limit cases) are derived from an underlying microscopic description. In biological examples, one often has to deal with large systems of interacting cells, and not only positions and velocities have to be considered, but a new microscopic state (termed activity) and representing biological functions at any level, has to be introduced. As of today, interesting results have been obtained in fields as tumor-immune competition (see Refs. [14, 15] for a review), but applications in the context of vascular morphogenesis have not been developed.

1.3.4 Individual-based and hybrid models

While continuous models are appropriate for describing the spatio-temporal dynamics of systems with a large number of particles (for instance, signalling molecules or large cell populations), they are not necessarily adequate in systems consisting of a small number of interacting discrete individuals. Instead, the so-called individual-based models appear as a useful choice when one has to deal with the dynamics of small populations or one tries to link the microscopic local behaviour with the macroscopic collective one.

Cellular Automata. A relevant group of individual-based models consist in Cellular Automata (CA). The notion of CA was proposed first by J. von Neumann and S. Ulam in the 1950s and was motivated by models of self-reproduction [21, 146]. In subsequent years the concept and applications of CA have been extended in many different ways. A rather general definition of CA can be made by means of a set of elements $(\mathcal{L}, \mathcal{E}, \mathcal{N}, \mathcal{R})$ [33], where $\mathcal{L}$ is a regular grid made up of regular polygons (usually termed as nodes or cells) that are labelled by its position $r \in \mathcal{L}$. These are not to be confounded with biological cells. When $\mathcal{L}$ is finite, appropriate boundary conditions must be specified. $\mathcal{E}$ is a finite (usually small) set of states (numbers, colours or any other objects) that characterizes nodes. Thus, for each node $r \in \mathcal{L}$, and each discrete time step $k \in \mathcal{N}$, a state value $s(r,k) \in \mathcal{E}$ is assigned. $\mathcal{N}$ is a finite set of nodes (usually symmetric) that describes the interaction neighbourhood of every node $r \in \mathcal{L}$. $\mathcal{R}$ is a local transition rule that determines the dynamic of the states of each of them as a function of its interaction-neighbourhood configuration in the previous m time steps (normally $m = 1$). $\mathcal{R}$ is generally spatially homogeneous, i.e., it does not depend explicitly on the cell position r. The CA is called synchronous if the local rule is time-independent and asynchronous if it is not. When the local rule is deterministic, we say that the CA is a deterministic one. In probabilistic CA the local transition rule specifies a probability distribution of subsequent states for each possible neighbourhood configuration.

A relevant type of CA is the Lattice-Gas Cellular Automata (LGCA). In LGCA, c channels are introduced at each node of the lattice, one for each node neighbour (called velocity channels) and a variable number of rest channels. A node configuration is prescribed by assigning the value 1 or 0 to each channel in the node; see Figure 1.10. In many applications, label 1 corresponds to a particle (or maybe a biological cell) being located at that node, which will change as specified by the LGCA rule. This rule is subdivided in two sequential stages: a first local interaction one, where particles can change channels and/or be created or

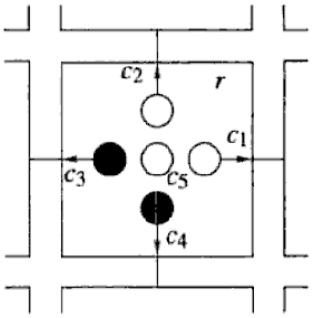

Figure 1.10: **Node configuration in a LGCA**. 4 velocity channels of node r in a two-dimensional square lattice with one rest channel. Filled dots denote the presence of a particle in the respective channel. Reprinted from [33] with permission from Prof. A. Deutsch.

destroyed, and a second propagation step, where particles are moved simultaneously to nodes in the direction assigned by their channels. The dynamics of these CA arises from iterations of combined interaction and propagation steps simultaneously applied at all lattice nodes at each discrete time step. The definitions of these steps have to satisfy the exclusion principle: there can be no more than one particle at each channel in each node. LGCA models are a fruitful approach for studying pattern formation in interacting biological cells systems. LGCA accounting for RD signalling, growth processes, chemotaxis, adhesive interactions, contact inhibition of movement, have been simulated and analysed [33]. Extended models accounting for several such behaviours together with subcellular and supracellular scales phenomena have been performed [3, 13, 54, 107]. However, little seems to be known about applications to de novo formation of vascular networks. It is to be noticed that cell morphology, a feature that becomes important to describe the vacular patterns at the cellular scale, seems to be difficult to incorporate into LGCA. An alternative individual-based model for overcoming such drawbacks is the hybrid Cellular Potts Model (CPM) that is present below.

Cellular Potts Model. The CPM was introduced by F.Graner and J.Glazier in Refs. [46,51]. The original model was designed to simulate differential-adhesion driven cell rearrangement resulting from cell adhesion molecules, and quantitatively reproduced cell-sorting experiments that include the separation of different cell phases. This process is observed both *in vivo* and *in vitro*. In fact, differential adhesion is nowadays considered as very important in embryogenesis, especially during histogenesis and organogenesis. Moreover, its relevance has also been suggested in pathological situations (like cancer) as well as in tissue engineering [111, 134].

Nowadays, the CPM is a versatile modelling framework used in many biological processes. Concerning embryonic morphogenesis, it has been applied to gastrulation, [62, 147] somitogenesis, [48, 59] limb development, [24, 116] mosaic patterning in chick inner ear epithelium, [113] as well as to study the complete life-cycle of the myxamoeba *Dyctiostelium discoideum* [84,85,128]. It is also used in many other situations, ranging from tumour growth [67,126,143] to the design of biofilms [117]. Purely discrete CPM began as an extension of the large-Q Potts Model, itself an extension of the Ising Model of ferromagnetism [65,106,118]. This explains many of choices of terms and symbols in its mathematical formalism. See Ref. [47] for a complete review about historical origins and further refinements. The fundamental idea of the CPM is to represent most cell behaviours by means of a generalized energy or Hamiltonian, which includes interactions between cells with other cells and with the ECM. Moreover, some constraints which determine individual-cell behaviours are taken into account, as for instance, a trend towards a fixed cell volume. The standard CPM uses a lattice-based Monte-Carlo method with Metropolis dynamics and generalized Boltzmann weighting function, but variations of this scheme have also been considered [7, 93]. Here we briefly introduce the model and discuss some works dealing with its application to vascular morphogenesis [92,94–96,129,137]. In these studies, besides the cellular adhesion and volume conservation assumptions made in the pioneering paper [51], other cell properties are included.

Let us briefly describe the structure of the CPM under consideration. Each of the N cells to be tracked is represented by a connected subdomain of a lattice (normally a quadrangular or hexagonal grid), made up of all the lattice sites with same index $\sigma \in \{1, 2, ..., N\}$. The index $\sigma = 0$ is kept for the extracellular medium (for instance, Matrigel), which is treated as a generalized cell. The interfaces between two different lattice sites x and x' with different indexes $\sigma_x \neq \sigma_{x'}$ represent membrane boundaries between cells or between cells and medium. To each of these boundaries, a characteristic binding energy is assigned, $J(\tau(\sigma_x), \tau(\sigma_{x'}))$. These energies are determined by the type and number of adhesion molecules involved between two cell types $\tau(\sigma_x)$ and $\tau(\sigma_{x'})$. In the cases under examination only one cell type is considered. It is labelled with the index $\tau(\sigma) = c$ for all $\sigma \in \{1, 2, ..., N\}$ corresponding to endothelial cells, while $\tau(0) = m$ is the index assigned to the generalized cell labelled by 0, extracellular medium.

If merely adhesion and volume conservation are taken into account, the corresponding Hamiltonian is:

$$H = \sum_{\{x,x'\}_n} J(\tau(\sigma_x), \tau(\sigma_{x'}))(1 - \delta_{\sigma_x \sigma_{x'}}) + \lambda \sum_{\sigma>0} (a_\sigma - A_{\tau(\sigma)})^2, \qquad (1.6)$$

where

$$\delta_{ij} = \begin{cases} 1 & i = j \\ 0 & i \neq j \end{cases}, \tag{1.7}$$

λ denotes resistance to compression, a_σ is the area occupied by the cell σ and A_τ is the target area for cells of type τ, which is selected according to data taken from experimental cultures. The symbol $\{x, x'\}_n$ in (1.6) denotes that the sum is taken for the n-order neighbours in each lattice site, see Figure 1.11. The second sum in (1.6) goes for all the cells except the generalized one representing the medium.

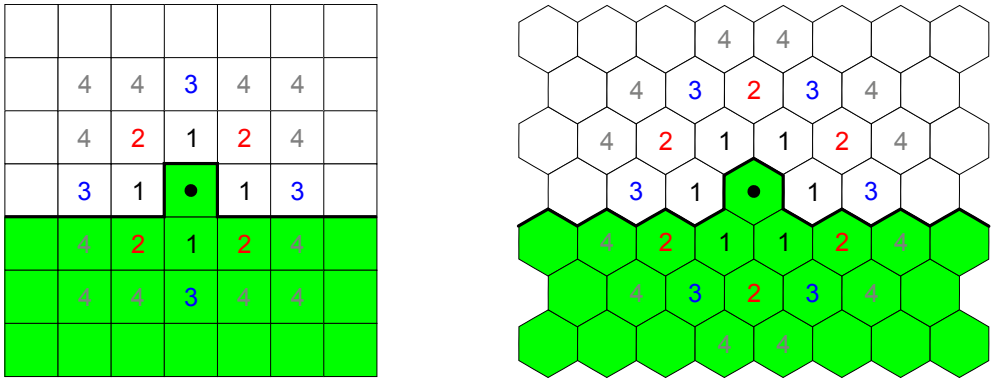

Figure 1.11: **Lattice neighborhoods**. The n-order neighbours of a lattice site (dark circle) for $n = 1, 2, 3, 4$ in regular quadrangular (left) and hexagonal (right) grids.

Chemotaxis, a major player in some of the models presented in Section 1.3.3, can be accounted for in the CPM. Specifically, the autocrine chemotaxis hypothesis described above can be modelled by coupling the CPM with a continuous RD equation for the dynamics of the chemoattractant [92]:

$$\frac{\partial c}{\partial t} = D\Delta c + \theta(1 - \delta_{\sigma_x 0}) - \epsilon c \delta_{\sigma_x 0}, \tag{1.8}$$

where θ accounts for the production rate of the chemoattracttant (whose diffusion coefficient is given by D) by the cells, and ϵ is a decay parameter related with the half-life of this substance. Equation (1.8) is numerically solved in the same mesh where the cells are represented. The inclusion of the function $\delta_{\sigma_x 0}$ (see (1.7)), allows the production of the chemical to be confined just to the sites occupied by cells, while chemical degradation takes place at sites occupied by the medium. A generalized Metropolis-Bolzmann algorithm that mimics cytoskeletally-driven membrane fluctuations is used for the simulation [47, 93]. The steps in that algorithm are: (i) For a given system configuration S_0, a lattice site x is randomly chosen; (ii) A neighbour site x' of order n is randomly selected. The effects of lattice anisotropy inherent in a discrete lattice can be avoided by choosing a

larger order of neighbours instead of a smaller one [63]; (iii) We call S_1 the configuration where x's index, σ_x, has been copied to x', we evaluate H in S_0 and S_1 and we define $\Delta H = H(S_1) - H(S_0)$; (iv) $\Delta H' = \Delta H - \mu(c(x',t) - c(x,t))$ is then evaluated, where μ accounts for the chemotactic response intensity, $c(x',t)$ (respectively $c(x,t)$) is the chemical concentration at x' (respectively at x) in time t; (v) The acceptance probability (of changing S_1 by S_0) is:

$$P(\Delta H') = \begin{cases} 1 & \text{if } \Delta H' \leq 0, \\ \exp\left(\frac{-\Delta H'}{T}\right) & \text{if } \Delta H' > 0, \end{cases} \tag{1.9}$$

where T is related with the intrinsic motility of cells. When the previous process has been done as many times as the total number of lattice sites, we say that a Monte-Carlo Step (MCS) has been performed. One thus has to select a relation between the time-scale for solving the PDEs involved and the MCS. Thus computational cells decisions, besides of being influenced by adhesion mechanisms or volume constraint, are also affected by chemical concentrations in such a way that they prefer to extend their membranes towards areas of high chemoattractant concentration. Furthermore, when neutral binding energies are used, the previous model displays velocities of simulated cells proportional to the strength of the gradient of the chemoattractant [94]. This is in contrast with the continuous chemotaxis model presented before, where cells accelerate due to chemical gradients. When the adhesion mechanisms are ruled out in the previous framework, but chemotaxis and volume conservation are maintained, a pattern of isolated patches of cells is obtained [95]: see Figure 1.12. Such pattern recalls the ones that the classic Keller-Segel model displays for chemotactic aggregation [57, 71]. As a matter of fact, the continuous chemotaxis model reduces to Keller-Segel model if a liner force-velocity response is applied (i.e. $F = mv$) [5].

Figure 1.12: **CPM - chemotaxis**. Chemotactic aggregation, without cell adhesion leads to the formation of isolated islands. As stated in ref. [95], in this simulation rounded cells are assumed but the results hold for unconstrained cells. Reprinted with permission from Ref. [95].

Then, besides chemotaxis, aditional mechanisms are needed for obtaining reticulated structures within the CPM framework. Interestingly, adding a number

of features including cell adhesion [92], steep gradients of chemoattractant [95], active cellular elongation [94], contact-inhibition of motility [96], is enough to produce reticular networks. For instance, when the first term in (1.6) is taken into account and strong adhesion for the cells (very small $J(c,c)$) is assumed, reticular networks can be obtained [92]. In this model cells experience passive elongation as a result of such strong adhesion. However the spatio-temporal dynamics of the simulation are noticed to be very slow compared with available experiments [96]; see Figure 1.13.

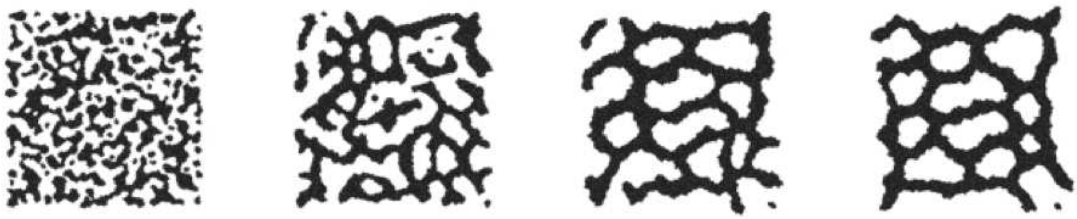

Figure 1.13: **CPM - adhesion**. Strong cellular adhesion causes the cells, whose shape is not constrained, to elongate and organize into reticulated networks. Reprinted with permission from Ref. [95].

On the other hand, neglecting cellular adhesion and assuming slow diffusion of the chemoattractant (which results in steepest gradients around cells) elongated cell shapes are obtained. As a result, reticulated structures are formed, see Figure 1.14. It has been noticed that the last two mechanisms depend on the cells having an elongated shape. If either mechanism is used but cells are imposed to have a rounded shape, patches (similar to those in Figure 1.12) instead of networks are obtained [95]. Extended, spindle shape of angioblasts and endothelial cells is observed both *in vivo* and *in vitro*. Nevertheless, it is not clear whether this is a consequence of other mechanisms (as suggested by previous remarks) or if instead this is an inherent property of cells.

Figure 1.14: **CPM - gradients**. Steep gradients also cause cells to elongate and organize into reticulated networks. Reprinted with permission from Ref. [95].

It is known that cells change from rounded to elongated and bipolar shape in response to growth factors, and by active remodelling of their cytoskeleton [38,98].

This behaviour can be added to the CPM by means of an extra term in the Hamiltonian, which penalizes configurations where the cells have different lengths than that of a target one. Specifically:

$$H_L = H + \nu \sum_{\sigma>0} (l_\sigma - L_{\tau(\sigma)})^2,$$

where ν denotes the intensity of the elongation constraint, l_σ is the actual length of cell σ, and L_τ is the target length, which is selected from experimental observations. In ref. [94], the authors claim that cell elongation, together with autocrine secretion of a chemoattractant, suffices to form vascular-like morphologies and is key to quantitatively reproduce some aspects of later remodelling observed *in vitro* experiments; see Figure 1.15. They also pointed out that the persistence needed in the continuous chemotaxis model takes actually place in the CPM simulations as a consequence of cell elongation and chemotaxis, without any additional assumption.

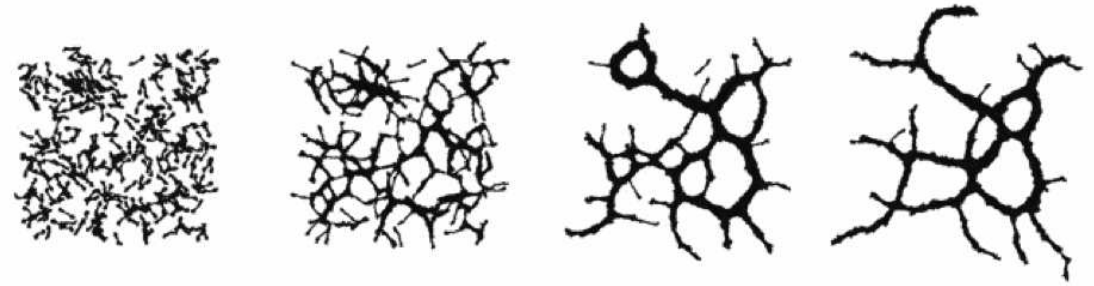

Figure 1.15: **CPM - elongation**. Autonomously elongating virtual cells organize into a vascular network with coarsening dynamics corresponding to in vitro observations. Reprinted with permission from Ref. [95].

Adding complication to the vascular patterning picture described so far, a further mechanism has been proposed in Ref. [96] which allows for network formation starting from dispersed or clustered cells and independently of cell shape. In this work it is supposed that binding of VE-cadherin, a prototypical endothelial cell adhesion molecule, acts locally to preclude the chemotactic response on cell-cell interfaces for chemoattractans, while cell surfaces in contact with the ECM keep the chemotactic activity unchanged. This contact-inhibition of motility is implemented in the CPM by using different values of the chemotactic response parameter, μ, for cell-cell interfaces ($\mu = \chi(c, c)$) and cell-ECM interfaces ($\mu = \chi(c, m)$). Some simulations of dispersed cells forming reticulated networks have been shown [95, 96]; see Figure 1.16. The aforementioned works present a study of contact-inhibited chemotaxis in sprouting clusters. Despite that some of the simulations mimic certain features of a knock-out VE-cadherin experiment

with mouse explants, many questions concerning the underlying molecular mechanisms remain unanswered.

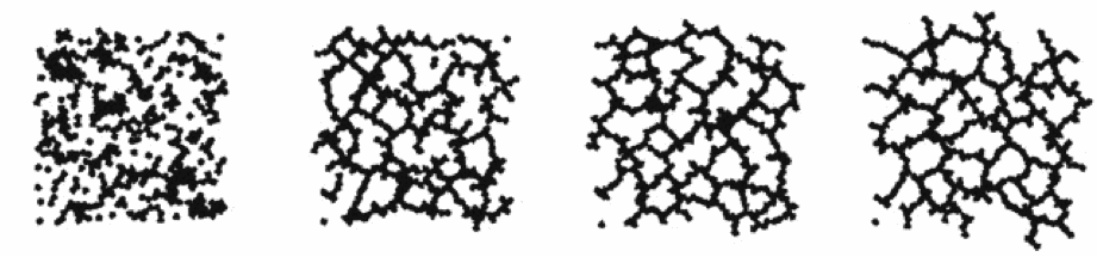

Figure 1.16: **CPM - contact-inhibition**. Conctact-inhibition of motility drives a cell-shape independent mechanism of vasculogenesis. Reprinted with permission from Ref. [95].

A few more CPM mechanisms have been recently proposed to study vascular development. For, instance, [137] focuses on the sprouting of cellular aggregates. In this and previous works by the authors it is suggested that the sprouting behaviour observed in several cell lines forming polygonal-like networks, might be a consequence of the preferential attraction of cells towards nearby elongated cells [29,112,136]. This feature was first included in a mathematical model representing cells as interacting point particles [136] by means of a stochastic Langevin equation. Cell shape is not explicitly taken into account. Thus, a cell infers elongation or local anisotropy from the configuration of the particles around it. On the other hand, in Ref. [137] an extended CPM is proposed which explicitly includes cell shapes. A standard Hamiltonian (1.6) accounting for cellular adhesion and volume conservation is considered. However, the probability acceptance function (1.9) is modified by a correction term that contains an asymmetric interaction bias. Specifically:

$$P(\Delta H') = \begin{cases} 1 & \text{if } \Delta H' \leq 0, \\ \exp\left(\frac{-\Delta H'}{T}\right) & \text{if } \Delta H' > 0, \end{cases} \tag{1.10}$$

where

$$\Delta H' = \Delta H - \gamma(\delta_{\tau(\sigma_x)c} - \delta_{\tau(\sigma_{x'})c}) \sum_{\varepsilon:\sigma_\varepsilon \notin \{0,\sigma_x,\sigma_{x'}\}} \theta_{\sigma_\varepsilon}. \tag{1.11}$$

The parameter γ in (1.11) represents the strength of the bias. The expresion $(\delta_{\tau(\sigma_x)c} - \delta_{\tau(\sigma_{x'})c})$ ensures that only cells (and not the medium) are affected, and that the amount of attraction depends only on the contact target. The symbol θ_i represents a messure of anisotropy for the cell i, obtained from the inertia tensor

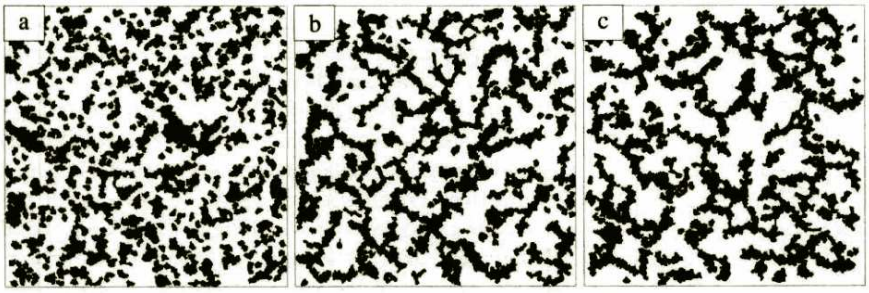

Figure 1.17: **CPM - biased motion**. The CPM model (1.6) (1.10) (1.11), when starting from dispersed cells reaches a quasi-stationary state where surface tension-driven coarsening is balanced by the formation of new sprouts. Configurations in the model are shown after 100 (a), 1000 (b) and 30000 (c) MCS. Reprinted with permission from Ref. [137].

of the domain occupied by the cell, and given by:

$$\theta_i = (\mu_i/\nu_i)^{1/2} - 1,$$

where $\mu_i \geq \nu_i$ are the two eigenvalues of the inertia tensor. The summation in (1.11) goes only over those neighbor sites of β that belong to cells other than σ_α and σ_β. Such bias preferentially guides cells towards their elongated neighbours, which eventually cause sprout and network pattern formation without any chemotactic assumption; see Figure 1.17. Cellular and molecular basis of such a possible cell preference in angioblasts remains unknown.

Finally, a very recent work proposes to model *in vitro* cultures of Tumour Endothelial Cells (TECs) in Matrigel by means of a multiscale hybrid approach [129]. This study uses a CPM formalism to represent TECs and a continuous PDE to describe the extracellular concentration of VEGF, similarly as described before. Moreover, it accounts for VEGF-induced calcium-dependent intracellular signals that are described by means of a PDE system for every cell. This allows for a more close relation of CPM parameters, including those related with cell shape, migration or chemical release, to the subcellular mechanisms. Specifically, the authors analyze the link between the subcellular dynamics and the macroscopic cell behavious by exploring the efficiency of some pharmacological interventions. The model is said to able to reproduce some features of network formation as well as the effect caused on this process by some anti-angiogenic therapies currently in used. As the continuos chemotaxis model, the main driving forces for cellular aggregation and network patterning in this case are autocrine chemotaxis and inertial motion. The former is accounted for in the CPM module as a new term in the Hamiltonian that penalizes desviations in cell velocity from past movements. [129].

1.4 Discussion

In this chapter, some key aspects of vascular development have been presented with a special emphasis on vasculogenesis, a process that constitutes the intial step in the formation of the vascular system. Out of the many features to be considered, this dissertation addresses the problem of the self-organization and patterning of vascular precursors into primitive blood vessel networks. The focus here is laid down on the mechanisms underlying patterning of angioblasts instead of on those related with the recruitment and differentiation of mesodermal cells to the endothelial lineage. In particular, the role of VEGF in providing local cues for angioblasts migration is study in detail. Progress in this direction is expected to have applications in biomedicine and tissue engineering. As a matter of fact, understanding how spatio-temporal aspects of vessel formation are regulated at the molecular at cellular level is critical to the ability to reconstitute vessels in patients or artificial tissues.

In Section 1.3 above, a number of representative mathematical models and theories proposed to explain some aspects of vascular patterning have been discussed. Those theories cannot be directly extrapolated to the *in vivo* situation under consideration, where different features have to be considered. For instance, accounting for the effect of VEGF on embryonic angioblasts requieres to consider VEGF essentially as a paracrine signal, in contrast to the autocrine one assumed in previous *in vitro* models. Moreover, the fact that VEGF is uniformly produced and distributed around angioblasts calls for a new theory to explain early embryonic vacular patterning based on VEGF signalling. On the other hand, some of the presented modelling formalisms are suitable to describe the cells and signals under consideration. While the dynamic of chemical signals can be adequately described by means of continuous PDE models, specially those accounting for diffusion mass transfer and chemical reactions, vascular cells are better described by means of discrete approaches. The cellular scale is certainly important to describe the network patterns generated during vasculogenesis. Two characteristic features of those structures are that they are composed of a small number of cells and that vascular chords are often formed by highly elongated cells (see Figure 1.3 B). Both features can be accurately described by means of the CPM framework. As shown above, this formalism can also be couple in a convenient way with continuous equations to describe specific interactions between cells and chemicals. In this way, the resulting hybrid models account for objects and process with different spatial and temporal scales.

1.5 References

[1] K. Abdi, L. Kobzik, X. Li and S. J. Mentzer, Expression of membrane glycoconjugates on sheep lung endothelium, Lab. Invest. **72** (1995) 445-452.

[2] M. Affolter, S. Bellusci, N. Itoh, B. Shilo, J. P. Thiery and Z. Werb, Tube or not tube: remodeling epithelial tissues by branching morphogenesis, Dev. Cell **4** (2003) 11-18.

[3] T. Alarcón, H. M. Byrne, P. K. Maini, A multiple scale model for tumor growth, Multiscale Model. Simul. **3**(2) (2005) 440-474.

[4] R. Alon, P. D. Kassner, M. W. Carr, E. B. Finger, M. E. Hemler and T. A. Springer, The integrin VLA-4 supports tethering and rolling in flow on VCAM-1, J. Cell Biol. **128** (1995) 1243-1253.

[5] D. Ambrosi, A. Gamba and G. Serini, Cell directionality and chemotaxis in vascular morphogenesis, Bull. Math. Biol. **66**(6) (2004) 1851-1873.

[6] D. Ambrosi, F. Bussolino and L. Preziosi, A review of vasculogenesis models, J. Theor. Med. **6** (2005) 1-19.

[7] A. R. A. Anderson, M. A. J. Chaplain and K. A. Rejniak (eds.), Single-Cell-Based Models in Biology and Medicine (Birkhuser, 2007).

[8] A. Anderson-Berry, E. A. O'Brien, S. B. Bleyl, A. Lawson, N. Gundersen, D. Ryssman, J. Sweeley, M. J. Dahl, C. J. Drake, G. C. Schoenwolf and K. H. Albertine, Vasculogenesis drives pulmonary vascular growth in the developing chick embryo, Dev. Dyn. **233** (2005) 145-153.

[9] D. Andreucci, M. A. Herrero and J. J. L. Velázquez, On the growth of filamentary structures in planar media, Math. Meth. Appl. Sci. **27** (2004) 1935-1968.

[10] Aristotle, Parts of animals, A. L Peck translator (Harvard University Press, 1961).

[11] Aristotle, The generation of animals, Book II (Loeb Classical Library, 1963).

[12] Y. Azar and H. Eyal-Giladi, Marginal zone cells - the primitive streak-inducing component of the primary hypoblast in the chick, J. Embryol. Exp. Morphol. **52** (1979) 79-88.

[13] D. Basanta, D. W. Strand, R. B. Lukner, O. E. Franco, D. E. Cliffel, G. E. Ayala, S. W. Hayward and A. R. Anderson, The role of transforming growth factor-beta-mediated tumor-stroma interactions in prostate cancer progression: an integrative approach. Cancer Res. **69** (2009) 7111-7120.

[14] N. Bellomo and B. Carbonaro, Toward a mathematical theory of living systems focusing on developmental biology and evolution: a review and perspectives. Phys. Life Rev. **8** (2011) 1-18.

[15] A. Bellouquid and M. Delitala, Mathematical Modelling of Complex Biological Systems, A Kinetic Theory approach (Birkhäuser, 2006).

[16] M. Boudreau and N. J. Bissell, Extracellular matrix signaling: integration of form and function in normal and malignant cells, Curr. Opin. Cell. Biol. **10** (1998) 640- 646.

[17] D. Bouïs, G. A. P. Hospers, C. Meijer, G. Molema and N. H. Mulder, Endothelium in vitro: A review of human vascular endothelial cell lines for blood-vessel-related research, Angiogenesis **4** (2001) 91-102.

[18] B. Brand-Saberi, R. Seifert, M. Grim, J. Wilting, M. Kuhlewein and B. Christ, Blood vessel formation in the avian limb bud involves angioblastic and angiotrophic growth, Dev. Dyn. **202** (1995) 181-194.

[19] G. Breier, U. Albrecht, S. Sterrer and W. Risau, Expression of vascular endothelial growth factor during embryonic angiogenesis and endothelial cell differentiation, Development **114** (1992) 521-532.

[20] R. Brusca and G. Brusca, Invertebrates (Sinauer Associates, Sunderland, MA, 2003).

[21] A. W. Burks (ed.), Essays on cellular automata. (Urbana IL: University of Illinois Press, 1970).

[22] J. P. Califano and C. A. Reinhardt-King, A balance of substrate mechanics and matrix chemistry regulates endothelial cell network assembly, Cell. Mol. Bioeng. **1(2-3)** (2008) 122-132.

[23] J. C. Chappell, S. M. Taylor, N. Ferrara and V. L. Bautch, Local guidance of emergin vessel sprouts requires soluble Flt-1, Dev Cell. **17** (2009) 377-386.

[24] R. Chaturvedi, C. Huang, J. A. Izaguirre, S. A. Newman, J. A. Glazier and M. Alber, A hybrid discrete-continuum model for 3-D skeletogenesis of the vertebrate limb, Sloot P.M.A., Chopard B. and Hoekstra (eds.) ACRI 2004, LNCS **3305** (2004) 543-552.

[25] T. Chihara and S. Hayashi, Control of tracheal tubulogenesis by Wingless signalling, Development **127** (2000) 4433-4442.

[26] J. D. Coffin and T. J. Poole, Endothelial cell origin and migration in embryonic heart and cranial blood vessel development, Anat. Rec. **231** (1991) 383-395.

[27] J. F. Colas and G. C. Schoenwolf, Towards a cellular and molecular understanding of neurulation, Dev. Dyn. **221** (2001) 117-145.

[28] F. Crick, Diffusion in embryogenesis, Nature **225** (1970) 420-422.

[29] A. Czirók, P. A. Rupp, B. J. Rongish and C. D. Little, Multi-field 3D scanning light microscopy of early embryogenesis, J. Microsc. **206**(3) (2002) 209-217.

[30] A. Czirók, E. A. Zamir, M. B. Filla, C. D.Little and B. J. Rongish, Extracellular matrix macroassembly dynamics in early vertebrate embryos, Curr. Top. Dev. Biol. **73** (2006) 237-58.

[31] A. Czirók, E. A. Zamir, A. Szabo and C. D. Little, Multicellular sprouting during vasculogenesis, Curr. Top. Dev. Biol. **81** (2008) 269-289.

[32] P. J. Del Vecchio, A. Siflinger-Birnboim, P. N. Belloni, L. A. Holleran, H. Lum and A. B. Malik, Culture and characterization of pulmonary microvascular endothelial cells, In Vitro Cell. Dev. Biol. **28**A (1992) 711-715.

[33] A. Deutsch and S. Dormann, Cellular Automaton Modeling of Biological Pattern Formation, Modeling and Simulatioin in Science Engineering and Technology (Birkhuser, Boston, 2005).

[34] D. Donovan, N. J. Brown, E. T. Bishop and C. E. Lewis, Comparison of three in vitro human "angiogenesis" assays with capillaries formed in vivo, Angiogenesis **4** (2001) 113-121.

[35] C. J. Drake and C. D. Little, Exogenous vascular endothelial growth factor induces malformed and hyperfused vessels during embryonic neovascularization, Proc. Natl. Acad. Sci. USA **92** (1995) 7657-7661.

[36] C. J. Drake, S. J. Brandt, T. C. Trusk C. D. Little, C.D, TAL1/SCL is expressed in endothelial progenitor cells/angioblasts and defines a dorsal-to-ventral gradient of vasculogenesis, Dev. Biol. **192** (1997) 17-30.

[37] C. J. Drake and C D. Little, VEGF and vascular fusion: implications for normal and pathological vessels, J. Histochem. Cytochem. **47** (1999) 1351-1356.

[38] C. J. Drake, A. LaRue, N. Ferrara and C. D. Little, VEGF regulates cell behavior during vasculogenesis, Dev. Biol. **224** (2000) 178-188.

[39] R. Eckert and D. Randall, Animal physiology: mechanisms and adaptations (W.H. Freeman & Co., New York, 1988).

[40] H.M. Eilken and R.H. Adams, Dynamics of endothelial cell behavior in sprouting angiogenesis, Curr. Opin. Cell Biol. **22** (2010) 617-625.

[41] R. A. Fisher, The wave of advance of advantageous genes, Ann. Eugenics **7** (1937) 353-369.

[42] J. Folkman and M. Klagsbrun, Angiogenic factors, Science **235** (1987) 442-447.

[43] A. Gamba, D. Ambrosi, A. Coniglio, A. de Candia, S. Di Talia, E. Giraudo, G. Serini, L. Preziosi and F. Bussolino, Percolation, morphogenesis and Burgers dynamics in blood vessels formation, Phys. Rev. Lett. **90**, 11810 (2003) 1-4.

[44] H. Gerhardt, M. Golding, M. Fruttiger, C. Ruhrberg, A. Lundkvist, A. Abramsson, M. Jeltsch, C. Mitchell, K. Alitalo, D. Shima and C. Betsholtz, VEGF guides angiogenic sprouting utilizing endothelial tip cell filopodia, J. Cell Biol. **161**(6) (2003) 1163-1177.

[45] A. Gierer and H. Meinhardt, A theory of biological pattern formation, Kybernetik **12** (1972) 30-39.

[46] J. A. Glazier and F. Graner, Simulation of the differential adhesion driven rearrangement of biological cells, Phys. Rev. E **47** (1993) 2128-2154.

[47] J. A. Glazier, A. Balter and N. J. Poplawski, Magnetization to Morphogenesis: A Brief History of the Glazier-Graner-Hogeweg Model, In Single-Cell-Based Models in Biology and Medicine, A. R. A. Anderson, M. A. J. Chaplain and K. A. Rejniak (eds.) (Birkhuser, 2007) 79-106.

[48] J. A. Glazier, Y. Zhang, M. Swat, B. Zaitlen and S. Schnell, Coordinated Action of N-CAM, N-cadherin, EphA4 and ephrinB2 Translates Genetic Prepatterns into Structure during Somitogenesis in Chick, Curr. Top. Dev. Biol. **81** (2008) 2005-247.

[49] F. González-Crussi, Vasculogenesis in the chick embryo. An ultrastructural study, Am. J. Anat. **130** (1971) 441-460.

[50] M. J. Goumans, F. Lebrin and G. Valdimarsdottir, Controlling the angiogenic switch: a balance between two distinct TGF-b receptor signaling pathways, Trends Cardiovasc Med. **13** (2003) 301-307.

[51] F. Graner and J. A. Glazier, Simulation of biological cell sorting using a two-dimensional extended Potts model, Phys Rev Lett. **69** (1992) 2013-2016.

[52] G. Grimmett, Percolation (Springer-Verlag, New York, 1999).

[53] J. A. Guadix, R. Carmona, R. Muñoz-Chapuli and J. M. Pérez-Pomares, In vivo and in vitro analysis of the vasculogenic potential of avian proepicardial and epicardial cells, Dev. Dyn. **235** (2006) 1014-1026.

[54] H. Hatzikirou, G. Breier and A. Deutsch, Cellular automaton models for tumor invasion. Encyclopedia of Complexity and Systems Science. Springer 2009.

[55] M. A. Herrero and J. J. L. Velázquez, Chemotactic collapse for the Keller-Segel model, J. Math. Biol. **35** (1996) 177-196.

[56] M. A. Herrero, Reaction-Diffusion Systems: a Mathematical Biology approach. In the volume Cancer Modelling and Simulation, L. Preziosi (Ed.) (Chapman and Hall, 2003) 367-420.

[57] M. A. Herrero, The Mathematics of Chemotaxis. Handbook of Differential Equations, Elsevier, vol. **3** (2007) 137-191.

[58] A. T. Hertig, Angiogenesis in the early human chorion and in the primary placenta of the macaque monkey, Contrib. Embryol. Carnegie Inst. **25** (1935) 37-81.

[59] S. D. Hester, J. M. Belmonte, J. S. Gens, S. G. Clendenon, J. A. Glazier, A Multi-cell, Multi-scale Model of Vertebrate Segmentation and Somite Formation, PLoS Comput Biol **7** (2011) e1002155. doi:10.1371/journal.pcbi.1002155.

[60] A. L. Hodgkin and A. F. Huxley, A qualitative description of membrane current and its application to conduction and excitation in nerves, J. Physiol. (London) **117** (1952) 500-544.

[61] B. L. Hogan and P. A. Kolodziej, Organogenesis: molecular mechanisms of tubulogenesis, Nat. Rev. Genet. **3** (2002) 513-523.

[62] P. Hogeweg, Evolving mechanisms of morphogenesis: on the interplay between differential adhesion and cell differentiation, J. Theor. Biol. **203** (2000) 317-333.

[63] E. A. Holm, J. A. Glazier, D. J. Srolovitz and G. S. Grest: Effects of Lattice Anisotropy and Temperature on Domain Growth in the Two-Dimensional Potts Model, Physical Review A **43**(6) (1991) 2662-2668.

[64] J. E. Hungerford and C. D. Little, Developmental biology of the vascular smooth muscle cell: building a multilayered vessel wall, J. Vasc. Res. **36** (1999) 2-27.

[65] E. Ising, Beitrag zur Theorie des Ferromagnetismus. Zeitschrift fr Physik, **31** (1925) 253-358.

[66] C. J. Jackson and M. Nguyen, Human microvascular endothelial cells differ from macrovascular endothelial cells in their expression of matrix metalloproteinases, Int. J. Biochem. Cell Biol. **29** (1997) 1167-1177.

[67] Y. Jiang, J. Pjesivac-Grbovic, I. C. Cantrel and J. P. Freyer, A Multiscale Model for Avascular Tumor Growth, Biophys. J. **89** (2005) 3884-3894.

[68] A. R. Kallianpur, J. E. Jordan, and S. J. Brandt, The SCL/TAL-1 gene is expressed in progenitors of both the hemopoietic and vascular systems during embryogenesis, Blood **83** (1994) 1200-1208.

[69] J. Kattan, R. W. Dettman and J. Bristow, Formation and remodeling of the coronary vascular bed in the embryonic avian heart, Dev. Dyn. **230** (2004) 34-43.

[70] P. J. Keck, S. D. Hauser, G. Krivi, K. Sanzo, T. Warren, J. Feder and D. T. Connolly, Vascular permeability factor, an endothelial cell mitogen related to PDGF, Science **246** (1989) 1309-1312.

[71] E. F. Keller and L. A. Segel, Initiation of slime mold aggregation viewed as an instability, J. Theor. Biol. **26** (1970) 399-415.

[72] J. King, T. Hamil, J. Creighton, S. Wu, P. Bhat, F. McDonald and T. Stevens, Structural and functional characteristics of lung macro- and microvascular endothelial cell phenotypes, Microvasc. Res. **67** (2004) 139-151.

[73] A. J. Koch and H. Meinhardt, Biological pattern-formation - from basis mechanisms to complex structures, Rev. Modern Physics **66** (1994) 1481-1507.

[74] A. A. Kolmogorov, I. G. Petrovsky and N. N. Piskunov, Study of the diffusion equation with growth of the quantity of matter and its application to a biology problem. Bul. Moskovskovo Gos, Univ. **17** 1-26 (in Russian). English Translation in The Dynamics of curved fronts, P. Pelc (ed.) (1988).

[75] R. Kowalczyk, A. Gamba and L. Preziosi, On the stability of homogeneous solutions to some aggregation models, Discr. Cont. Dynam. Sys. Series B **4** (2004) 203-220.

[76] R. Kowalczyk, Preventig Blow-up in a Chemotaxis Model, J. Math. Anal. Appl. **305** (2005) 566-588.

[77] V. Lanza, D. Ambrosi and L. Preziosi, Exogenous control of vascular network formation in vitro: A mathematical model, Netw. Heterog. Media **1** (2006) 621-637.

[78] L. Lai, B. L. Bohnsack, K. Niederreither and K. K. Hirschi, Retinoic acid regulates endothelial cell proliferation during vasculogenesis, Development **130** (2003) 6465-6474.

[79] B. Larrivée and A. Karsan, Signaling pathways induced by vascular endothelial growth factor (review), Int. J. Mol. Med. **5**(5) (2000) 447-456.

[80] J. C. Magee, A. E. Stone, K. T. Oldham and K. S. Guice, Isolation, culture, and characterization of rat lung microvascular endothelial cells, Am. J. Physiol. **267** (1994) L433-L441.

[81] J. N. Maina, Comparative respiratory morphology: themes and principles in the design and construction of the gas exchangers, Anat Rec. **261** (2000) 25-44.

[82] D. Manoussaki, S. R. Lubkin, R. B. Vernon and J. D. Murray, A mechanical model for the formation of vascular networks in vitro, Acta Biotheor. **44** (1996) 271-282.

[83] D. Manoussaki, A mechanochemical model of vasculogenesis and angiogenesis, ESAIM, Math. Model. Num. Anal. **37**(4) (2003) 581-599.

[84] A. F. M. Marée and P. Hogeweg, How amoeboids self-organize into a fruiting body: Multicellular coordination in *Dictyostelium discoideum*, Proc. Natl. Acad. Sci. USA **98** (2001) 3879-3883.

[85] A. F. M. Marée and P. Hogeweg, Modelling *Dictyostelium discoideum* morphogenesis: the culmination, Bull Math Biol. **64** (2002) 327-353.

[86] D. A. McDonald, Blood flow in arteries (Williams and Wilkins, Baltimore, 1960).

[87] H. Meinhardt, Morphogenesis of lines and nets. Differentiation, **6** (1976) 117-123.

[88] H. Meinhardt, Models of biological pattern formation (Academic Press, London, 1982).

[89] H. Meinhardt, Biological Pattern Formation as a complex dynamic phenomenon, Int. J. Bif. Chaos **7** (1997) 1-26.

[90] H. Meinhardt, Models for the formation of netlike structure. In Vascular Morphogenesis: In Vivo, In Vitro, In Mente, Little C.D., Mironov V. and Sage E.H. (eds.), (Birkhuser, 1998) 147-172.

[91] H. Meinhardt, Modeling pattern formation in hydra: a route to understanding essential steps in development, Int. J. Dev. Biol. in press (2012) doi: 10.1387/ijdb.113483hm.

[92] R. M. H. Merks, S. A. Newman and J. A. Glazier, Cell-oriented modelling of in vitro capillary development. In: Soot P.M.A., Chopard B., Hoekstra A.G. (eds.). Cellular Automata: 6th International Conference on Cellular Automata for Research and Industry. Springer Verlag, Lect. Notes Comput. Sci. **3305**, (2004) 425-434.

[93] R. M. H. Merks and J. A. Glazier, A Cell-centered Approach to Developmental Biology, Physica A **352** (2005) 113-130.

[94] R. M. H. Merks, S. V. Brodsky, M. S. Goligorsky, S. A. Newman and J. A. Glazier, Cell elongation is key to in silico replication of in vitro vasculogenesis and subsequent remodelling, Dev Biol. **289**(1) (2006) 44-54.

[95] R. M. H. Merks and J. A. Glazier, Dynamic mechanisms of blood vessel growth, Nonlinearity **19** (2006) C1-C10.

[96] R. M. H. Merks, E. D. Perryn, A. Shirinifard and J. A. Glazier J.A., Contact-inhibited chemotactic motility in de novo and sprouting blood vessel growth, PLoS Comput. Biol. **4**(9) (2008) e1000163.

[97] B. Millauer, S. Wizigmann-Voos, H. Schnurch, R. Martinez, N. P. Moller, W. Risau and A. Ullrich, High affinity VEGF binding and developmental expression suggest Flk-1 as a major regulator of vasculogenesis and angiogenesis, Cell **72** (1993) 835-846.

[98] T. M. Moore, G. H. Brough, P. Babal, J. J. Kelly, M. Li and T. Stevens, Store-operated calcium entry promotes shape change in pulmonary endothelial cells expressing Trp1, Am. J. Physiol.: Lung Cell Mol. Physiol. **275** (1998) L574-L582.

[99] J. D. Murray and G. F. Oster, Cell traction models for generation of pattern and form in morphogenesis, J. Math. Biol **19** (1984) 265-279.

[100] J. D. Murray and G. F. Oster, Generation of biological pattern and form, IMA J. Math Appl. Med. Biol. **1** (1984) 51-75.

[101] J. D. Murray, Mathematical Biology. Vols. I and II (Springer, 2000).

[102] P. Namy, J. Ohayon and P. Traqui, Critical conditions for pattern formation and in vitro tubulogenesis driven by cellular traction fields, J. Theor. Biol. **227** (2004) 103-120.

[103] D. M. Noden, Origins and assembly of avian embryonic blood vessels, Ann. N. Y. Acad. Sci. **588** (1990) 236-249.

[104] D. M. Noden, Development of craniofacial blood vessels. In: Feinberg, R.N., Sherer, G. K., Auerbach, R. (eds.) The development of the vascular system (Karger, Basel, 1991) 1-24.

[105] S. V. Nolte, H. O. Rennekampff and H. P. Rodemann, Diversity of fibroblasts - a review on implications for skin tissue engineering, Cells Tissues Organs **187** (2008) 165-176.

[106] L. Onsager, Crystal Statistics I. A Two-Dimensional Model with an Order-Disorder Transition, Phys. Rev. **65** (1944) 117-149.

[107] M. R. Owen, T. Alarcón, P. K. Maini and H. M. Byrne, Angiogenesis and vascular remodelling in normal and cancerous tissues, J. Math. Biol. To appear. DOI: 10.1007/s00285-008-0213-z.

[108] K. J. Painter and T. Hillen, Volume-filling and quorum-sensing in models for chemosensitive movement, Canadian Appl. Maths. Quart. **10**(4) (2002) 501-543.

[109] J. M. Pérez-Pomares, R. Carmona, M. González-Iriarte, G. Atencia, A. Wessels and R. Muñoz-Chápuli, Origin of coronary endothelial cells from epicardial mesothelium in avian embryos, Int. J. Dev. Biol. **46** (2002) 1005-1013.

[110] J. M. Pérez-Pomares and R. Muñoz-Chápuli, Epithelial-mesenchymal transitions: a mesodermal cell strategy for evolutive innovation in Metazoans, Anat. Rec. **268** (2002) 343-351.

[111] J. M. Pérez-Pomares and R. A. Foty, Tissue fusion and cell sorting in embryonic development and disease: biomedical implications, Bioessays **28** (2006) 809-821.

[112] E. D. Perryn, A. Czirók and C. D. Little, Vascular sprout formation entails tissue deformations and VE-cadherin-dependent cell-autonomous motility, Dev. Biol. **313** (2008) 545-555.

[113] G. J. Podgorski, M. Bansal and N. S. Flann, Regular mosaic pattern development: A study of the interplay between lateral inhibition, apoptosis and differential adhesion, Theor. Biol. Med. Modl. **4**(43) (2007) 1-19.

[114] T. J. Poole and J. D.Coffin, Vasculogenesis and angiogenesis: two distinct morphogenetic mechanisms establish embryonic vascular pattern, J. Exp. Zool. **251** (1989) 224-231.

[115] T. J. Poole, E. B. Finkelstein and C. M. Cox, The role of FGF and VEGF in angioblast induction and migration during vascular development, Dev. Dyn. **220** (2001) 1-17.

[116] N. J. Poplawski, M. Swat, J. S. Gens and J. A. Glazier, Adhesion between cells, diffusion of growth factors and elasticity of the AER produce the paddle shape of the chick limb, Phys. Stat. Mech. Appl. **373**C (2007) 521-532.

[117] N. J. Poplawski, A. Shirinifard, M. Swat and J. A. Glazier, Simulation of single-species bacterial-biofilm growth using the Glazier-Graner-Hogeweg model and the compucell3D modeling environment, Math. Biosci. Eng. **5** (2008) 255-288.

[118] R. B. Potts, Some Generalized Order-Disorder Transformations, Proc. Camb. Phil. Soc. **48** (1952) 106-109.

[119] A. Raya, Y. Kawakami, C. Rodríguez-Esteban, M. Ibañes, D. Rasskin-Gutman, J. Rodríguez-León, D. Büscher, J. Feijó and J. C. Izpisúa Belmonte, Notch activity acts as a sensor for extracellular calcium during vertebrate left-right determination, Nature **427**-6970 (2004) 121-128.

[120] W. Risau and V. Lemmon, Changes in the vascular extracellular matrix during embryonic vasculogenesis and angiogenesis, Dev. Biol. **125** (1988) 441-450.

[121] W. Risau, Differentiation of endothelium, FASEB J. **9** (1995) 926-933.

[122] W. Risau and I. Flamme, Vasculogenesis, Annu. Rev. Cell. Dev. Biol. **11** (1995) 73-91.

[123] W. Risau, Mechanisms of angiogenesis, Nature **386** (1997) 671-674.

[124] C. Roca and R. H. Adams, Regulation of vascular morphogenesis by Notch signaling, Development **21** (2007) 2511-2524.

[125] F. Rothe, Global Solutions of Reaction-Diffusion Systems, Lecture Notes in Mathematics **1072** (Springer, Heidelberg, 1984).

[126] B. M. Rubenstein and L. J. Kaufman, The role of extracellular matrix in glioma invasion: a cellular Potts model approach, Biophys J **95** (2008) 5661-5680.

[127] P. A. Rupp, A. Czirók and C. D. Little, alphavbeta3 integrin-dependent endothelial cell dynamics in vivo, Development **131** (2004) 2887-2897.

[128] N. J. Savill and P. Hogeweg, Modelling morphogenesis: from single cells to crawling slugs, J. Theor. Biol. **184** (1997) 229-235.

[129] M. Scianna, L. Munaron and L. Preziosi, A multiscale hybrid approach for vasculogenesis and related potential blocking therapies, Prog Biophys Mol Bio **106** (2011) 450-462.

[130] G. Schlosser and G. P. Wagner (eds.), Modularity in Development and Evolution (The University of Chicago Press, 2004).

[131] G. Serini, D. Ambrosi, E. Giraudo, A. Gamba, L. Preziosi, F. Bussolino, Modeling the early stages of vascular network assembly, EMBO J. **22** (2003) 1771-1779.

[132] G. K. Sherer, Vasculogenic mechanisms and epithelio-mesenchymal specificity in endodermal organs, In: R. N. Feinberg, G. K. Sherer and R. Auerbach (eds.), The development of the vascular system (Karger, Basel, 1991) 37-57.

[133] D. Stauffer and A. Aharony, Introduction to Percolation Theory (Taylor & Francis, London, 1994).

[134] M. S. Steinberg, Differential adhesion in morphogenesis: a modern view, Curr. Opin. Genet. Dev. **17**(4) (2007) 281-286.

[135] S. Suchting, C. Freitas, F. le Noble, R. Benedito, C. Bréant, A. Duarte and A. Eichmann, The Notch ligand Delta-like 4 negatively regulates endothelial tip cell formation and vessel branching, Proc. Natl. Acad. Sci. USA **104**(9) (2007) 3225-3230.

[136] A. Szabo, E. D. Perryn and A. Czirók, Network formation of tissue cells via preferential attraction to elongated structures, Phys. Rev. Lett. **98**(3) (2007) 038102.

[137] A. Szabo, E. Mehes, E. Kosa and A. Czirók, Multicellular sprouting in vitro, Biophys. J. **95**(6) (2008) 2702-2710.

[138] D. W. Thompson, On growth and form (Cambridge University Press, 1917).

[139] A. Tosin, D. Ambrosi and L. Preziosi, Mechanics and chemotaxis in the morphogenesis of vascular networks, Bull. Math. Biol. **68** (2006) 1819-1836.

[140] L. Tranqui and P. Traqui, Mechanical signalling and angiogenesis. The integration of cell-extracellular matrix couplings, C. R. Acad. Sci. Paris, Science de la Vie **323** (2000) 31-47.

[141] A. Tufro, V. F. Norwood, R. M. Carey and R. A. Gomez, Vascular endothelial growth factor induces nephrogenesis and vasculogenesis, J. Am. Soc. Nephrol. **10** (1999) 2125-2134.

[142] A. M. Turing, The Chemicals basis of morphogenesis. Philos. T. Roy. Soc. London **237** (1952) 37-72.

[143] S. Turner and J. A. Sherratt, Intercellular adhesion and cancer invasion: a discrete simulation using the extended Potts model, J. Theor. Biol. **216** (2002) 85-100.

[144] S. A. Vokes and P. A. Krieg, Endoderm is required for vascular endothelial tube formation, but not for angioblast specification, Development **129** (2002) 775-785.

[145] G. von Dassow, E. Meir, E. M. Munro and G. M. Odell, The segment polarity network is a robust developmental module, Nature **406** (6792) (2000) 188-192.

[146] J. von Neumann, The theory of self-reproducing automata, A. W. Burks (ed.) (Urbana, IL: University of Illinois Press, 1966).

[147] M. Zajac, G. L. Jones and J. A. Glazier, Simulating convergent extension by way of anisotropic differential adhesion, J. Theor. Biol. **222** (2003) 247-259.

[148] H. Zhang and A. C. Issekutz, Down-modulation of monocyte transendothelial migration and endothelial adhesion molecule expression by fibroblast growth factor: reversal by the anti-angiogenic agent SU6668, Am. J. Pathol. **160** (2002) 2219-2230.

Part II

Research Work

Chapter 2

A key problem in early embryonic vasculogenesis: vascular patterning by matrix-mediated VEGF signalling

Contents

2.1 Abstract

In this chapter, a new mathematical model for embryonic vasculogenesis is introduced. It is based on the assumption that binding of paracrine signals to angioblast-produced ECM regulates early vascular patterning in the embryo by creating spatially-restricted guidance cues required for directed cell migration and coalescence (see Figure 2.1). Detailed morphometric analysis of simulated networks and images obtained from *in vivo* quail embryos reveals the model mimics the vascular patterns with high accuracy. The robustness of the mathematical model is checked by performing a sensitivity analysis with respect to the parameters involved. Finally, the dynamics of network formation as well as the role of cell shape and cell density in this process are explored. These results show that paracrine signalling can result in the formation of fine-grained cellular networks when mediated by angioblasts-produced ECM.

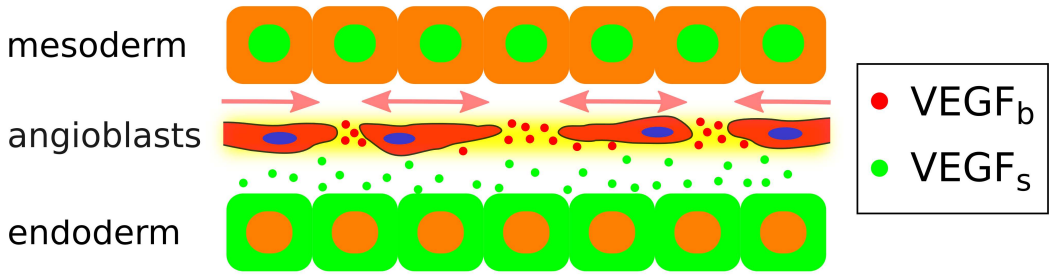

Figure 2.1: **Paracrine chemotaxis model for vasculogenesis**. Angioblasts (endothelial progenitor cells) are derived from mesodermal cells and assemble into polygonal networks under instructive paracrine signalling provided by the endoderm. Endodermal cells express pro-vascular growth factors such as VEGF. Angioblasts are located in the space between endoderm and mesoderm, surrounded by extracellular matrix (ECM). Angioblasts produce ECM molecules (such as heparan sulphates and fibronectin) with VEGF binding domains (depicted in yellow). This matrix thus acts to store chemotactic growth factors, which provides spatial cues for cell migration.

2.2 Introduction: autocrine vs paracrine signalling

Various recent studies summarized in Chapter 1 hypothesize that autocrine regulation of the chemoattractant vascular endothelial growth factor (VEGF) is responsible for the formation of vascular networks *in vitro* [14, 26–28, 40]. These studies assume that mature endothelial cells seeded in gels produce a chemoattractant, typically identified as VEGF, that provides themselves the spatial cues

driving their migration. This autocrine model may provide insight on certain *in vitro* settings, but does not fit well with reported data on early embryonic vascular formation *in vivo*.

Chemotactic mechanisms are indeed compatible with biological data on the migration of angioblasts and their coalescence to form early blood vessels in the embryo, as well as with some theoretical principles on the role of molecular signalling gradients [50]. However, the autocrine regulation mechanism, in which endothelial cells stimulate themselves by both producing and responding to growth factors, does not seem to be fully supported by the biological evidence so far reported in the literature. As a matter of fact, angioblasts are known to express receptors for chemoattractants (VEGFR-2 and CXCR-4, [47, 52]), but there is no evidence that, in the embryo, they produce biologically significant amounts of their ligands as well (VEGF and SDF-1, respectively) [10, 34, 37]. Instead, it is known that most relevant pro-vascular signals, including VEGF, are expressed by the adjacent endoderm [32, 37]. A further problem concerns an assumption related to the diffusivity of the signalling molecule. Some autocrine models require a slowly diffusing, quickly inactivating chemoattractant in order to produce stable cellular networks [28]. The assumed rate of diffusion in these mathematical models is typically orders of magnitude lower than that reported for most common VEGF isoforms [28, 30]. Thus, both the source of VEGF and its biophysical properties assumed in models of autocrine regulation are not in aggrement with the reported data on early vascular development.

In view of these problems, an alternative mechanism for vascular patterning in the embryo is proposed in this study. Specifically, VEGF is assumed to be a paracrine signalling agent, in accordance with its reported endodermal origin *in vivo* [32, 37]. Yet, paracrine signalling seems at odds with tight regulation of fine-grained network patterns. In the absence of additional regulatory mechanisms, diffusive signals from nearby tissues lack the ability to create precise spatially restricted cues. Interestingly, however, angioblasts are known to produce extracellular matrix (ECM) molecules that are able to bind pro-vascular growth factors, including VEGF [23, 36, 43, 49]. These ECM molecules can immobilize diffusive signalling molecules and thereby provide fine-grained spatial motility cues. For this reason, we assume angioblasts produce ECM molecules with VEGF binding domains. Next, a concise overview of the key biological evidence on the interaction of VEGF and the ECM that supports these assumptions is provided.

2.2.1 VEGF and the ECM

Angioblasts express some endothelium-specific markers like VEGFR-2/FLK-1/KDR; SCL/TAL-1; PECAM/CD31, VE-cadherin or Tie2/Tek [7, 48, 52]. Some of these molecules are receptors for growth factors essential to vascular morphogenesis, VEGF-A being the most relevant example of a pro-vascular secreted factor considered in the literature. VEGF-A is a glycoprotein with several isoforms arising from the alternative splicing of a unique gene. Splice variants differ in their ability to bind the ECM. Smaller forms are able to diffuse through the ECM, while larger forms bind to heparan sulphate and other characteristic ECM domains with high affinity, thus modulating the distribution of the growth factor in the tissues [11, 19, 33, 43].

VEGF signalling is believed to be at the core of the vascular patterning process as suggested by multiple studies [8, 34, 46]. VEGF expression has been detected in the whole endoderm and some other mesodermal cells, but has not been unambiguously reported in angioblasts [12, 32]. As a matter of fact, angioblasts express a variety of VEGF receptors, of which VEGFR-2 is the most relevant one for vascular development [31]. Although different routes can be identified in the transduction of the signal by angioblasts, that one including p38MAPK-MAPKAPK2/3-HSP27 is key in mediating patterning, as it regulates angioblast protrusive activity towards the signal, thereby modulating cell shape and motility [51]. It has been argued that heparin-binding VEGF isoforms provide spatially restricted cues that polarize and thereby guide sprouting endothelial cells [39]. This suggests a more active role of the ECM in vascular development than previously thought. Indeed several recent reports indicate that the ECM is pivotal to a variety of morphogenetic events including blood vessel formation [54, 55]. The specific mechanisms through which the ECM influences angioblast and endothelial cell functions are complex and involve both external structural support and regulation of multiple signalling pathways. Such mechanisms include modulation of growth, differentiation, migration, determination of cell shape and survival, as well as providing storage of growth factors [6, 15, 43].

From the above, it is clear that the ECM can provide crucial cues for early vascular developmental events, but its involvement in such processes tends to be overlooked. This is surprising since it is known that vascular abnormal patterning is characteristic of many animal models where expression/function of a variety of ECM molecules is deficient [1]. A highly relevant finding obtained in knock-out screens is that fibronectin, an ECM glycoprotein essential to the migration of multiple cell types, was found to be the most relevant molecule in early vascular development, closely followed by elements of the VEGF and retinoid signalling

pathways and some cell-matrix adhesion molecules [1]. Interestingly, VEGF can bind fibronectin and other ECM molecules and this may affect its downstream effect on cells [2,5,49]. All these findings have motivated this study to investigate mechanisms in which the ECM, and matrix-binding VEGF isoforms can lead to coalescence of angioblasts into a polygonal vascular network.

2.3 Mathematical model

Before turning to the mathematical formulation of the model, the key assumptions together with the published biological data on which these are based are summarized:

(1) A significant number of early embryonic blood vessels develop from isolated angioblasts distributed in the thin, planar surface of the lateral splanchnic mesoderm [37]. Therefore, the system is studied in a two dimensional domain where planar cells are initially distributed. Previous developmental events related to the origin of angioblasts are neglected.

(2) VEGF is known to be produced homogeneoulsy by the endoderm [32], and binds to various ECM molecules such as fibronectin and heparan sulphates [43,49]. VEGF production by the endoderm is represented in the model by a constant source of VEGF all over the domain. VEGF molecules are then modelled as diffusible particles that become non-diffusive when bound to ECM molecules following the mass action law.

(3) Early vascular cells are known to migrate in an ECM rich in fibronectin and heparan sulphates, that can be deposited by endothelial cell precursors themselves [23, 36, 43]. Likewise, in the model, angioblasts are assumed to produce directly or indirectly non-diffusive ECM components able to bind VEGF.

(4) ECM-bound VEGF provides stronger signalling cues for cell motility or shape remodeling than the freely diffusive forms [5, 39]. Consequently, in the model motility is strongly biased towards upward gradients of anchored growth factors rather than to gradients of the freely diffusive forms.

(5) Binding of VEGF to heparan sulphates in ECM molecules offers protection to growth factors against enzymatic degradation [19, 42]. Therefore, degradation or removal of bound growth factors is neglected in the model.

(6) Although it is commonly accepted that endothelial cells have a low proliferation rate in the adult and a high one in the embryo, the reported proliferation rates for angioblasts *in vivo* are not high [4, 22, 29]. Moreover, administration of exogenous VEGF in the embryo results in dysmorphogenesis by hyperfusion,

rather than increased cell numbers [9]. Here it is assumed that proliferation is not a major limiting factor during the first steps of early vascular formation. Accordingly, the number of cells is considered constant.

Once particular hypotheses have been established, a mathematical formalism which unambiguously describes them has to be chosen. In this study, a hybrid cell-based/continuous framework from previous works [26] is adopted and modified. This model formalism represents the multi-scale nature of the problem under consideration in a simple way. Moreover, it explicitly accounts for cell shape, which is key for reproducing the observed network patterns at a cellular scale. The model consists of two interconnected modules. On the first one, angioblasts are represented as discrete and geometrically extended objects using a cellular Potts model (CPM) [16]. On the other one, growth factors and ECM molecules are modeled as continuous fields whose distribution is governed by partial differential equations (PDEs).

Let us consider this second module first. Bearing in mind the diffusivity and binding reactions of growth factors and ECM molecules, the following system of differential equations is proposed:

$$\begin{aligned} \frac{\partial u}{\partial t} &= D\triangle u + \gamma_1 - f(u,v) - \epsilon u \\ \frac{\partial v}{\partial t} &= \gamma_2 \delta_{\sigma_{x,0}} - f(u,v) \\ \frac{\partial w}{\partial t} &= f(u,v) \end{aligned} \tag{2.1}$$

where u, v and w denote the concentrations of soluble VEGF, ECM molecules with free heparan binding domains and bound VEGF, respectively. Parameter D is the diffusion coefficient of VEGF, γ_1 is the constant rate of VEGF production and ϵ is related to the half-life of VEGF. Parameter γ_2 is the production rate of ECM molecules by cells ($\delta_{\sigma_{x,0}} = 1$ inside cells and $\delta_{\sigma_{x,0}} = 0$ outside cells). VEGF-heparan sulfate interaction is assumed to take place according to mass action with second order kinetics, so that $f(u,v) = \alpha uv$ with effective kinetic rate α. Note that this simple reaction-diffusion model does not include terms for saturated production, enzymatic kinetics or cooperative binding. The focus, thus, is on the feedback mechanisms between the molecular and cellular levels, coupled through ECM-mediated chemotaxis. In this way, the assumptions on the underlying biochemical kinetics, about which little is known, is reduce to a minimum.

Cells are modeled using a CPM in which each of the N cells to be tracked is

represented by a connected subdomain of a 2D square lattice. The same index $\sigma = \{1, 2, ..., N\}$ labels all the lattice sites of a particular cell while the special index $\sigma = 0$ labels the medium, i.e. all lattice sites not occupied by cells. In this formalism a cell has finite volume and deformable shape. The interfaces between two different lattice sites x and x' with different indexes $\sigma_x \neq \sigma_{x'}$ represent membrane boundaries between cells or between cells and the ECM. To each of these boundaries, a characteristic binding energy is assigned: J_{cc}, when the interface is between two different cells and J_{cm}, when it lies between a cell and the surrounding ECM. An energy penalty increasing with the cell's deviation from a selected target area A imposes an area constraint on the cells.

The corresponding Hamiltonian is defined as follows:

$$H = \sum_{\{x,x'\}_n} J_{\tau(\sigma_x)\tau(\sigma_{x'})}(1 - \delta_{\sigma_x,\sigma_{x'}}) + \lambda \sum_{\sigma>0}(a_\sigma - A)^2 \tag{2.2}$$

where $\tau(\sigma)$ represents the type of object occupying a grid space σ, which in this case can only be angioblast (c) or medium (m). The term $(1 - \delta_{\sigma_x,\sigma_{x'}})$ ensures binding energies are only considered between different cells. The term $(a_\sigma - A)$ represents a cell's deviation from its target area and λ represents the cell's resistance to such deformations. The first summation is taken for the n^{th}-order neighbors in each lattice site. The second summation goes for all cells with the exception of the medium.

Cell dynamics are generated in the CPM by a modified Metropolis algorithm. The latter randomly chooses a lattice site, x', and computes what the difference in energy, ΔH, would be if a randomly selected neighboring site, x, would copy its state into this site. The probability of accepting the change, P, depends on the difference in the energy costs:

$$P(\Delta H) = \begin{cases} 1 & if\ \Delta H \leq 0 \\ e^{\frac{-\Delta H}{T}} & otherwise, \end{cases} \tag{2.3}$$

so that cell extensions that diminish H are given priority. In this way, the cell shape is updated locally. Parameter T, henceforth referred to as fluctuation energy, is a biological analogue to the energy of thermal fluctuations in statistical physics [3] and it is considered here as a measure of cell motility. Chemotaxis is modelled as a bias in the direction of higher VEGF concentrations. More precisely, P is considered to depend on:

$$\Delta H_{chemotaxis} = \Delta H - \mu_b(w(x') - w(x)) \\ -\mu_s(u(x') - u(x)),$$

where a distinction is made between bound and soluble VEGF. The strength of signalling provided by the bound and soluble forms can be varied by setting the parameter μ_b and μ_s while preserving their total value $\mu_t = \mu_s + \mu_b$. Stronger chemotaxis towards bound VEGF is accounted for by setting $\mu_b > \mu_s$. Finally, the unit of time in the simulation is defined as one Monte Carlo step (MCS) that corresponds to a number of random update attempts equal to the total number of lattice sites.

2.4 Methods

2.4.1 Experimental images

Blood vessels of quail embryos are labelled with the QH1 antibody (endothelial membrane), using DAPI for nuclear counterstain, at 36-40 hours after incubation. Confocal microscopy allows to visualize the developing vasculature and all nuclei in the tissue. Images are then taken of wide areas of the embryo where angioblasts have just assembled into networks (see Figure 2.2). QH1 labeling of the cellular structures is achieved by segmentation of the appropriate fluorescence channel. This results in a binary image where vascular zones are labelled with one and avascular zones or lacunae are labelled with zero. Segmentation of DAPI fluorescent stain, marking all nuclei in the confocal plane, is used to estimate angioblast cell density by co-localization of identified nuclei with the QH1 membrane label using the segmented binary image.

The simulation software produces binary images in which cells and lacunae are labelled as described before so that both series can be examined and compared by means of the same morphometric techniques.

2.4.2 Morphometric methods

Experimental and simulated networks represented in binary images are characterized by quantifying the lacunae (number, size and roundness of avascular zones), the vascular structures (number of connected components, coverage and widths), network properties (number of nodes, degree distribution, percolation and span-

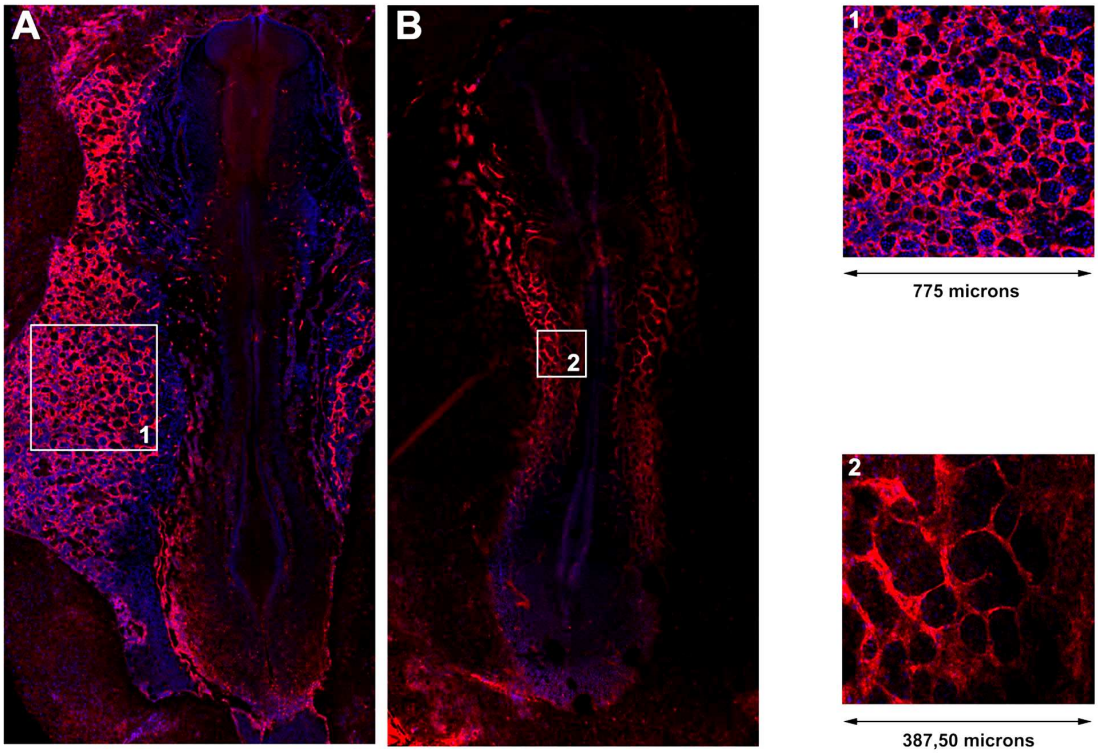

Figure 2.2: ***In vivo* vascular network in the quail embryo**. Laser confocal microscope reconstruction of the extra-embryonic (A) and intra-embryonic (B) vasculature of early quail embryos (3640 hours of incubation). Embryonic blood vessels are identified by the QH1 antibody (red). Cell nuclei have been counterstained with DAPI (blue). The inserts depict extra-embryonic (1) and intra-embryonic (2) vascular networks in more detail; the former are used in analysis and validation of the mathematical model.

ning length) and fractal properties (fractal dimension and lacunarity). Image processing and statistical analysis have been performed in Matlab 2009b using morphological functions supplied by the Image Processing Toolbox (version 6.4) supplemented by custom-made routines. Together, the set of morphometric features provides us with detailed quantification of vascular patterns obtained *in vivo* and *in silico*.

The number of connected vascular zones and lacunae are two key network characteristics and correspond to the 0^{th} and 1^{st} Betti number used in algebraic topology (see [38] and references therein). These are identified by tracing the exterior boundaries of objects in the binary image. The sizes of lacunae and vascular structures equal the number of pixels they occupy, while the roundness of lacunae is measured using the isoperimetric quotient, defined as the ratio of the measured area to that of a circle having the same perimeter, $R = 4\pi A_l/P_l^2$, where A_l and P_l are the lacuna area and perimeter, respectively. The coverage of

angioblasts is recorded as the ratio of the number of nonzero pixels to the size of the binary image. The network is said to be percolative when a vascular structure exists that spans the image both horizontally and vertically.

Assessing some of the morphometric features requires computation of a skeletonization of the network, using a morphological operation known as thinning. Thinning reduces the network structures to a skeletal remnant that largely preserves the extent and connectivity of the original one while pruning away redundant foreground pixels. The spanning length of the network is then measured as the sum of nonzero elements. The widths of cellular cords are assessed by measuring the Euclidean distance from each nonzero pixel on the thinned structure to its closest lacuna. Nodes in the thinned structure are usually identified as nonzero points with 3 or more nonzero pixels among the 8 adjacent sites, indicating a point at which the structure branches. Although this method is often used [18, 25], it actually overestimates the number of nodes when no further processing is applied. To improve the measurement, proximate nodes are merged whenever the distance between them is smaller than the distance from the node to the nearest lacuna. This procedure reduces the number of nodes on the thick vascular segments while preserving them on thin cords. Moreover, using this method we gain information on the degree distribution, i.e. on the distribution of connections or edges a node has to other nodes. Finally, fractal analysis is performed to quantify the complexity and space filling properties of network patterns. Informally, the fractal dimension D_f measures how a fractal-like structure fills the space for decreasing scales, while the lacunarity L_f assesses its 'gappiness', i.e. the distribution and size of the empty domains [24]. These properties have been previously applied to characterize vascular growth in e.g. chick chorioallantoic membrane (CAM) angiogenesis [17, 21]. The fractal properties of the the thinned network structure were estimated by applying the box counting methods and gliding box method [41, 44], using the FracLac plugin for ImageJ [20, 35].

2.4.3 Simulation set-up

When selecting simulation scenarios, several choices are determined by the experimental setup. For instance, the size of the lattice where CPM and PDE are simulated is adjusted to resemble 775x775 mm^2 experimental images. Specifically, a square lattice of 400x400 pixels is considered, where each lattice node represents 2 mm^2, thus giving a total simulated tissue of 800x800 mm^2 or 0.64 mm^2. Cell densities are estimated from experimental images by co-localization of nuclei with the vascular structure, resulting in an average density of $\approx$1750 cell mm^2, which is used as a reference in the simulations (1100 cells over 800x800 mm^2).

Parameter	Symbol	Value	Source
PDE			
Diffusion coefficient $VEGF_s$	D	10 $\mu m^2 s^{-1}$	[30]
Production rate $VEGF_s$	γ_1	10^{-3} $a.u.s^{-1}$	estimated
Production rate ECM	γ_2	10^{-3} $a.u.s^{-1}$	estimated
Binding rate $VEGF_s$+ECM	α	10^{-1} $a.u.^{-1}s^{-1}$	estimated
Degradation rate $VEGF_s$	ϵ	10^{-2} s^{-1}	estimated
CPM			
Fluctuation energy	T	50	[25–27]
Target area	A	95 pixels	empirical
Cell rigidity	λ	25	[26, 28]
Cell-cell binding energy	J_{cc}	20	[26]
Cell-medium binding energy	J_{cm}	10	[26]
Chemotaxis strength	$\mu_t = \mu_s + \mu_b$	2000	[26, 27]
Signalling strength $VEGF_b$	μ_b/μ_t	0.75	[5, 39]
Signalling strength $VEGF_s$	μ_s/μ_t	0.25	[5, 39]

Table 2.1: **Parameters of the simulation model**.

As initial condition, cells are distributed over the lattice in either a regular or a semi-random mesh. The latter is constructed by randomly displacing cells from the regular mesh, where displacements are smaller than one cell diameter.

Parameter choices in the CPM module have been made as in previous works [25, 26, 28], see Table 2.1. In particular, we neglect surface tension between cells and the ECM for sake of simplicity, by setting $\gamma_{cm} = J_{cm} - J_{cc}/2 = 0$.

The criteria for selecting PDE module parameters are different. A value for the diffusion coefficient of VEGF has been taken similar to those reported in the literature [30], although we shall see later that our results are largely insensitive with respect to this coefficient. The rest of the parameters has been chosen on the basis of estimated time scales of processes. For instance, binding is fast relative to VEGF and ECM production, and the corresponding parameters are selected so as to fit experimental data (see Table 2.1). Then, a sensitivity analysis on these parameters is performed to give us an idea of the expected variability in terms of some of the quantified morphometric properties.

Each MCS in simulation corresponds to one second. For this choice, the total simulated time is about one hour, agreeing well with the estimated time scale in which the process takes place *in vivo* (from minutes to a few hours).

Simulations have been implemented using a C++ based modeling environment called Morpheus. Multiple simulation repetitions are performed ($n = 10$, unless stated otherwise) with different random seeds, of which the mean and standard deviation are shown.

2.5 Results

2.5.1 Model simulations yield vascular-like reticular patterns

Vascular networks obtained from quail embryos *in vivo* are compared to those resulting from model simulations, along a series of morphometric properties, summarized in Figure 2.3. Examples of binary images used in this comparison are shown with their thinned skeleton (red pixels) and detected nodes (blue circles) in panel A. We found that the morphometrics of simulated networks correspond well to experimental observations, as shown in the statistical comparison in Figure 2.3 B. Despite small deviations, the number of nodes and edges, network length and interface length, as well as fractal properties and coverage measured in the simulated networks are remarkably similar to the corresponding values obtained from experimental images. Lacunarity, a measure for lack of translation and rotational invariance, is observed to be slightly higher in the *in vivo* situation. This may be due to the spatial heterogeneity in tissue density along the mediolateral axis, which is not reflected in the model. Although the number of cells used in simulation has been estimated from experimental images, the observed coverage (the relative size of the area covered by angioblasts) is also seen to be slightly higher *in vivo*. The differences in network and interface length are related to the previous feature, since denser vascular structures have more and longer edges at the cost of cell-lacuna interface length.

In order to further characterize the vascular network, distributions of several measured morphometric properties are quantified, shown in Figure 2.3 C. As a result of the procedure to merge proximate nodes, the number of connections per node is recovered, known as the node degree (indicated as size of blue circles in Figure 2.3 A). Although the range of observed node degrees is rather small, an exponential decay can be recognized in their distribution, with high frequency of small degree and rare high-degree nodes. Using both the skeletonized structure and the underlying binary image, the distribution of cord widths is assesed by measuring the shortest distance of each pixel on the skeletonized image to an avascular region. The distribution thus obtained reveals a right-skewed distribution of cellular cord widths with thin cords forming the highest frequency, while thick cords are relatively rare. Simulated networks display less right-skewness, which may again be related to the mediolateral heterogeneity in the experimental images. Nevertheless, the modes of both distributions coincide and both show a distinct pattern of high and low frequencies around the mode. These peaks are caused by the discreteness of the number of cells involved in a cord, a fact

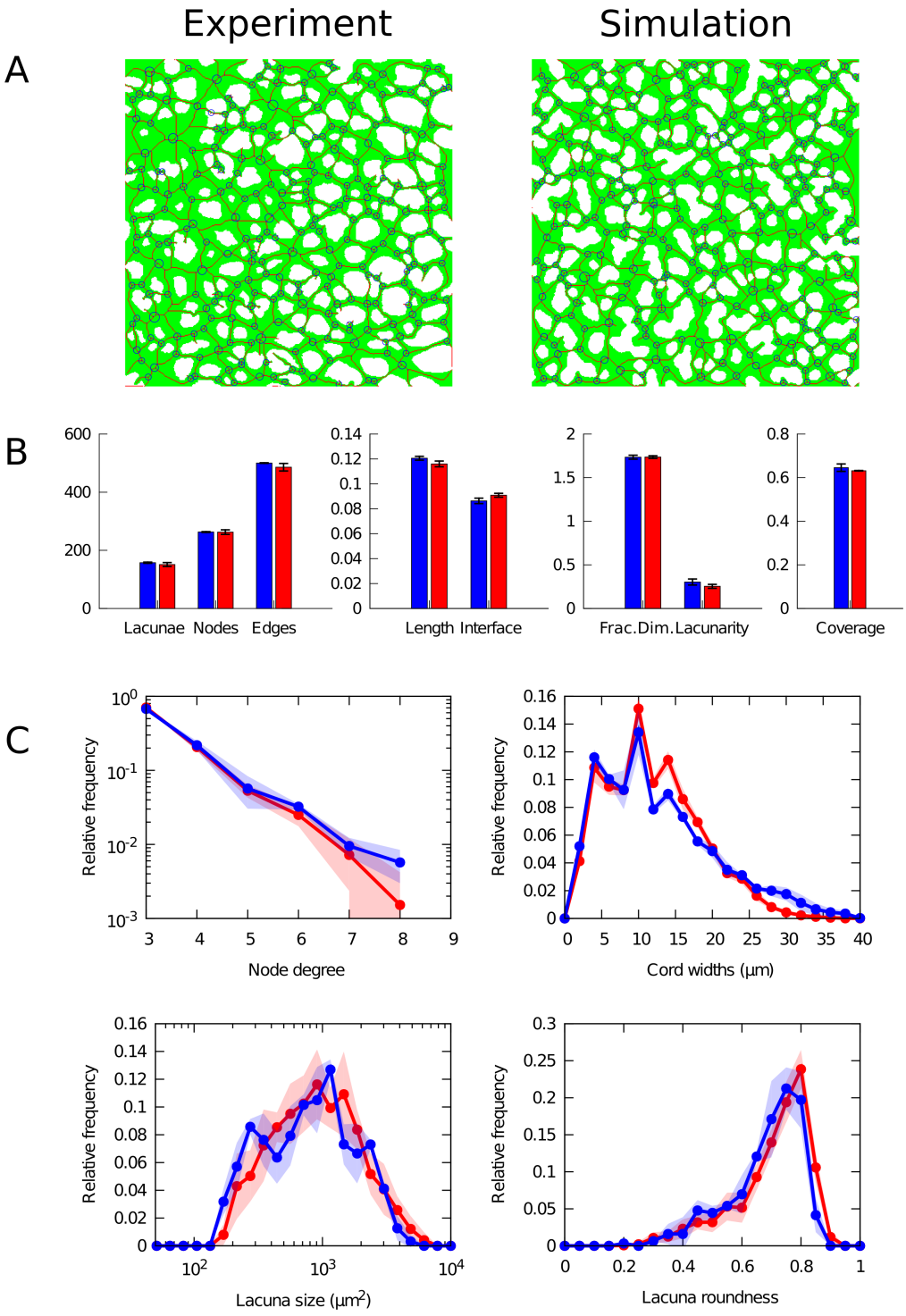

Figure 2.3: **Morphometric comparison**. Comparison between experimental (in blue) and simulated (in red) vascular networks (after 3000 MCS). (A) Binary images over cellular structures (green) overlayed with skeletonized network (red), detected branching points (blue points) and corrected nodes (blue circles). (B) Morphometric statistics. Boxes show average values (n = 2 for experiments; n = 10 for simulation) and error bars indicate standard deviation. (C) Distributions of morphometric properties. Lines show average values; filled areas indicate standard deviations.

that is captured by the discrete cell-based submodel. Interestingly, the mode of the distribution ($10\mu m$) is well below the diameter expected for isotropic cells which indicates a strong contribution of elongated cells (discussed in more detail below). Finally, the size and shape distribution of lacunae are compared. In both experiment and simulation, a wide lognormal distribution can be discerned in lacuna size distribution, spanning almost two orders of magnitude around the most frequent size at approx. $1000\mu m^2$. The distribution of roundness of lacunae is left-skewed with most holes being nearly circular. Note that these two quantities are related to each other by the fact that larger holes tend to have a less circular shape. Lacunae size and roundness are thus negatively correlated, although this effect is more clearly seen in simulations (Pearson correlation $r = -0.81$) than in the segmented experimental image ($r = -0.27$).

In summary, detailed morphometric analysis shows that a model based on chemotaxis towards growth factors bound to ECM secreted by angioblasts is able to produce reticular patterns as those observed in vascular networks in quail embryos. The main reasons to describe and compare the vascular networks using a broad spectrum of morphometric properties are as follows. First, detailed quantitative morphological characterization of early vascular networks is needed to characterize normal vascular development. It can also prove helpful to detect defects in experiments in which specific processes are perturbed. On the other hand, a fact relevant for this study is that, in order to ascertain geometrical and functional similarities, multiple shape descriptors are required to compare vascular shapes. In principle, this represents a difficulty since an accurate fit with respect to one shape parameter (e.g. number of nodes) needs not be compatible with a similar fit with respect to another such parameter (e.g. distribution of cord widths). A remarkable fact that results from the simulations below is that a good fitting can be obtained simultaneously with respect to a large number of morphometric parameters.

2.5.2 Sensitivity analysis

In order to check the robustness of the model, the sensitivity of the simulation results with respect to their parameters was investigated. First, a sensitivity analysis was performed on the coefficients specifying the rates of production (γ_1 and γ_2), binding (α) and degradation (ϵ) of VEGF and ECM, respectively. Simulations were performed in which these parameters are varied independently over two orders of magnitude from their reference values (see Table 2.1). The change in morphometric properties with respect to the reference simulation described above was measured, shown in Figure 2.4 A. As shown there, a 10-fold decrease

and increase of the VEGF-ECM binding rate α and VEGF decay rate has only moderate or negligible effects on the network morphology. However, variation of the VEGF and ECM production rates (γ_1 and γ_2) does have large impact on the structure of the network. Upon decrease of these production rates a marked decline in the number of lacunae is observed, indicative of vascular dysmorphogenesis. This is readily understood under the model assumptions, since effective removal of either VEGF or ECM disrupts binding of growth factor to the matrix, which normally provides the spatial cues for cellular patterning. The analysis further shows that a 10-fold increase in VEGF production (γ_1) has little impact on network formation. Interestingly, however, a similar increase in matrix production (γ_2) does disturb proper morphogenesis. This happens because overproduction of ECM allows fast accumulation of the bound VEGF. Due to chemotaxis towards bound VEGF, this causes premature immobilization of cells and hampers the coalescence of cells and their assembly into a polygonal pattern.

The sensitivity of the results with respect to VEGF diffusivity was further explored. Previous model of vasculogenesis were dependent on unrealistically slow diffusion of VEGF, for instance in [25]. To understand the role of VEGF diffusion in the present model model, simulations with different scenarios concerning VEGF diffusion were perforemed: no diffusion ($D = 0$), normal diffusion ($D = 10\,\mu m^2/s$) and a well-mixed system ($D = \infty$). The latter is modeled by redistributing the total amount of VEGF homogeneously over the lattice after every reaction step. Remarkably, the results in Figure 2.4 B show that the model is extremely robust against variation in that parameter. This virtual independence on VEGF diffusivity can be explained by reference to the assumed homogeneous production of growth factor over the modeled area. Therefore, even in the absence of diffusion, binding of VEGF to ECM will occur throughout the tissue and guide motility. On the other hand, under high diffusivity, VEGF is not only produced but also redistributed in instantaneously homogeneous manner, leaving matrix binding and motility relatively unaffected.

Additionally, the dependency of the resulting network pattern on chemotaxis was investigated. Based on experimental evidence [5, 39], it is assumed in the present study that ECM-bound VEGF provides stronger signalling cues than soluble VEGF. Accordingly, cells in the model have a stronger chemotactic response to bound VEGF (μ_b) than to soluble VEGF (μ_s) in a $3:1$ ratio. To ensure that network pattern formation is not dependent on a particular choice of these parameters, the relative strengths of chemotaxis towards bound and soluble VEGF were explored. Effectively, this alters the relative strength of the signalling cues on cells. Figure 2.5 shows that network formation is perturbed when soluble VEGF is the major signalling agent ($\mu_s > \mu_b$), which is due to a lack of

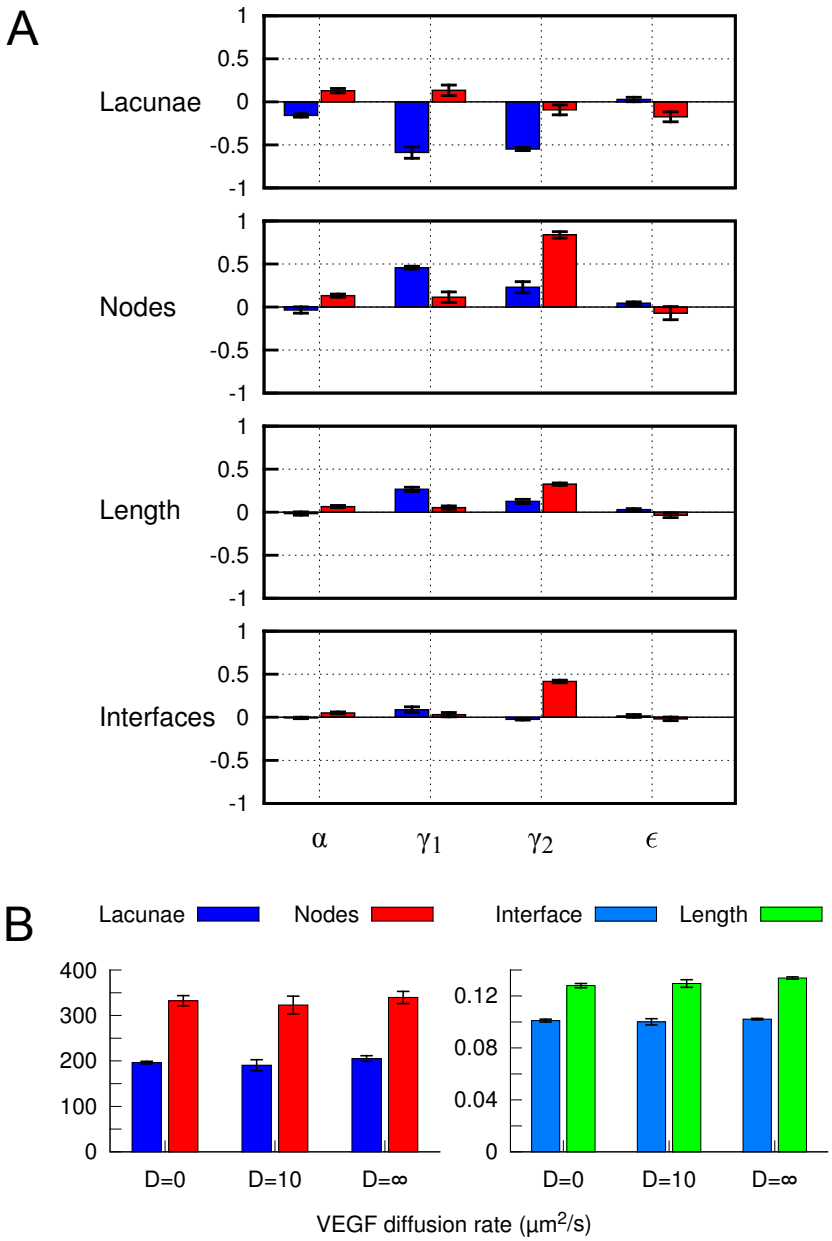

Figure 2.4: **Sensitivity analysis of PDE parameters**. Sensitivity to rates of binding (α), VEGF and ECM production (γ_1) and (γ_2), and degradation of soluble VEGF (ϵ). Changes in various morphometric properties were measured for simulations (n = 3) in which each parameter was independently varied by a 10-fold decrease (blue) and a 10-fold increase (red). (B) Sensitivity to VEGF diffusivity. Morphometric quantities are shown for simulations (n = 3) with non-diffusive VEGF ($D = 0$), with normal VEGF diffusion ($D = 10$), and with well-mixed VEGF ($D = \infty$).

spatially restricted cues. On the other hand, when cells react more strongly to ECM-bound VEGF ($\mu_b \geqq \mu_s$), network formation is relatively stable in a broad domain. The reference values of these parameters (arrowhead in Figure 2.5; table 2.1) are within this region.

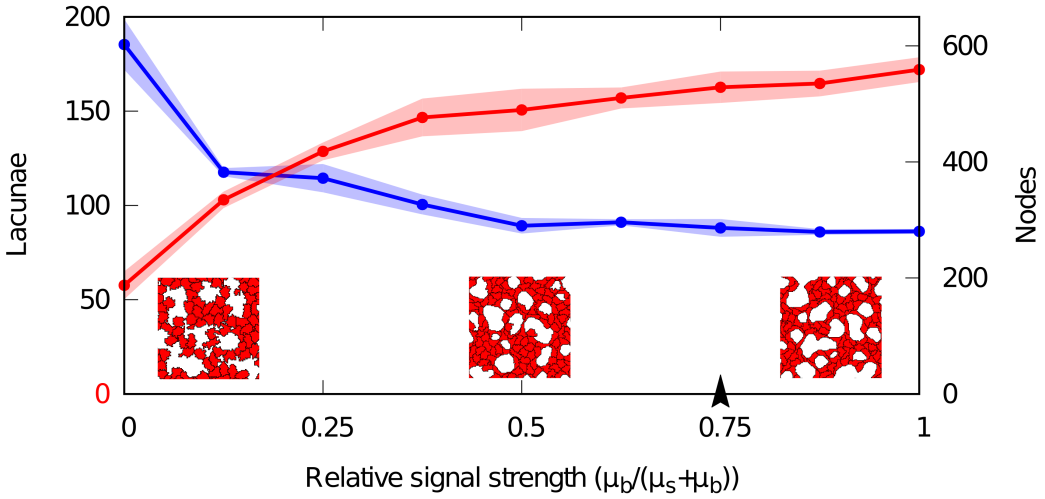

Figure 2.5: **Sensitivity analysis chemotactic signal strength**. Sensitivity of morphometric parameters to relative strength of bound (μ_b) and soluble (μ_s) VEGF. Red points (lacunae) and blue points (nodes) show averages of measured quantities in simulations (n = 3), filled regions represent standard deviations. Insets show portions of networks (200x200 μm^2) where the relative signalling strength (μ_b/μ_t) is set to soluble-VEGF-only ($\mu_b = 0$, left), bound-VEGF-only ($\mu_b = \mu_t$, right) and equal strengths ($\mu_b = \mu_s$, center). Arrowhead indicates the reference value.

2.5.3 Model dynamics display fast coalescence and slow remodelling

Experimental images are obtained by fluorescent staining which requires fixation of the embryo. Therefore, no temporally resolved data are available that would enable to track the development of a vascular bed *in vivo*. Based on simulation results, however, it is possible to look into the dynamics of vasculogenetic development. Although proliferation is known to occur during the assembly of the vascular bed, this is omitted from the model for simplicity. Instead, a constant population size of 800 cells (1250 $cells/mm^2$) is assumed, a figure that lies between a rough estimate of newly differentiated angioblasts and the cell density measured in our experimental images. The influence of cell density on the network morphology is explored below. Also, modelling cell proliferation is briefly discussed in the future perspectives section 4.2 below.

Although the initial population of cells is distributed in a regular mesh, a network pattern forms rapidly during simulation, as shown in Figure 2.6. The top panel (Figure 2.6 A) displays a typical simulation showing the shapes and positions of simulated angioblasts, and the relative concentrations of matrix-bound VEGF. The evolution of the number of connected cellular structures and

that of the number of holes in Figure 2.6 B shows that these quantities move towards a steady state, indicating the dynamic stability of the reticular structure. This stabilization property is in contrast with some models based on autocrine chemotaxis hypothesis [45].

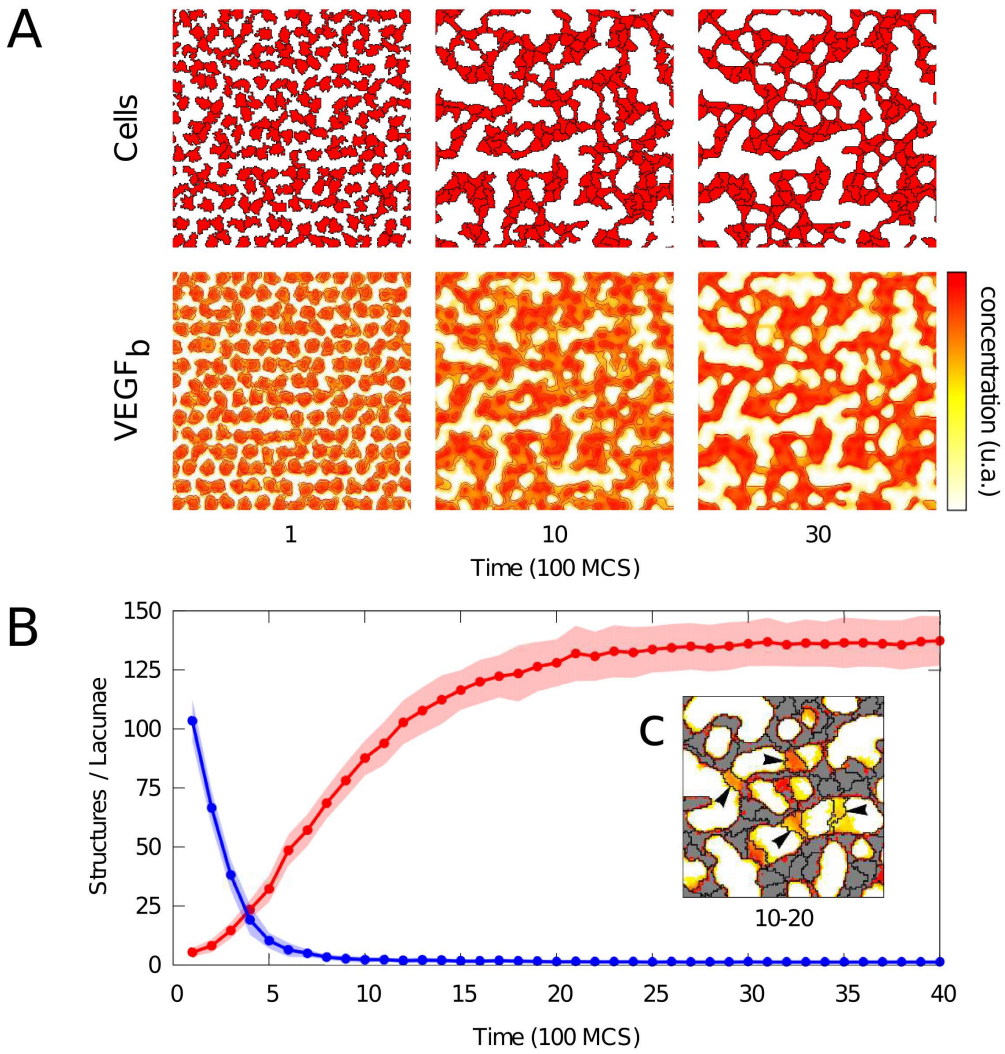

Figure 2.6: **Dynamics of vascular network formation**. (A) Detail of simulated tissue at various time points, showing the cells (top) and relative concentrations of bound VEGF with isolines (bottom). (B) Dynamics of number of isolated cellular structures (blue) and number of lacunae (red), filled regions indicates standard deviation (n = 10). (C) Inset depicts remodeling in a small region. This occupancy map is constructed by averaging over binary images in the interval between 1000 and 2000 MCS; lines show cell boundaries at 2000 MCS. Grey/white pixels are cells/lacuna which remained unchanged over this period; colored pixels indicates how long a pixel has been occupied by cells. It shows the creation of new connections (arrows) increasing the number of lacunae.

Further, the dynamics considered in Figure 2.6 B operate on separate timescales.

On the one hand, cells rapidly coalesce from a mostly isolated configuration to form a percolative and closed network consisting of a single connected component (between 0 and 1000 MCS). On the other hand, the number of lacunae changes over a longer time scale, and keeps increasing after all cells have assembled into a single network (between 1000 and 3000 MCS). In other words, subsequently to the assembly of a closed network, cells continue to rearrange and remodel the network and thereby increase the number of lacunae. Substantial remodeling is performed by cells creating new connections across lacunae, resulting in cords with a single cell width (indicated by arrows). Figure 2.6 C depicts a close-up of remodeling occurring in the period (1000-2000 MCS) after a percolative network has formed. In addition to increasing the number of lacunae in this way, the resulting holes are smaller and have a more regular and round shape. This remodeling is driven by cell motility over tracks of previously secreted ECM that are subsequently primed by VEGF binding.

2.5.4 Cell elongation results from chemotaxis towards matrix-bound VEGF

Using the same data, the shape of cells during simulation is tracked and their lengths are quantified by computing the inertia tensor of an elliptic shape approximation [25,53]. Taking the length of isotropic cells as a reference, the distribution of cell shapes before and after tissue remodeling was compared, as shown in figure 2.7. Before remodelling, cell lengths are skewed towards isotropic length, indicating roundish cells. Afterwards, the position of the mode of the distribution (i.e. the most frequent cell length) has remained unchanged. However, the tail of the distribution has grown, showing that the contribution of elongated cells has markedly increased. Some cells extend up to almost three times the default isotropic length. Importantly, this is not caused by constraining cell shape in our model (as in was done in [25]). Instead, the observed cell elongation follows as a natural consequence of chemotaxis towards matrix-bound VEGF. Thus, in the present model elongation is an effect rather than a cause for the formation of a reticular pattern in the vascular bed.

2.5.5 Morphological dependence on cell density

To explore the influence of cell density on the morphology of the vascular network, a set of simulations was performed in which the number of cells is varied, while keeping the simulated tissue size constant, and the morphometric properties were analyzed. The results, shown in figure 2.8, point out the presence of various

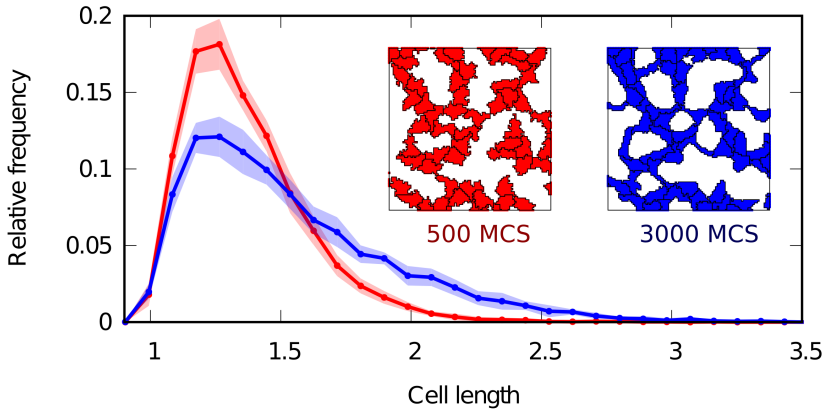

Figure 2.7: **Cell elongation**. Distribution of cell lengths at different time points during the simulation. Red line and inset depict early, blue depicts late in development. Lengths are normalized to isotropic cells given the target area ($\sqrt{s4A_\sigma/\pi}$....), where $s = 4$... is the scaling factor per pixel). Cells become increasingly anisotropic and elongated during vascular patterning. Filled regions represent standard deviation.

thresholds or maxima at increasing cell densities.

The first threshold appears at a density of ≈900 cells/mm^2, where the network exhibits percolation. This percolative threshold is the critical density above which a network first exhibits long-range connectivity. Related to this, the point at which the vascular structure forms a single connected component (so that all cells lie within a single network structure) is found at only slightly higher densities. Both aspects are important for blood transport through the tissue and are established at low cell densities.

At medium cell densities (≈1500 cells/mm^2), a maximum in the number of nodes and the length of cell-lacunae interfaces exists. A high number of nodes indicates a complex branched network structure. Unsurprisingly, such networks show a maximum in the interface length between vascular and avascular regions. Biologically, it is this surface area between endothelium and surrounding tissue which is crucial to the supply of oxygen and nutrients to that tissue.

When density is further increased (≈2000 cells/mm^2), interface length decreases as the size of the avascular region decreases. Instead, the number of lacunae and total network length are maximized. This cell density corresponds to that estimated in *in vivo* vascular networks in quail embryos at 36-40 hours after incubation.

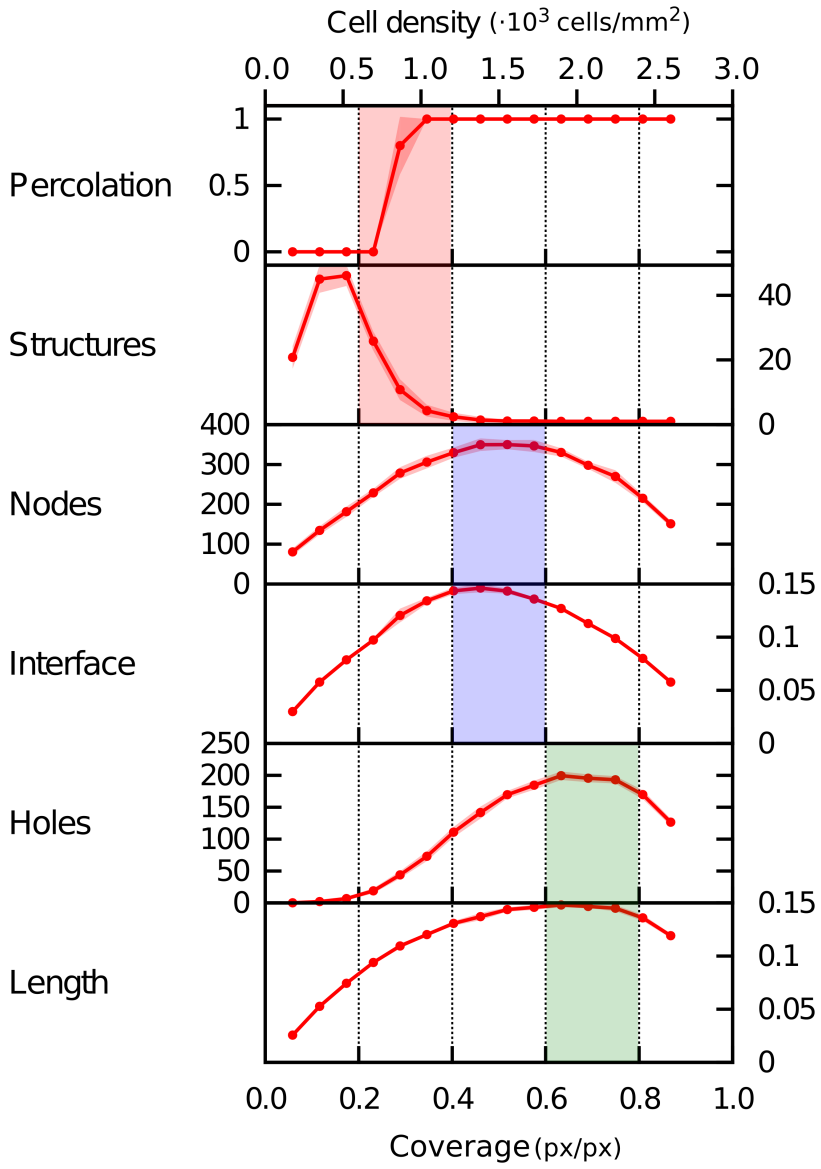

Figure 2.8: **Morphometric dependence on cell density**. A number of morphometric properties of simulated networks are presented as a function of both cell density (number of cells per area) and coverage (the ratio of angioblasts-covered pixels to the total number of pixels). Averaged over 10 simulation runs, filled regions around curves represent standard deviation. Three optima are shown from top to bottom, at increasing cell densities. Parameters as in table 1.

2.6 Discussion

In this chapter, a new mathematical model to describe vascular patterning during early stages of embryonic vasculogenesis has been presented. The prevalent view that the formation of vascular network patterns is regulated by autocrine chemotaxis has been formulated largely based on *in vitro* studies. Instead, the present

model was developed making use of the current biological knowledge on early vasculogenesis in the embryo. In accordance to hypotheses made by other authors [10, 37], the role of paracrine signalling in embryonic vascular development has been explored. In particular the role of the extracellular matrix (ECM) in providing spatial cues for angioblasts by storing and/or activating chemoattractive growth factors have been mathematically simulated. Actually, the significance of the ECM during vasculogenesis has long been known [36] and continues to be an active research field both in vasculogenesis and angiogenesis [5, 39, 43, 49, 55], although its capacity for pattern formation by providing signalling cues has not received much attention (see however [5, 39]).

The presented model combines a 2D discrete cellular Potts model (eq. 3.21 and 3.22) with a continuous reaction-diffusion model (eq. 3.20) under the assumptions that angioblasts are chemotactically attracted towards paracrine VEGF that binds to angioblast-produced ECM. As demonstrated by morphometric analysis, this model is able to produce polygonal cellular patterns that accurately resemble the *in vivo* early vascular bed in quail embryos, recorded by confocal microscopy. The simulated networks show high degree of similarity with respect to a broad spectrum of morphological descriptors, including lacunae number/sizes/shapes, network and interface lengths, cord widths, degree distribution and fractal properties.

At the same time, the model circumvents certain drawbacks of autocrine mathematical models in the context of early embryonic vascular patterning. Indeed, a key problem of the autocrine regulation hypothesis is that no experimental evidence exists that angioblasts produce significant amounts of VEGF, while it is known that the adjacent endodermal tissue produces many pro-vascular growth factors, including VEGF [32, 37]. Thus, for the autocrine model to account for early embryonic vasculogenesis, it remains to be explained how embryonic angioblasts could respond more efficiently to low mesodermal VEGF levels rather than to the high amounts of the same growth factor produced by the adjacent endoderm. The mathematical model proposed here does not consider VEGF production by angioblasts, and assumes instead an external source of VEGF. Angioblast-secreted or modified ECM molecules bind and immobilize the paracrine signalling agent in close proximity of cells. Thus, fine-grained spatial cues for chemotactic cell migration can be generated without postulating unrealistically low VEGF diffusion rates [25, 28]. Furthermore, the stability of the network structures increases over time, instead of collapsing after a transient time, as in previous models [14, 28, 45]. Another interesting observation is that cell elongation, a fact which is experimentally observed, needs not be postulated a priori as in [25]. Instead, cells elongate in our model as a natural consequence

of chemotaxis towards matrix-bound VEGF.

Simulations of the paracrine model yields several results that are coherent with most of the biological data on embryonic vasculogenesis published up to date. In general, downregulation of VEGF or the ECM molecules where VEGF can bind, as fibronectin or heparan sulphates, is known to severely impair early vascular patterning [11,13,43]. In particular, administration of exogenous soluble VEGF receptors during vasculogenesis, which decreases the level of endogenous VEGF, results in a lack of network formation [8]. The relevance of VEGF matrix binding in providing precise spatial cues has also been addressed in several studies. For instance, embryos that expressed only VEGF isoforms lacking ECM interaction domains lead to greatly reduced vessel branching and network complexity [39]. However, to unravel the interaction between ECM molecules with heparin domains and VEGF matrix-binding isoforms as well as their influence in angioblasts responses, further experimental work is needed.

On the other hand, simulations of the mathematical model here considered, reveal some interesting features of networks formation, which however remain to be experimentally validated. For instance, for a fixed number of cells, pattern formation dynamics on two time scales are observed. First, a fully connected network is formed, so that percolation is attained and middle-long range connectivity is achieved. This can be interpreted as a basic requirement for any functional blood vessel network. On a longer timescale, tissue remodeling takes place, whereby the number of lacunae continues to increase so that the surface area keeps increasing too, thus ensuring an efficient distribution of nutrients and waste removal. On the other hand, when cell densities are varied, three maxima in the morphometric quantities can be distinguished. At increasing cell densities, these mark the onset of percolation, the attainment of optimal interface length, and that of a maximal number of lacunae, a fact related to the total spanning length. Interestingly, the densities measured in *in vivo* vascular networks correspond to the latter maximum.

In summary, I have proposed and studied a mathematical model based on the assumption that matrix-binding of paracrine signals mediates early stages in *in vivo* vascular patterning. Simulation of the model suggests that the assumptions made are sufficient to generate vascular networks comparable to those observed during quail embryonic vascular development.

2.7 References

[1] W S Argraves and C J Drake. Genes critical to vasculogenesis as defined by systematic analysis of vascular defects in knockout mice. *Anat Rec Part A*, 286A:875–884, 2005.

[2] S Ashikari-Hada, H Habuchi, Y Kariya, and K Kimata. Heparin regulates vascular endothelial growth factor 165-dependent mitogenic activity, tube formation, and its receptor phosphorylation of human endothelial cells. *J Biol Chem*, 35:1508–3151, 2005. Comparison of the effects of heparin and modified heparins.

[3] D A Beysens, G Forgacs, and J A Glazier. Cell sorting is analogous to phase ordering in fluids. *P Natl Acad Sci USA*, 97:9467–9471, 2000.

[4] G Breier, U Albrecht, S Sterrer, and W Risau. Expression of vascular endothelial growth factor during embryonic angiogenesis and endothelial cell differentiation. *Development*, 114:521–532, 1992.

[5] T T Chen, A Luque, S Lee, S M Anderson, T Segura, and M L Iruela-Arispe. Anchorage of VEGF to the extracellular matrix conveys differential signaling responses to endothelial cells. *J Cell Biol*, 188(4):595–609, 2010.

[6] G E Davis and D R Senger. Endothelial extracellular matrix: Biosynthesis, remodelling and functions during vascular morphogenesis and neovessel stabilization. *Circ Res*, 97:1093–1107, 2005.

[7] S Davis, T H Aldrich, P F Jones, A Acheson, D L Compton, V Jain, T E Ryan, J Bruno, C Radziejewski, P C Maisonpierre, and G D Yancopoulos. Isolation of angiopoietin-1, a ligand for the TIE2 receptor, by secretion-trap expression cloning. *Cell*, 87(7):1161–1169, 1996.

[8] C J Drake, A LaRue, N Ferrara, and C D Little. VEGF regulates cell behavior during vasculogenesis. *Dev Biol*, 224:178–188, 2000.

[9] C J Drake and C D Little. Exogenous vascular endothelial growth factor induces malformed and hyperfused vessels during embryonic neovascularizarion. *P Natl Acad Sci USA*, 92:7657–7661, 1995.

[10] D J Dumont, G H Fong, M C Puri, G Gradwohl, K Alitalo, and M L Breitman. Vascularization of the mouse embryo: a study of Flk-1, Tek, Tie, and vascular endothelial growth factor expression during development. *Dev Dyn*, 203(1):80–92, May 1995.

[11] N Ferrara. Molecular and biological properties of vascular endothelial growth factor. *J Mol Med*, 77(7):527–543, 1999.

[12] I Flamme, G Breier, and W Risau. Vascular endothelial growth factor (VEGF) and VEGF receptor 2 (Flk-1) are expressed during vasculogenesis and vascular differentiation in the quail embryo. *Dev Biol*, 169(2):699–712, 1995.

[13] S E Francis, K L Goh, K Hodivala-Dilke, B L Bader, M Stark, D Davison, and R O Hynes. Central roles of alpha5beta1 integrin and fibronectin in vascular development in mouse embryos and embryoid bodies. *Arterioscler Thromb Vasc Biol*, 22(6):927–933, 2002.

[14] A Gamba, D Ambrosi, A Coniglio, A de Candia, S Di Talia, E Giraudo, G Serini, L Preziosi, and F Bussolino. Percolation, morphogenesis, and Burgers dynamics in blood vessel formation. *Phys. Rev. Lett.*, 90:118101., 2003.

[15] A L Georges and M A Nugent. pH regulates vascular endothelial growth factor binding to fibronectin: A mechanism for control of extracellular matrix storage and release. *J Biol Chem*, 279(3):2307–2315, 2004.

[16] J A Glazier and F Graner. Simulation of the differential adhesion driven rearrangement of biological cells. *Phys Rev E*, 47:2128–2154, 1993.

[17] D Guidolin, B Nico, G Mazzocchi, A Vacca, G G Nussdorfer, and B Ribatti. Order and disorder in the vascular network. *Leukemia*, 18:1745–1750, 2004.

[18] D Guidolin, A Vacca, and G G Nussdorferand D Ribatti. A new image analysis method based on topological and fractal parameters to evaluate the angiostatic activity of docetaxel by using the matrigel assay in vitro. *Microvasc Res*, 67(2):117–124, 2004.

[19] K A Houck, D W Leung, A M Rowland, J Winer, and N Ferrara. Dual regulation of vascular endothelial growth factor bioavailability by genetic and proteolytic mechanisms. *J Biol Chem*, 267(36):6031–2603, 1992. 27.

[20] A Karperien. Fraclac for ImageJ, version 2. http://rsbweb.nih.gov/ij/plugins/fraclac/fraclac.html, 1999–2007.

[21] L Kirchner and P Schmidtand B Gruber. Quantitation of angiogenesis in the chick chorioallantoic membrane model using fractal analysis. *Microvasc Res*, 51:2–14, 1996.

[22] L Lai, L Bohnsack, K Niederreither, and K K Hirschi. Retinoic acid regulates endothelial cell proliferation during vasculogenesis. *Development*, 120:6465–6474, 2003.

[23] J Larsson, M J Goumans, L J Sjöstrand, M A van Rooijen, D Ward, P Levéen, X Xu, P ten Dijke, C L Mummery, and S Karlsson. Abnormal angiogenesis but intact hematopoietic potential in TGF-*beta* type I receptor-deficient mice. *EMBO J*, 20(7):1663–1673, 2001.

[24] Daniele Mancardi, Gianfranco Varetto, Enrico Bucci, Fabrizio Maniero, and Caterina Guiot. Fractal parameters and vascular networks: facts & artifacts. *Theor Biol Med Model*, 5:12, 2008.

[25] R M H Merks, S V Brodsky, M S Goligorksy, S A Newman, and J A Glazier. Cell elongation is key to in silico replication of in vitro vasculogenesis and subsequent remodelling. *Dev Biol*, 289:44–54, 2006.

[26] R M H Merks and J A Glazier. Dynamics mechanisms of blood vessel growth. *Nonlinearity*, 19:C1–C10., 2006.

[27] R M H Merks, S A Newman, and J A Glazier. Cell oriented modelling of in vitro capillary development. *LNCS*, 3305:425–434, 2004.

[28] R M H Merks, E D Perryn, A Shirinifard, and J A Glazier. Contact-inhibited chemotaxis in de novo and sprouting blood-vessel growth. *PLoS Comput Biol*, 4(9):e1000163., 2008.

[29] B Millauer, S Wizigmann-Voos, H Schnurch, R Martinez, N P Moller, W Risau, and A Ullrich. High affinity VEGF binding and developmental expression suggest Flk-1 as a major regulator of vasculogenesis and angiogenesis. *Cell*, 72:835–846, 1993.

[30] T Miura and R Tanaka. *In Vitro* vasculogenesis models revisited - measurement of VEGF diffusion in matrigel. *Math Model Nat Phenom*, 4(4):118–130, 2009.

[31] G Neufeld, T Cohen, S Gengrinovitch, and Z Poltorak. Vascular endothelial growth factor (VEGF) and its receptors. *FASEB J*, 13(1):9–22, 1999.

[32] B Nico, A Vacca, M De Giorgis, L Roncali, and D Ribatti. Vascular endothelial growth factor and vascular endothelial growth factor receptor-2 expression in the chick embryo area vasculosa. *Histochem J*, 33(5):283–286, 2001.

[33] J E Park, G A Keller, and N Ferrara. The vascular endothelial growth factor (VEGF) isoforms: Differential deposition into the subepithelial extracellular matrix and bioactivity of extracellular matrix-bound VEGF. *Mol Biol Cell*, 4:1317–1326, 1993.

[34] T J Poole, E B Finkelstein, and C M Cox. The role of FGF and VEGF in angioblast induction and migration during vascular development. *Dev Dyn*, 220(1):1–17, 2001.

[35] W S Rasband. Imagej. http://rsb.info.nih.gov/ij, 1997–2009.

[36] W Risau and V Lemmon. Changes in the vascular extracellular matrix during embryonic vasculogenesis and angiogenesis. *Dev Biol*, 125(2):441–450, 1988.

[37] W Rissau and I Flamme. Vasculogenesis. *Annu Rev Cell Dev Biol*, 11:73–91, 1995.

[38] V Robins. Computational topology for point data: Betti numbers of α-shapes. *Lect Notes Phys*, pages 261–274, 2002.

[39] C Ruhrberg, H Gerhardt, M Golding, R Watson, S Ioannidou, H Fujisawa, C Betsholtz, and D T Shima. Spatially restricted patterning cues provided by heparin-binding VEGF-A control blood vessel branching morphogenesis. *Genes Dev*, 16:2684–2698, 2002. Genes Dev 16.

[40] G Serini, D Ambrosi, E Giraudo, A Gamba, L Preziosi, and F Bussolino. Modelling the early stages of vascular network assembly. *EMBO J*, 22:1771–1779, 2003.

[41] T G Smith, G D Lange, and W B Marks. Fractal methods and results in cellular morphology - dimensions, lacunarity and multifractals. *J Neurosci Meth*, 69:123–136, 1996.

[42] S Soker, C M Svahn, and G Neufeld. Vascular endothelial growth factor is inactivated by binding to alpha 2-macroglobulin and the binding is inhibited by heparin. *J Biol Chem*, 268:7685–7691, 1993.

[43] SE Stringer. The role of heparan sulphate proteoglycans in angiogenesis. *Biochem Soc Trans*, 34(3):451–453, 2006.

[44] C Tolle, T Mcjunkin, and D Gorsich. An efficient implementation of the gliding box lacunarity algorithm. *Physica D*, 237:306–315, 2008.

[45] A Tosin, D Ambrosi, and L Preziosi. Mechanics and chemotaxis in the morphogenesis of vascular networks. *Bull Math Biol*, 68:1819–1836, 2006.

[46] S A Vokes and P A Krieg. Endoderm is required for vascular endothelial tube formation, but not for angioblast specification. *Development*, 129(3):775–785, 2002.

[47] M V Volin, L Joseph, M S Shockley, and P F Davies. Chemokine receptor CXCR4 expression in endothelium. *Biochem Biophy Res Co*, 242(1):46–53, 1998.

[48] S M Watt, S E Gschmeissner, and P A Bates. PECAM-1: Its expression and function as a cell adhesion molecule on hemopoietic and endothelial cells. *Leuk Lymphoma*, 17:229–244, 1995.

[49] E S Wijelath, S Rahman, M Namekata, J Murray, T Nishimura, Z Mostafavi-Pour, Y Patel, Y Suda, M J Humphries, and M Sobel. Heparin-II domain of fibronectin is a vascular endothelial growth factor-binding domain: Enhancement of VEGF biological activity by a singular growth factor/matrix protein synergism. *Circ Res*, 99(8):853–860, 2006.

[50] L Wolpert, J Smith, T Jessell, P Lawrence, E Robertson, and E Meyerowitz. *Principles of Development*. Oxford University Press, Oxford, third edition, 2006.

[51] L W Wu, L D Mayo, J D Dunbar, K M Kessler, M R Baerwald, E A Jaffe, D Wang, R S Warren, and D B Donner. Utilization of distinct signalling pathways by receptors for vascular endothelial cell growth factor and other mitogens in the induction of endothelial cell proliferation. *J Biol Chem*, 275(7):5096–5103, 2000.

[52] T P Yamaguchi, D J Dumont, R A Conlon, M L Breitman, and J Rossant. Flk-1 and Flt-related receptor tyrosine kinase is an early marker for endothelial cell precursors. *Development*, 118(2):489–498, 1993.

[53] M Zajac, G L Jones, and J A Glazier. Simulation of convergent extension by way of anisotropic differential adhesion. *J Theor Biol*, 222:247–259, 2003.

[54] E A Zamir, A Czirók, C Cui, C D Little, and B J Rongish. Mesodermal cell displacements during avian gastrulation are due to both individual cell-autonomous and convective tissue movements. *P Natl Acad Sci USA*, 103(52):9806–1981, 2006. 11.

[55] X Zhou, R G Rowe, N Hiraoka, J P George, D Wirtz, D F Mosher, I Virtanen, M A Chernousov, and S J Weiss. Fibronectin fibrillogenesis regulates three-dimensional neovessel formation. *Genes Dev*, 22(9):1231–1243, 2008.

Chapter 3

Accumulation of exogenous VEGF around endothelial cells guides *in vitro* vasculogenesis

Contents

3.1 Abstract

In this chapter several aspects of the theory of vascular patterning under consideration are tested in a controlled situation using an *in vitro* Matrigel assay

of HUVEC cells with exogenous administration of fluorescently labelled VEGF. In line with the theory of matrix-mediated VEGF signalling, experiments show that exogeneous VEGF accumulates around endothelial cells, matching up the regions where specific VEGF matrix molecules are also found. Combined mathematical and experimental analysis allows to estimate key kinetic parameters of VEGF, including the diffusion coefficient or the binding, unbinding and decay rates. Moreover, a specific and parametrized version of the proposed model for the Matrigel assays confirms that the retention of exogenous VEGF around HUVECs provides the necessary signals for *in vitro* vascular patterning.

3.2 Introduction

The theory for vascular patterning during embryonic vasculogenesis proposed in Chapter 2 holds that specific ECM molecules produced by vascular precursors are able to retain diffusive VEGF signals coming from adjacent tissues. The retention of those signals by the ECM would create spatially restricted guidance cues that in turn would allow cells to organize into reticular networks. Mathematical modelling and morphometric methods have shown that the matrix-mediated signalling mechanism under consideration is able to produce realistic vascular networks, and has provided specific, testable hypotheses on the spatial distribution of cells and signals. In particular, the model predicts the retention of VEGF in the vicinity of cells as a consequence of matrix-binding. In this chapter the accumulation of VEGF in the proximity of cells is tested in a controlled situation using an *in vitro* Matrigel assay of HUVECs with exogenous administration of fluorescent-labelled VEGF.

More precisely, it is shown that administration of exogenous VEGF is key for the *in vitro* vascular patterning process. Fluorescence recovery after photobleaching (FRAP) techniques are used to estimate the diffusion coefficient of VEGF in Matrigel. Also, it is shown that when HUVECs are present in Matrigel, exogenous VEGF accumulates around cultured HUVECs within 60 minutes. Moreover, the binding and unbinding rates of VEGF in those areas are estimated by FRAP analysis. Immunohistochemistry reveals that heparan sulfate proteglycans (HSPGs) and fibronectin are major candidates to retain VEGF. Also, ELISA assays allow to estimate VEGF decay in culture medium and shows that it is decreased in a cell density-dependent manner, suggesting the absorption of VEGF by the cells-produced ECM. Simulation of a mathematical model using actual concentrations and estimated kinetic constants confirms that network patterning is possible under the proposed theory. Moreover, perturbation of the spatially restricted cues

by addition of collagenase causes reduced network complexity or absence of network formation both *in vitro* and in simulation. Taken together, these observations demonstrate that vascular network formation in Matrigel assays depends on matrix-mediated retention of exogenous VEGF.

3.3 Mathematical modelling and analysis

3.3.1 Estimating local mass transfer: FRAP analysis

In order to get insight into the dynamics of exogenous VEGF molecules, we used FRAP methods. FRAP is a widely used technique to investigate transport and interactions of molecules [1, 5, 9, 12]. In FRAP experiments, fluorescence tagged molecules are irreversibly photobleached in a small region of interest (ROI) by a high-powered focused laser beam. Subsequent displacement of surrounding non-bleached fluorescent molecules into the bleached area leads to a recovery of fluorescence, which is recorded at low laser power. This allows for quantitative analyses that provide information about the motility and interactions of fluorescent molecules. In this study we fit experimental recovery curves to theoretical models and estimate kinetic rate constants such as the diffusion coefficient or binding/unbinding rates of fluorescently-labelled VEGF molecules present in Matrigel cultures.

First, the diffusion coefficient of VEGF in Matrigel in the absence of cells was estimated. To do this, a thin layer of Matrigel containing fluorescently-labelled VEGF was prepared (see Section 3.6 for the details). After the gel has solidified, a circular area of it is bleached and the recovery of the fluorescence in it is tracked until recovery saturates (see Figure 3.1 A). If the increase in fluorescence is interpreted on the basis of a linear diffusion model, a formula for the recovery of the fluorescence can be derived [5]:

$$frap(t) = F_\infty exp\left(-\frac{2}{1+8Dt/a^2}\right), \tag{3.1}$$

where F_∞ is the fluorescence after the recovery is complete, t is time and a is the radius of the bleached ROI. The unknown parameter D, the diffusion coefficient of VEGF, can be estimated by fitting (3.1) to the observed recovery. Doing so for eight different recovery data, the following estimate was obtained:

$$D \approx 5.87 \times 10^{-7} cm^2/s \quad \pm 1.7159 \times 10^{-7}, \tag{3.2}$$

which is consistent with estimates obtained by different methods [10].

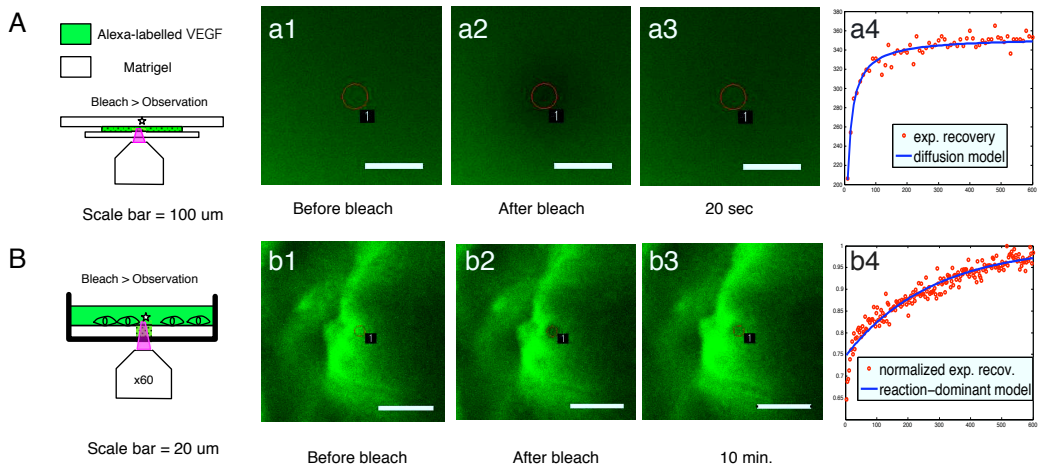

Figure 3.1: **FRAP analysis**. Two different FRAP experiments are shown in top and bottom lines. (A) FRAP experiment in Matrigel in the absence of endothelial cells. Panels (a1), (a2) and (a3) show the observed VEGF fluorescence in three different time points, while (a4) shows a fitting of the linear diffusion model to the obtained experimental recovery. (B) FRAP experiment in a culture of HUVECs in Matrigel. In this case the photobleached region is a small circunference in the proximity of an endothelial cell. Panels (b1), (b2), (b3) and (b4) are as in the previous case. The theoretical model used in this case to fit the obtained experimental recovery is the reaction-dominant model. Note that the spatial and temporal scales in both cases are different.

Next, the dynamics of exogenous VEGF was analyzed in the areas around HUVECs where VEGF accumulation can be observed (see Section 3.4.2 below). More precisely, a small circular region around a cell was photobleached (see Figure 3.1 B), the recovery of fluorescence was observed and models were used to obtain estimates for it. Contrary to the recovery in absence of cells, theoretical curves due to diffusion do not fit well the observed experimental data. Moreover, the closest theoretical curve (in the least-squares sense) to the experimental data gives a very small diffusion coefficient. As a matter of fact, the estimated diffusion of VEGF in the previous case cannot be observed in this experiment due to the small size of the ROI and the time scale of the fluorescence measurements that are used. In order to show the previous statement in a rigorous way, one can use an analytical formula for the concentration of the fluorescent molecule after photobleaching. Then, one can substitute therein the particular size and the estimated diffusion coefficient of VEGF and look at the time evolution of the concentration in the time scale of the experiment. More precisely, the concentration, c, of the fluorescent molecule at position r, and at time t is given by [5]:

$$c(r,t) = c_0 \left(1 - \frac{exp(-r^2/4Dt)}{2Dt} \int_0^a exp(-r'^2/4Dt) I_0 \left(\frac{rr'}{2Dt}\right) r' dr'\right), \qquad (3.3)$$

where D is the diffusion of the molecule, r is the distance from the optical axis, t is time, a is the radius of the bleached ROI, c_0 is the initial concentration for all $r > a$, and I_0 is the modified Bessel function of the first kind of order zero. Figure 3.2 shows the time evolution of the concentration c in (3.3) using the estimated diffusion coefficient shown in (3.2), and the size of the ROI, a, used in Figure 3.1 B. Note that after 3 seconds, which is the time interval used in the experiment under consideration, the concentration is almost constant and very close to the concentration of the fluorescence outside the ROI, c_0. Therefore, the recovery due to diffusion of free VEGF is not captured in this experiment. Thus, the observed recovery of fluorescence in this case involves a different underlying mechanism.

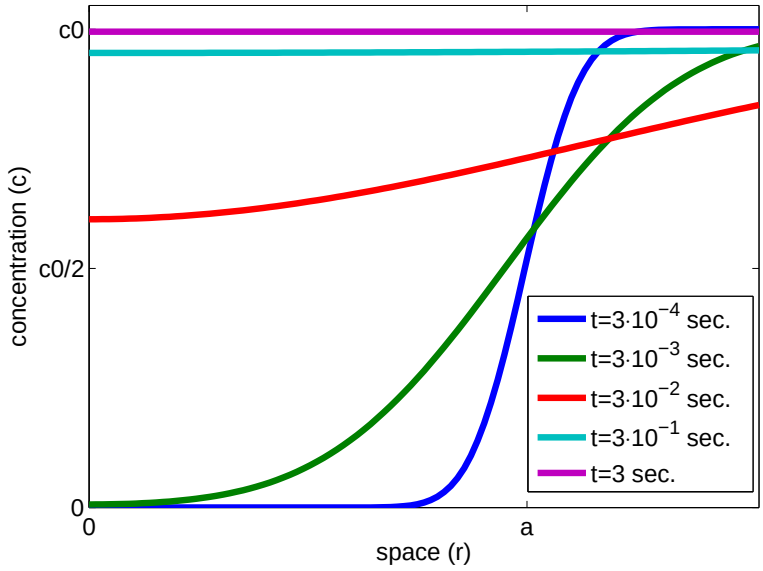

Figure 3.2: **Diffusion in a circular region (CR) after photobleaching**. The evolution in time of the concentration of fluorescent VEGF is shown with respect to the radial distance from the optical axis. After photobleaching, the concentration profile inside the CR ($r < a$) increases from zero to c_0 in 3 seconds.

As shown in Section 3.4.3 below, the regions where VEGF is accumulated match the distribution of some VEGF binding molecules of the ECM. Therefore, it seems reasonable to fit fluorescence recovery with a model that accounts for binding processes. A realistic case of binding that can be analyzed by FRAP con-

sist of a single binding interaction, described by the following chemical equation:

$$VEGF_u + ECM_s \underset{k_{on}}{\overset{k_{off}}{\leftrightarrows}} VEGF_b, \tag{3.4}$$

where $VEGF_u$ and ECM_s denote unbound VEGF molecules and specific binding sites of the ECM, respectively, and $VEGF_b$ represents bound VEGF. In general, the equations describing the preceding binding reaction also incorporate diffusion:

$$\frac{\partial u}{\partial t} = D_u \Delta u - k_{on} us + k_{off} b \tag{3.5}$$

$$\frac{\partial s}{\partial t} = D_s \Delta s - k_{on} us + k_{off} b \tag{3.6}$$

$$\frac{\partial b}{\partial t} = D_b \Delta b + k_{on} us - k_{off} b \tag{3.7}$$

where $u = [VEGF_u], s = [ECM_s]$ and $b = [VEGF_b]$ denote the corresponding concentrations. These equations can be simplified by a number of assumptions that are applicable in the biological situation under consideration [1]. A first simplifying assumption is that binding sites are part of a large, relatively immobile complex, at least on the time- and lenght-scale of the FRAP measurement. Then, diffusion of binding sites and bound complexes can be ignored, i.e, $D_s = D_b = 0$. Another simplifying assumption is based on the fact that fluorescence molecules and binding sites are typically at a constant level by the time the FRAP experiment is performed (from seconds to several minutes). Accordingly, we can assume that the system has reached equilibrium before photobleaching. We denote the corresponding equilibrium concentrations of $VEGF_u, ECM_s$ and $VEGF_b$ by U_{eq}, S_{eq} and B_{eq}. Althought the act of bleaching changes the number of visible free and complexed molecules $VEGF_u$ or $VEGF_b$, it does not change the number of free binding sites. Therefore $s = S_{eq}$ is a constant throughout the photobleaching recovery. Then we can eliminate equation (3.6) and also replace the variable s in (3.5) and (3.7) with the constant value. As a result, we can define a pseudo-first-order rate constant as $k^*_{on} = k_{on} S_{eq}$. Then, equations (3.5), (3.6), (3.7) reduce to:

$$\frac{\partial u}{\partial t} = D_u \Delta u - k^*_{on} u + k_{off} b \tag{3.8}$$

$$\frac{\partial b}{\partial t} = k^*_{on} u - k_{off} b \tag{3.9}$$

While an analytical solution for (3.8), (3.9) can be obtained [1], here a particular case of that model is used that adequately describes the recovery of the fluorescence in a tiny bleached area near a HUVEC cell. This particular case is commonly known in this context as reaction-dominant model and describes a sce-

nario where diffusion is very fast compared both to binding and to the timescale of FRAP measurements [1]. In other words, diffusion is not detected in the FRAP recovery, as it was shown before. As a consequence, one can assume that free molecules instantly equilibrate after the bleach, i.e., $u = U_{eq}$. Thus, (3.8) disappears and (3.9) becomes:

$$\frac{\partial b}{\partial t} = -k_{off} b + k^*_{on} U_{eq} \tag{3.10}$$

Note that the second term on the right hand side in the preceding equation is constant, so this is a first-order linear equation whose solution is given by:

$$b(t) = (k^*_{on} U_{eq}/k_{off}) + Ae^{-k_{off}t} \tag{3.11}$$

In order to evaluate the constant A in (3.11) recovery data can be normalize to lie between 0 and 1. More precisely, we assumes that after normalization the concentration of fluorescence in the bleached zone is zero, i.e., $b(0) = 0$. Then, $A = -k^*_{on} U_{eq}/k_{off}$, which leads to:

$$b(t) = k^*_{on} U_{eq}/k_{off} \left(1 - e^{-k_{off}t}\right) \tag{3.12}$$

Due to normalization, we also assume:

$$U_{eq} + B_{eq} = 1 \tag{3.13}$$

Equation (3.12) yields the behaviour for the bound complex of fluorescent protein. Total fluorescence is:

$$frap(t) = b(t) + u(t) = U_{eq} + k^*_{on} U_{eq}/k_{off} \left(1 - e^{-k_{off}t}\right) \tag{3.14}$$

Before the bleach, as noted above, the system is at equilibrium, and U and B have achieved steady-state values, U_{eq} and B_{eq}, then:

$$\frac{\partial u}{\partial t} = \frac{\partial b}{\partial t} = 0 \;\; \Rightarrow \;\; k^*_{on} U_{eq} = k_{off} B_{eq} \;\; \Rightarrow \;\; k^*_{on} U_{eq}/k_{off} = B_{eq} \tag{3.15}$$

Using (3.13), (3.14) and (3.15), we obtain:

$$frap(t) = u(t) + b(t) = 1 - \frac{k^*_{on}}{k^*_{on} + k_{off}} e^{-k_{off}t} \tag{3.16}$$

Then, fitting the previous formula to the experimental FRAP recovery yields estimates for k^*_{on} and k_{off}. Doing so for six different recovery data, the following

figures were obtained:

$$k_{on}^{*} \approx 1.5 \times 10^{-3} s^{-1} \pm 2.87 \times 10^{-4} \tag{3.17}$$

$$k_{off} \approx 3.6 \times 10^{-3} s^{-1} \pm 3.68 \times 10^{-4} \tag{3.18}$$

In order to estimate k_{on} from k_{on}^{*} we would need the equilibrium concentration of binding sites, S_{eq}, which is unknown. However, we can use estimated dissociation constants of VEGF to matrix molecules as fibronectin or HSPG, defined as $K_d = k_{off}/k_{on}$, that are available in the literature [8]. In this study, K_d has been shown to depend on pH and Heparin concentration, but a suitable estimate for such parameter would be around $100nM = 10^{-7}M$. Therefore,

$$k_{on} = \frac{k_{off}}{K_d} = 3.6 \times 10^{4} M^{-1} s^{-1}, \tag{3.19}$$

a figure that is consistent with reported binding rates of VEGF to HSPG [18].

3.3.2 A parametrized mathematical model for *in vitro* vasculogenesis

The quantitative analysis by means of FRAP provides insight into the dynamics of VEGF in Matrigel assays. Importantly, these results are in line with the hypothesis that specific ECM molecules produced by HUVECs act to retain VEGF around cells. To study whether this mechanism can guide cells into the formation of network patterns a parametrized version of the hybrid model use in Chapter 2 is used. The mechanisms and the main structure of the mathematical model describing vasculogenesis *in vivo* remain unchanged. However, several changes have been made to adapt the model to the particular *in vitro* experimental conditions, where most model parameters have been estimated. Below, the main assumptions made for the formulation of the model are summarized:

(1) HUVECs are seeded on top of a planar Matrigel surface and once they lie on it, their vertical displacement is small. Therefore, the problem can be reduced to a 2D configuration.

(2) Initially, the culture medium contains a homogeneous concentration of soluble, unbound VEGF. VEGF diffuses through the medium and the Matrigel and it can bind (and unbind) to various ECM molecules such as heparan sulphates or fibronectin. For simplicity, it is assumed that such a reversible binding reaction follows the mass action law.

(3) HUVECs produce ECM components able to bind VEGF, such as fibronectin and heparan sulphates. As those molecules have a higher molecular weight than VEGF and they can bind to many other molecules of the ECM, the effective diffusivity of molecules with VEGF binding capacity, as well as VEGF bounded to them is assumed to be very small compared with the diffusivity of unbound VEGF.

(4) Bound forms of VEGF provide stronger signalling cues for cell motility than freely difusive forms [2, 13]. Consequently, motility is biased in the model towards upward gradients of anchored growth factors, while chemotaxis towards freely diffusive forms is neglected.

(5) Binding of VEGF to ECM molecules offers protection to growth factors against enzymatic degradation [4,16]. Therefore, degradation or removal of bound growth factors are neglected in the model.

(6) No proliferation or cell death is taken into account during the modelled time window.

Let u, s and b be the concentrations of $VEGF_u$, ECM_s and $VEGF_b$, respectively. Bearing in mind assumptions (2) and (3) above, the following reaction-diffusion system is proposed:

$$\begin{aligned} \frac{\partial u}{\partial t} &= D_u \Delta u - k_{on} u s + k_{off} b - \epsilon u \\ \frac{\partial s}{\partial t} &= D_s \Delta s + \gamma - k_{on} u s + k_{off} b \\ \frac{\partial b}{\partial t} &= D_b \Delta b + k_{on} u s - k_{off} b, \end{aligned} \tag{3.20}$$

where D_u, D_s and D_b are the diffusion coefficients of $VEGF_u$, ECM_s and $VEGF_b$ respectively. The parameters k_{on}, k_{off} and ϵ represent the binding, unbinding and decay rates of VEGF respectively. The function γ represents the production rate of VEGF binding sites by HUVECs ($\gamma = 0$ in sites that are not occupied by cells).

Cells are represented on a discrete square lattice. The same index $\sigma = 1, 2, ..., N$ labels all the lattice sites, x, occupied by a particular cell, while the special index $\sigma = 0$ labels all lattice sites occupied by the extracellular medium. The interfaces between two different lattice sites, x and x' with different index σ_x and $\sigma_{x'}$ represent the membrane boundaries between two cells or between a cell and the medium. Cell shape and position of cells is determined by volume and perimeter constraints plus a biased (chemotactic) movement towards bound VEGF. More precisely, the state of the system is defined by means of the following Hamiltonian:

$$H = \sum_{\sigma>0} (\lambda_a (a_\sigma - A)^2 + \lambda_p p_\sigma), \tag{3.21}$$

where the term $(a_\sigma - A)$ represents the deviation of a cell labelled with the index σ from a target area A and p_σ is the total perimeter of the same cell. The parameters λ_a and λ_p represent the strength of the area and perimeter constraints respectively.

Dynamics in the discrete lattice are generated by a modified Metropolis algorithm that randomly chooses a lattice site, x', and computes what the difference in energy, ΔH, will be if a randomly selected neighboring site, x, would copy its state into this site. The probability of accepting the change, P, depends on the difference in the energy and a chemotactic energy term $\Delta H_c = \Delta H - \mu(b_{\mathbf{x}'} - b_{\mathbf{x}})$:

$$P(\Delta H_c) = \begin{cases} 1 & \Delta H_c \leq 0 \\ e^{-\Delta H_c} & otherwise \end{cases} \tag{3.22}$$

In this way, cell shape and position is updated locally such that cells shape is biased towards a target area and minimum perimeter and the movement is biased up the gradients of $VEGF_b$.

In order to parameterize the model according to the *in vitro* situation, the estimates obtained in this chapter using own experimental data for VEGF concentrations, diffusion coefficient, half-life, and binding/unbinding rates will be used. Moreover, quantitative image processing allows to estimate also average cell sizes and cell densities in the Matrigel cultures. On the other hand, the chemotactic sensitivity parameter μ has been estimated by comparison to the response of HUVEC cells to quantified gradients of VEGF as reported in Reference [15]. Using a microfluidic device, those authors generated stable and precise linear gradients (14 ng/mL/mm) of VEGF with concentrations between $18 - 32$ ng/mL in the presence of fibronectin (10 μg/mL), and measured the migration of cells towards regions of higher concentrations. These concentrations are reported below receptor saturation concentrations [19] and comparable to the ones used in our in vitro assays. In line with the experimental setup, a stable gradient of bound VEGF and a random distribution of cells is simulated and then cell displacement are measured over a period of 6 hours by recording the change in occupancy in four equally sized regions (250μm). Fitting the results from simulation with the reported cell migration, an estimate for chemotactic sensitivity $\mu = 10^7$, can be obtained, see Figure 3.3.

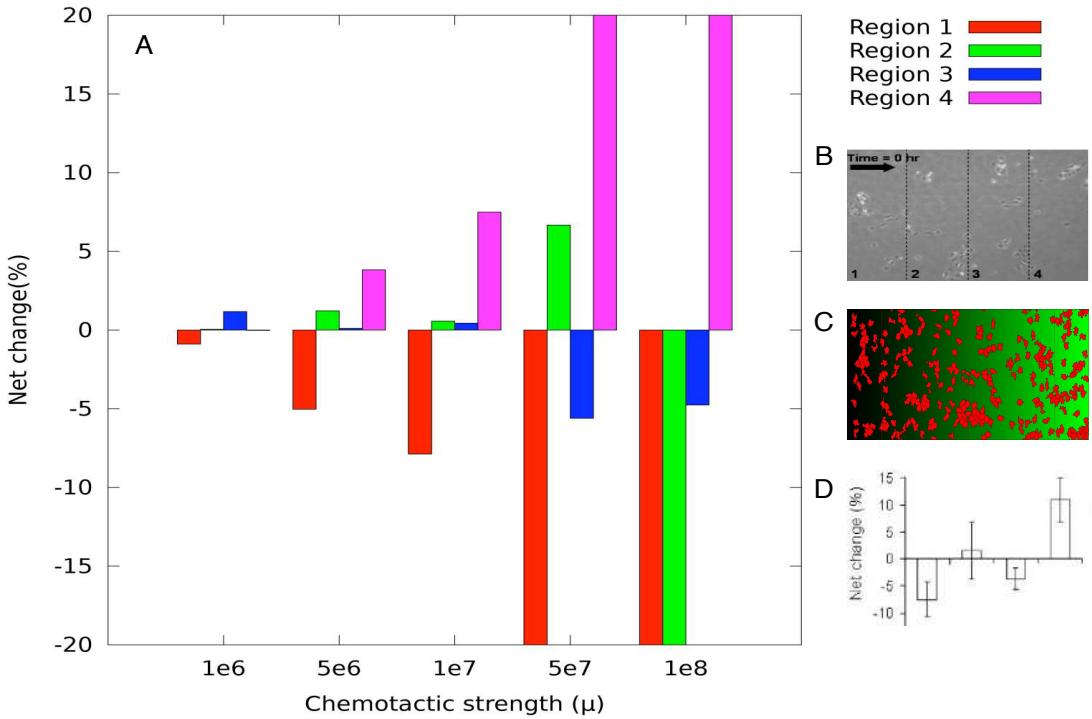

Figure 3.3: **Chemotactic strength estimate**. (A) Simulation results using different values for the chemotactic strenght parameter, μ, are shown. The net change in cells occupancy after 6 hours was quantified in four equally sized regions of the simulated cultures. (B) Experiments used in Ref. [15]. (C) Simulated experiment displaying cells in red and the VEGF gradient in green. (D) Experimental results reported in Ref. [15] after 6 hours.

3.4 Results

3.4.1 Exogenous VEGF is key for network patterning

In previous studies discussed in Chapter 1, it is assumed that VEGF secreted by cells plays a key role during *in vitro* vascular patterning [7, 14]. However, considerable amount VEGF not produced by cells exists in the culture medium. To evaluate the relevance of exogenous VEGF in the specific experimental conditions under consideration, HUVEC cultures containing exogenous VEGF (control) are compared with cultures where VEGF was previously removed from the culture medium. Specifically, normal EGM-2 medium (containing VEGF) is used for control cultures and additional cultures are prepared with VEGF-free EGM-2 medium. It was observed that network formation is dramatically reduced in the VEGF-free case as compared with the network formed in the presence of VEGF (see Figure 3.4). In particular, the number and total length of cell protrusions were decreased, indicating that exogenous VEGF in the culture medium, instead

of VEGF produced by HUVECs, if any, is key for network patterning.

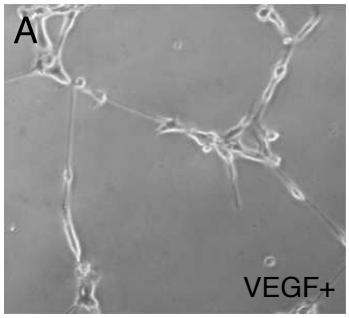

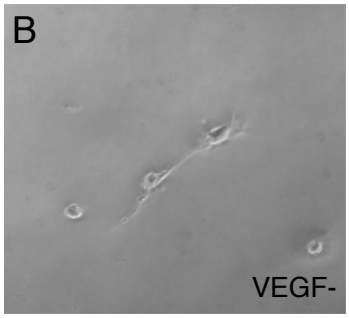

C	VEGF+	VEGF-
No of protrusion	297	117
Average length	29.2	27.6

Figure 3.4: **Exogenous VEGF is key for *in vitro* vascular patterning**. (A), (B) show representative images of HUVECs in the control (VEGF+) and VEGF-free (VEGF-) settings. (C) Quantitative comparison of cells protrusion number and average length of protrusions between the two cases.

3.4.2 Exogenous VEGF is absorbed around cultivated HUVECs

In order to experimentally test the accumulation of VEGF around cells, HUVECs on a thin layer of Matrigel were cultured for 10 hours. Then, 1 µg/ml solution of fluorescently-labelled VEGF was applied on the culture dish and observed for 60 min as described in Appendix 3.6 on Materials and Methods. Accumulation of fluoresecently-labelled VEGF around cells was observed within 5-10 minutes. The fluorescence became saturated after that and the concentration around cells did not change much. However, there were subtle background changes after that period, that resulted in equilibrium after 60-90 minutes. A comparison of fluorescent and brightfield images shows that the absorption occurs mainly at the extracellular region near the cells and is not confined to the cell membrane (see Figure 3.5).

3.4.3 VEGF binding molecules colocalize with VEGF absortion areas

To investigate the reason behind the accumulation of fluorescently-labelled VEGF in the proximity of HUVECs, VEGF binding molecules were labelled in cultures by means of immunohistochemistry. We found out that two ECM molecules that bind strongly to VEGF, fibronectin and HSPG, colocalize with VEGF absorption areas in the vecinity of HUVECs (see Figure 3.6). To what extent those

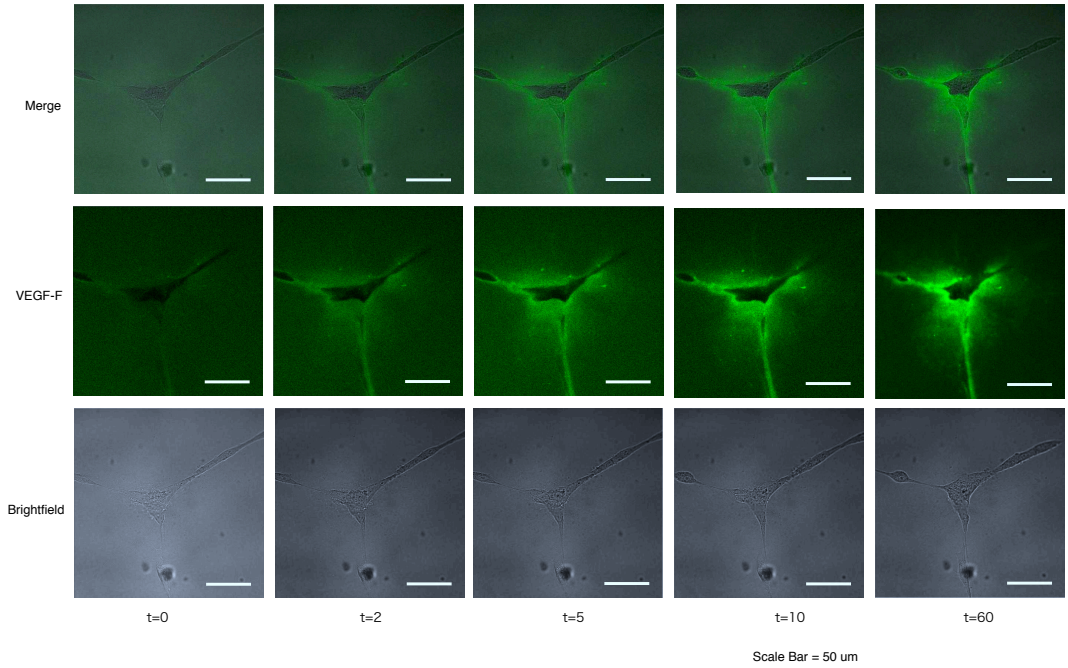

Figure 3.5: **Absorption of VEGF around endothelial cells**. Time-lapse of fluorescent and brightfield images showing typical observed accumulation of fluorescently-labelled VEGF (VEGF-F) around HUVECs (Brightfield). A superposition of both image types is shown in the top line (Merge).

ECM molecules are secreted or redistributed by HUVECs is not clear. Although expressions of both fibronectin and HSPG in HUVECs have been reported, an active reorganization by endothelial cells of the existing VEGF binding molecules in Matrigel cannot be excluded. Transmission Electron Microscopy (TEM) was used to examine the structure of Matrigel in the cultures. TEM does not reveal regions devoid of Matrigel in the cultures but a considerably uniform structure of Matrigel with a slightly denser fiber texture in the proximity of cells. Consequently, the reason for localization of VEGF and VEGF binding molecules in the proximity of cells is not the accumulation of the whole extracellular material around them. Taken these results together, fibronectin and HSPG are considered as candidates that retain VEGF in the proximity of HUVECs.

3.4.4 VEGF in the cultured medium is decreased in a cell density-dependent manner

VEGF decay in the culture medium was quantified by means of ELISA assays (see Materials and Methods in Appendix 3.6). More precisely, ELISA assay was used to measure the evolution of VEGF concentration in culture medium alone (without Matrigel or cells) and in mediums extracted from cell cultures contain-

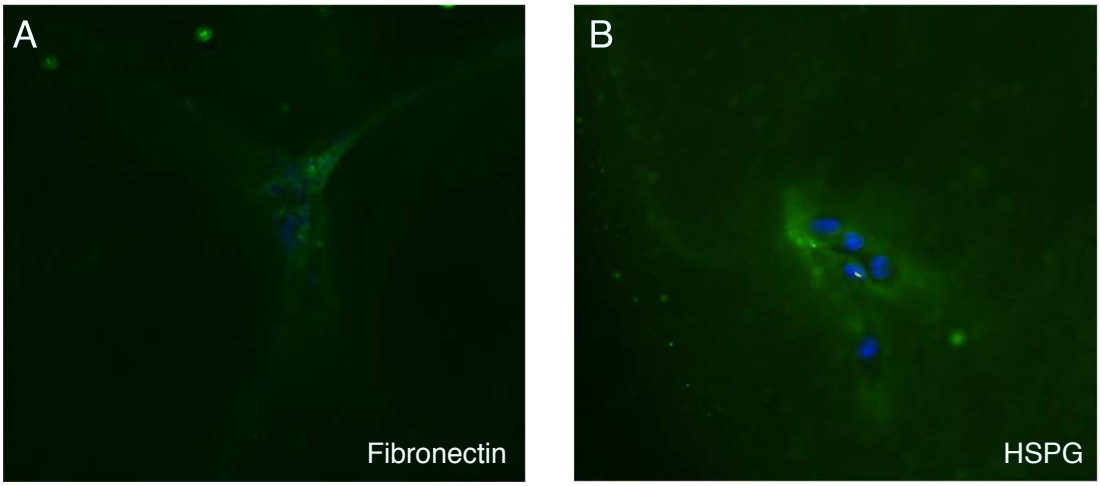

Figure 3.6: **Immunohistochemistry of VEGF binding molecules**. Fluorescent staining of fibronectin (A) and HSPG (B) around HUVECs. Cells nuclei are stained in blue.

ing different cell densities. In the first case, decay is mainly due to molecular degradation. According to ELISA results, an estimate of VEGF half-life is above 72 hours (see Figure 3.7), which is much higher than that used in previous studies [14]. In the second case, decay is a result not only of molecular degradation but also due to matrix-binding or cell uptake. It was found that VEGF concentration in the culture medium is reduced in a cell density-dependent manner. Specifically, VEGF concentration was measured in the culture medium before and after HUVEC culture on Matrigel for 18 hours. A significant reduction of VEGF was detected (see Figure 3.8). Moreover, the reduction was greater when cell density was higher, indicating that the decrease of VEGF is not due to general absorption by Matrigel or culture dish.

3.4.5 Model simulations mimic *in vitro* HUVEC cultures

After investigating VEGF dynamics in HUVEC cultures, the mathematical model described in Section 3.3.2 was used to see whether the estimated kinetics of VEGF can drive HUVECs aggregation and patterning. Model simulations show that cells form reticular network patterns based on matrix-mediated retention of chemoattractant signals within the estimated range of biophysical parameters provided that the cell density is high enough (see Figure 3.9). Moreover, the model is able to mimic an experiment where network formation is perturbed. More precisely, if network formation depends on spatially restricted guidance cues of VEGF absorped on cell-produced ECM, perturbing these spatial cues is expected to hamper

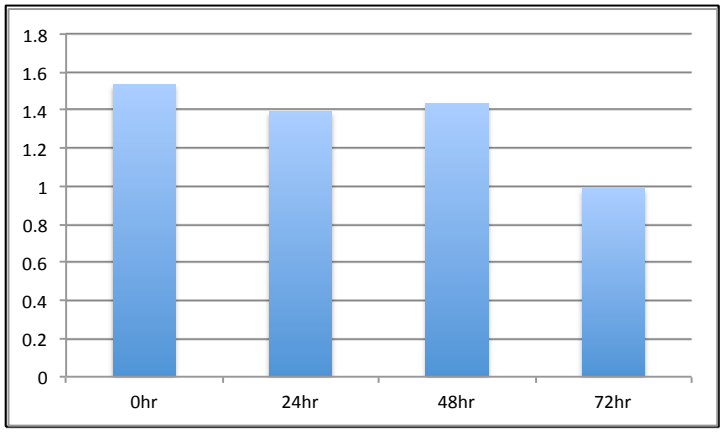

Figure 3.7: **VEGF decay**. VEGF concentration measured in EGM-2 culture medium at different incubation times.

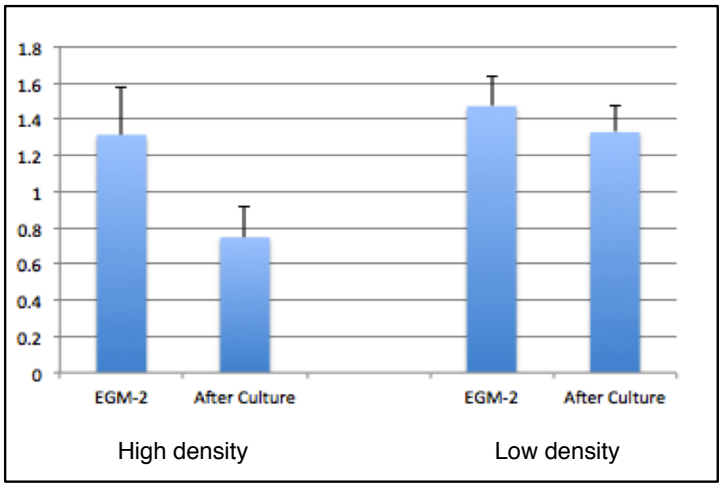

Figure 3.8: **VEGF decay in HUVEC cultures**. VEGF concentration in the culture medium measured before (EGM-2) and after HUVEC culture on Matrigel for 18 hours (After Culture). Two different cell densities were used and VEGF was found to decrease faster in the high density case.

network formation. In HUVEC assays, adding collagenase to the medium breaks peptide bonds in collagen, an abundant component in Matrigel, which presumably increases the motility of those matrix molecules. Because the main candidates for VEGF binding molecules in our culture system (HSPG and fibronectin) are known to strongly bind collagen, administration of collagen is assumed to distort the fine-grained spatial cues. In our model, increasing the diffusion coefficients of VEGF binding sites and the associated bound VEGF (D_s and D_b) has a similar effect. Indeed, comparison of model simulations with *in vitro* assays under varying amounts of collagenase shows that an increase in motility of matrix components

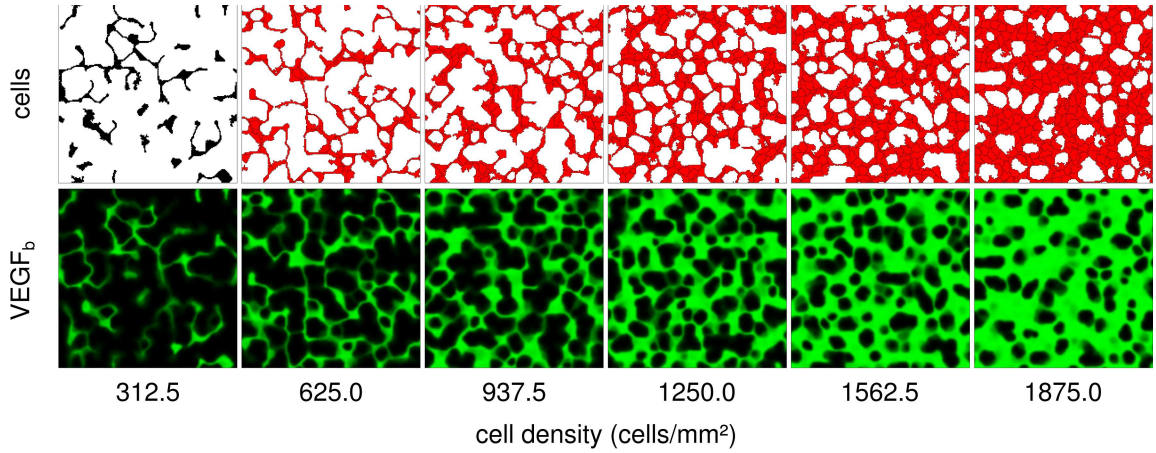

Figure 3.9: **Model simulations**. Simulated cellular patterns and bound VEGF distributions at 4000 MCS are shown over a range of different cell densities. Initially, cells were distributed all over the domain on a regular grid while the concentration of soluble VEGF was constant and equal to the one used in the Matrigel assays. The initial concentration of bound VEGF was assumed to be zero.

with VEGF binding sites sharply reduces network complexity (see Figure 3.10). These results further indicate that HUVECs make use of guidance cues retained by cell-produced matrix molecules.

3.5 Discussion

In order to unravel the role of VEGF in guiding angioblasts during embryonic vasculogenesis, it is necessary to describe in detail the spatiotemporal dynamics of VEGF molecules during this process. VEGF gene expression in the embryo has been reported in several studies (see for instance Ref. [11]). However, no data are available in the literature on the precise distribution and concentrations of VEGF molecules during embryonic vasculogenesis. As a matter of fact, the physiological concentration of VEGF seems to be very low and this complicates the task of labelling and imaging those molecules. Moreover, fixing the embryo, a usual procedure for molecular labelling, does not allow to analyze the dynamics and kinetic properties of VEGF. In view of these problems, this study used an *in vitro* Matrigel assay of HUVECs with exogenous administration of fluorescently-labelled VEGF, where dynamic and quantitative analysis of VEGF is possible provided that the used concentrations are high enough to be dectected under confocal microscopy. As high concentrations of VEGF are known to severly impact cell behaviours, studies with fluorerescent VEGF were only used in this study to test the accumulation of VEGF around cells and to investigate the kinetic properties

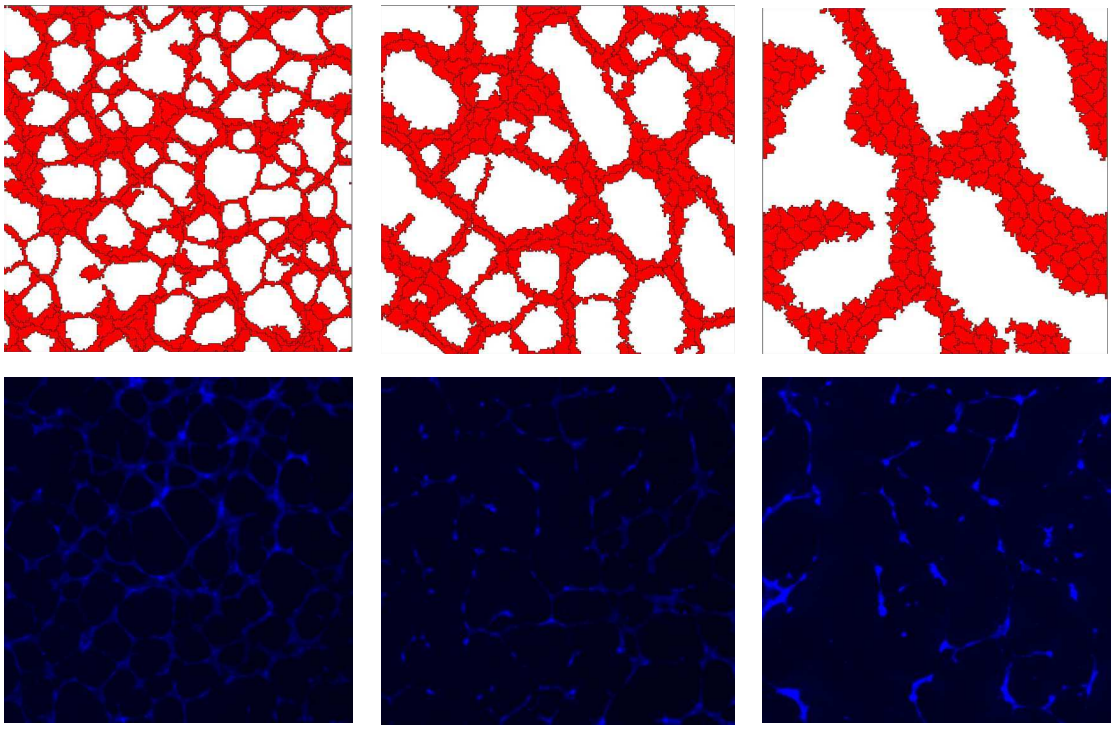

Figure 3.10: **Collagenease experiment**. Three HUVEC cultures containing different amounts of collagenease are compared with model simulations where the diffusion of binding sites and bound VEGF, D_s and D_b in model (3.20), respectively, was increased from 0 to 0.5.

of VEGF in the assays by means of FRAP. However, to study network formation of HUVECs low concentrations of VEGF were used, see Section 3.6.

Despite the large differences between *in vivo* vasculogenesis and the Matrigel assays under consideration, this study suggests that there are paralelisms in the mechanisms underlying patterning. As shown by means of mathematical modelling and simulations, a uniform distribution of VEGF (produce by the endoderm *in vivo* and externally added *in vitro*) can result in non-homogeneous configurations that drive cells into network patterns, when bound to specifc ECM molecules produced by cells. This view is is contrast with previous models for similar Matrigel assays that have assumed an autocrine source of VEGF as the driving force for patterning [3, 7, 14]. The autocrine hypothesis was supported in Reference [14] by showing that individual cell trayectories were directed toward zones of high cell concentration. However, those data are also in line with the matrix-binding theory proposed here. Moreover, the fact that Matrigel cultures without exogenous administration of VEGF fail to generate networks invalidates the autocrine hypothesis, at least in the experimental setup used here. Another important difference between previous works and this study is that the estimated

half-life of VEGF used for simulations was very small compared to the one estimated here. As a matter of fact the decay in VEGF concentration measured in those studies was performed in mediums cultured with cells for different times (see [14]). Therefore, the decay was not only due to molecular degradation, but also due to other processes as cell uptake or matrix-binding.

An important insight obtained in the present study is that the dynamics of VEGF in Matrigel is different when cells are present. Fluorerescent labelling clearly shows that exogenous VEGF accumulates in extracellular regions around HUVECs. In thoses areas close to cells, the binding and unbinding rates of VEGF were estimated by means of FRAP. As the size of those areas are of the order cell size, the bleached area in the experiment has to be small and it does not allow to observe diffusion of free VEGF molecules, which is a faster process than binding.

The parametrized model used in this chapter generates networks from disperse, isolated cells, but quantification and comparison of simulated and experimental patterns have not been accomplish yet. Although the tools developend in Chapter 2 can be used to quantify both patterns further work is needed to obtain and segment images from *in vitro* cultures that are needed for quantification. Preliminary work in this direction indicates that the model is able to reproduce only the initial period of the culture. As a matter of fact, it has been shown in other studies (see Refs. [6, 17]) that after after an initial period of 2-3 hours, mechanical tractions of cells in Matrigel, a mechanism that has been neglected in the present model, have an important effect in the observed patterns.

3.6 Appendix: Materials and Methods

Simulations

Numerical simulations were performed using the modeling software Morpheus developed by members of Prof. A. Deutsch group at Technische Universität Dresden in collaboration with the author. The modified Metropolis algorithm governing cell motility in the cellular Potts module (CPM) was specified with temperature T=1 and a 8-pixel neighborhood. Random numbers were generated using Mersenne Twister algorithm (mt19937) available in C++ TR1 library extensions. Reactions in the PDE module were solved using the 4th order Runge-Kutta method with time step dt=1.0, i.e. once every Monte Carlo step. Diffusion was solved using Euler forward diffusion using time steps that are chosen as to satisfy the Courant-Friedrichs-Lewy condition for the given length interval and diffusion coefficient. Space discretization was chosen equal for the CPM and PDE

models.

Network formation assay

Human Umbilical Vein Endothelial Cells (HUVECs) were purchased from Lonza Inc. and maintained in EGM-2 culture medium. Culture medium was changed every 2 days. Cells with less than 10 passages were used for experimentation. Matrigel solution (BD Biosciences) was prepared on ice. 50 µl of Matrigel was spread in the center well of 35 mm glass-bottom dish (Matsunami Glass inc.). The dish was kept at room temperature for 10 min to allow the Matrigel to solidify. HUVECs in a different chamber were detached from dish using 0.1% Trypsin-EDTA solution (Nacalai Tesque inc). The cells were centrifuged, trypsin solution was removed and resuspended in EGM-2 culture medium. Cells were seeded on Matrigel-covered dish in various cell densities. In some cases Type I Collagenase (Sigma) was added to the culture medium. The dish was cultivated 18 hours, and pattern formation was observed using inverted microscope (Nikon TMD or Nikon Eclipse). For VEGF-free condition, we prepare EGM-2 culture medium without VEGF supplement and use it for the experiment.

Absorption of fluorescently-labelled VEGF around HUVECs

Recombinant Human VEGF protein was purchased from Peprotech Inc. 100 µg of the protein were covalently conjugated with Alexa-488 fluorescent dye using microscale protein labeling kit according to the manufacturers protocol (Molecular Probes Inc.). We used 4.7 µl dye solution for labeling 100 µg VEGF protein, and fluorescently-labelled protein was purified from unbound dye using gel filtration column according to the manufacturers protocol. The labelled protein has a biological acitivity monitored by induction of dpERK in HUVEC (data not shown). HUVECs were seeded on a thin layer of Matrigel on 35 mm glass-bottom dish as described above. The cells were cultivated for additional 10 hours at 37 °C in a humidified atomosphere. Then the dish was moved to stagetop incubator on Nikon C1 confocal microscope. 1 µg/ml of fluorescently-labeled VEGF was prepared by mixing the EGM-2 culture medium with 1 µg/ml stock solution. The working solution was prewarmed in the stagetop incubator. The culture medium in the culture dish was completely removed, and fluorescent VEGF-containing culture medium was added to the culture dish. Then the absorption of fluorescently-labeled VEGF was observed at x60 magnification using Nikon C1 confocal microscope. Brightfield and fluorescence images were captured every minute.

Fluorescence Recovery After Photobleaching (FRAP)

FRAP experiments in the Matrigel region were done using thin layer of Matrigel. First we mixed 1 µg of fluorescently-labeled VEGF to 100 µl of phenol-red free Matrigel (BD Biosciences) on ice. 3 µl of VEGF-F containing Matrigel solution was put on a slideglass, and covered by a coverglass of 18 x 18 mm size (Matsunami Glass Inc.). The Matrigel on the slide was allowed to solidify for 10 min at room temperature in a moisture chamber. Then the slide was put in the stagetop incubator, and the sample was photobleached at x20 lens. The bleach spot size is around 2000 μm^2, and the recovery time is 60 frames with 10 second interval.

FRAP experiments in the proximity of cells were performed using the HUVEC after absorption of fluorescently-labelled VEGF has reached equilibrium, which occurs in 60-90 minutes. The spot size was kept 10 μm^2, and the recovery was observed for every 3 seconds for 200 frames.

Immunohistochemistry

HUVECs were cultivated for 18 hours on thin layer of Matrigel as described above. The cells were fixed in 100% Methanol for 10 minutes. The nonspecific binding was blocked using 1.5% NGS, and primary antibody against HSPG (Seikagaku Kogyo Inc. 10E4) or fibronectin (SC-69682 Santa Cruz biotechnology inc.) was added overnight at 4 degree. For HSPG, the culture dish was washed three times with PBS to remove unbound primary antibody. Then the biotin-conjugated secondary antibody was added to the dish, incubated for 30 min at room temperature, and FITC-avidin was used to visualize the distribution. For Fibronectin immunohistochemistry, we washed the dish, incubate in Alexa 488-labelled secondary antibody. In both cases, nuclei were stained with Hoechst 33342 to clarify the location of cells.

Sandwich ELISA

100 µl of capture antibody were applied to each well of the 96-well plate and incubated overnight. Then each well were washed with wash buffer. Nonspecific binding was blocked by blocking buffer. After these preparations, dilutions of unknowns and standards were applied to the wells, and incubated for two hours at room temperature. Then the wells were washed with wash buffer. Biotynilated detection antibody was applied to the well and incubated for 2 hours at room temperature. After wash, 100 µl of Streptavidin-HRP was added to each well and incubation was performed for for 20-30 minutes at room temperature. Then

the substrate was washed away, 100 µl of substrate solution (R&D systems) was added to each well and incubated for 20-30 minutes at room temperature to develop color. Then 50 µl of stop solution was added to each well. The optical density of each well was determined within 30 minutes with microplate reader (Thermo Fisher Multiskan FC).

3.7 References

[1] B L Sprague. andR L Pego, D A Stavreva, and J G McNally. Analysis of binding reactions by fluorescence recovery after photobleaching. *Biophys J*, 86(6):3473–3495, Jun 2004.

[2] T T Chen, A Luque, S Lee, S M Anderson, T Segura, and M L Iruela-Arispe. Anchorage of VEGF to the extracellular matrix conveys differential signaling responses to endothelial cells. *J Cell Biol*, 188(4):595–609, 2010.

[3] A Gamba, D Ambrosi, A Coniglio, A de Candia, S Di Talia, E Giraudo, G Serini, L Preziosi, and F Bussolino. Percolation, morphogenesis, and Burgers dynamics in blood vessel formation. *Phys. Rev. Lett.*, 90:118101., 2003.

[4] K A Houck, D W Leung, A M Rowland, J Winer, and N Ferrara. Dual regulation of vascular endothelial growth factor bioavailability by genetic and proteolytic mechanisms. *J Biol Chem*, 267(36):6031–2603, 1992. 27.

[5] K Jacobson, E Wu, and G Poste. Measurement of the translational mobility of concavalin a in glycerol-saline solutions and on the cell surface by fluorescence recovery after photobleaching. *Biochim Biophys Acta*, 433:215–22, 1976.

[6] D Manoussaki, S R Lubkin, R B Vernon, and J D Murray. A mechanical model for the formation of vascular networks in vitro. *Acta Biotheor*, 44(3-4):271–282, Nov 1996.

[7] R M H Merks and J A Glazier. Dynamics mechanisms of blood vessel growth. *Nonlinearity*, 19:C1–C10., 2006.

[8] M Mitsi, Z Hong, C E Costello, and M A Nugent. Heparin-mediated conformational changes in fibronectin expose vascular endothelial growth factor binding sites. *Biochemistry*, 45(34):10319–10328, Aug 2006.

[9] F Mueller, D Mazza, T J Stasevich, and J G McNally. Frap and kinetic modeling in the analysis of nuclear protein dynamics: what do we really know? *Curr Opin Cell Biol*, 22(3):403–411, Jun 2010.

[10] D A Nu nez. Experimental estimate of the diffusivity of vascular endothelial growth factor. Master's thesis, Massachusetts Institute of Technology, Dept. of Mechanical Engieneering, 2006.

[11] B Nico, A Vacca, M De Giorgis, L Roncali, and D Ribatti. Vascular endothelial growth factor and vascular endothelial growth factor receptor-2 expression in the chick embryo area vasculosa. *Histochem J*, 33(5):283–286, 2001.

[12] E A J Reits and J J Neefjes. From fixed to frap: measuring protein mobility and activity in living cells. *Nat Cell Biol*, 3(6):E145–E147, June 2001.

[13] C Ruhrberg, H Gerhardt, M Golding, R Watson, S Ioannidou, H Fujisawa, C Betsholtz, and D T Shima. Spatially restricted patterning cues provided by heparin-binding VEGF-A control blood vessel branching morphogenesis. *Genes Dev*, 16:2684–2698, 2002. Genes Dev 16.

[14] G Serini, D Ambrosi, E Giraudo, A Gamba, L Preziosi, and F Bussolino. Modelling the early stages of vascular network assembly. *EMBO J*, 22:1771–1779, 2003.

[15] A Shamloo, N Ma, M Poo, L L Sohn, and S C Heilshorn. Endothelial cell polarization and chemotaxis in a microfluidic device. *Lab Chip*, 8(8):1292–1299, Aug 2008.

[16] S Soker, C M Svahn, and G Neufeld. Vascular endothelial growth factor is inactivated by binding to alpha 2-macroglobulin and the binding is inhibited by heparin. *J Biol Chem*, 268:7685–7691, 1993.

[17] A Tosin, D Ambrosi, and L Preziosi. Mechanics and chemotaxis in the morphogenesis of vascular networks. *Bull Math Biol*, 68(7):1819–1836, Oct 2006.

[18] P Vempati, A S Popel, and F Mac Gabhann. Formation of vegf isoform-specific spatial distributions governing angiogenesis: computational analysis. *BMC Syst Biol*, 5:59, 2011.

[19] D Zicha, G A Dunn, and A F Brown. A new direct-viewing chemotaxis chamber. *J Cell Sci*, 99 (Pt 4):769–775, Aug 1991.

Part III

Perspectives and Conclusions

Chapter 4

Perspectives

Contents

4.1 General remarks

The last decade have seen great progress in our understanding of blood vessel morphogenesis. However, many questions remain open at every level. For instance, the genetic information leading to the generation of vascular networks has not been fully deciphered. The molecular players that mediate genetic instructions and their mutual interaction have not been identified yet and the biophysical mechanisms that translate such plans into vascular shape are not understood. In addition, morphogenesis, as many other phenomena in Biology, is governed by very complex dynamic interactions that involve many players and span a range of different spatiotemporal scales. These features would make it difficult to understand morphogenesis even if all the players and interactions involved were known. As a matter of fact, modern biological techniques can nowadays generate extensive amounts of data on specific processes, but they are often hard to be accounted for since the underlying dynamics are extremely complex. Progress in such a complicated scientific landscape requires effective approaches to identify main issues and neglect secondary information. In general, there is a need for integrative approaches that combine experimentation with theoretical and quantitative multiscale methods. In particular, the prospects of mathematical and computational techniques to address such complex problems in Biology are becoming more and more promising.

As for the specific problem in vasculogenesis addressed in this thesis, further developments can be made in different directions. Regarding the proposed mechanism of vascular patterning during vasculogenesis, several aspects need to be investigated in more depth. In particular, in the context of embryonic vasculogenesis few data are available about the interaction between ECM molecules with heparin domains and VEGF matrix-binding isoforms. Also, the influence on embryonic angioblasts of matrix-bound VEGF versus free, unbound VEGF has not been addressed. Progress in this direction would allow to design specific experiments to test, in combination with suitable modifications of the model, the core of the proposed patterning mechanism. On the other hand, in this study an attempt has been made to identify key underlying mechanisms during vascular patterning. On the contrary, many molecular and cellular aspects that have an impact in angioblasts coalescence and early vascular patterning have been neglected. Possible approaches to extend this study are to include in the analysis other pro- and anti-angiogenics signals, to study the impact of cell proliferation or the interaction of angioblasts with other cell types in network patterning. Moreover, juxtacrine cell-cell communication, ECM degradation by cells and aspects related to cell mechanosensing seem interesting mechanisms to be explored. Some of those model extensions have created interest in the biological community and are already being jointly developed by the author together with experimental partners (see Sections 4.2 and 4.3 below).

At the mathematical level, there are important issues that need to be studied in more detail. Regarding the model formalism to be used for this and other similar problems, there are different views. However, very few comparative studies exist that allow to establish relations and differences among them. A formulation of exactly the same biological mechanisms and hypothesis proposed here by means different types of mathematical models would allow to clarify this issue. Accordingly, the derivation of continuous PDE equations from the hybrid model proposed here would point in that direction. As a matter of fact, an important drawback of the discrete CPM module used in this study is the lack of analytical tools to investigate the properties of model solutions. Also, some phenomenological parameters in the CPM module do not have a clear physical and measurable meaning. Both problems could be addressed by deriving suitable PDE equations from the original model, since in that case many analytical tools exist and parameters could perhaps be easier to relate to biophysical processes.

4.2 Role of cell proliferation in early vascular patterning

Proliferation and differentiation are mutually exclusive biological phenomena [6]. This developmental paradigm is crucial to understand the formation of patterned structures in the embryo, which require a limited proliferation in order not to distort patterning via hyperplasia. In the context of vascular development, several studies have shown that increasing endothelial cell numbers causes severe alteration of blood vessel patterning and morphology [7]. Therefore, analysing the regulation of proliferation in embryonic angioblasts/endothelial cells is important to further understand early vascular development.

Experimental data on this topic available in the literature are confusing, mostly because the mitogenic properties of growth factors like VEGF have been extensively proven *in vitro* and using late fetal or adult endothelial cells, but not tested on angioblasts or early embryonic endothelial cells. As a matter of fact, supplying extra VEGF to the developing embryo does not seem to increase endothelial proliferation, but rather causes the formation of dysmorphic, large endothelial lacunae thought to result from hyperfusion of endothelial cells [3]. Therefore, the results obtained in *in vitro* experimental settings using mature endothelial cells can not be directly extrapolated to the developing embryo. Instead, and according to available data, it is logical to hypothesize that: 1) embryonic endothelial cells might not proliferate as much as suggested by *in vitro* experiments in which mature endothelial cells (displaying a low mitotic rate under normal conditions) are induced with supraphysiological concentrations of VEGF; and 2) angioblast/endothelial cell proliferation is controlled by inhibitory signals that could balance the promotion of cell division induced by other molecules. An excellent candidate to act as negative regulator of endothelial proliferation is retinoic acid (RA), a biologically active derivative of VitaminA. Embryos deficient for Raldh2, the main RA-synthesizing enzyme in the mesoderm, show a remarkable increase in endothelial cell proliferation and evident defects in blood vessel morphology [7].

On the other hand, existing mathematical models of vasculogenesis, including the ones proposed in this dissertation, have neglected cell proliferation (see Sections 1.3 and 2.3 above). Few studies have analyzed the impact of cell density in network patterning by exploring a range of different cell densities that remain constant along simulations (see Section 2.5 and Refs. [5, 11]). A natural further step in these studies is therefore to extend the proposed models to include cell proliferation and to analyze the impact in network patterning. In the case of

the hybrid model proposed here, where cells consist of a connected subset of lattice sites, mitoses or cell divisions can be accounted for by spliting cells into two daughter cells along a defined axis [12]. More precisely, lattice sites ocupied by one of the daughter cells keep the index of the mother cell, while a new index (different to those identifying other cells) has to be assigned to the lattice sites occupied by the other (see Figure 4.1). After division, daughter cells will growth towards a predefined target size according to a usual CPM cell size contraint. If necessary, target size could be time-dependent to reproduce for instance gradual growth. Besides defining the dividing axis and a suitable dynamical system for the evolution of the target volume, a key problem to be addressed when modelling proliferation in this framework is to determine the precise time when each cell of the developing network has to undergo mitosis. This could be in principle accounted for by coupling a more or less complex cell-cycle model to every simulated cell. Ideally, those internal clocks that tell every cell when to divide should account for positive and negative mitotic signals perceived by cells. However, little is known about the nature of those signals and their subcellular mechanisms regulating them during vasculogenesis. Therefore, a different approach based on estimating average dividing rates is proposed here as a first approximation to the problem that is expected to provide information on the biological hypothesis mentioned above.

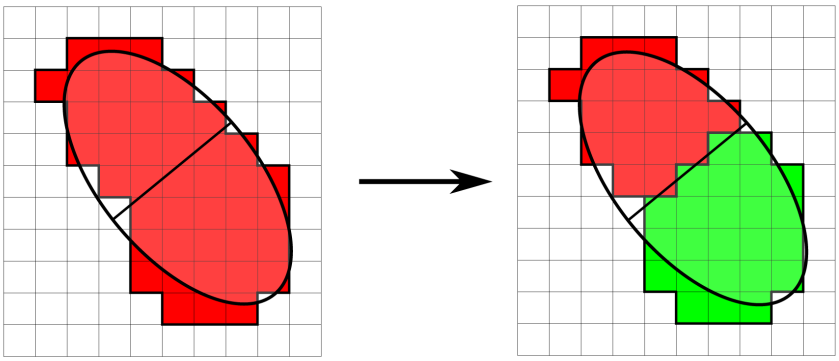

Figure 4.1: **An example of cell division in the CPM**. The lattice sites occupied by a cell (in red) are approximated by an ellipse [16]. Then the minor axis of the ellipse is use to divide the cell in two daughter cells (red and green)

In order to quantify proliferation of vascular cells in embryos, BrdU treatment can be used, see Figure 4.2. This procedure labels all cells that are in the S phase of the cell cycle and allows to estimate an average value for the cell-cycle length and the rate of division in the tissue [13, 15]. The same method can also be used for embryos where proliferation has been perturbed. For instance, colchicine treatment inhibits proliferation in embryos while downregulation of the

enzyme Raldh2, or chemical inhibition of RA synthesis, is expected to increase the proliferation rates of vascular cells. The different estimates obtained in by this method can then be used as inputs to the model that will generate different types of networks. Analyzing and quantifying both simulated and experimental networks is expected to provide information of the impact that proliferation has in developing networks as well as to test related biological hypothesis. In particular, this analysis will allow to explore the correlation between expression of Raldh2 along the embryo (and therefore the production of RA), angioblasts proliferation, and network patterning.

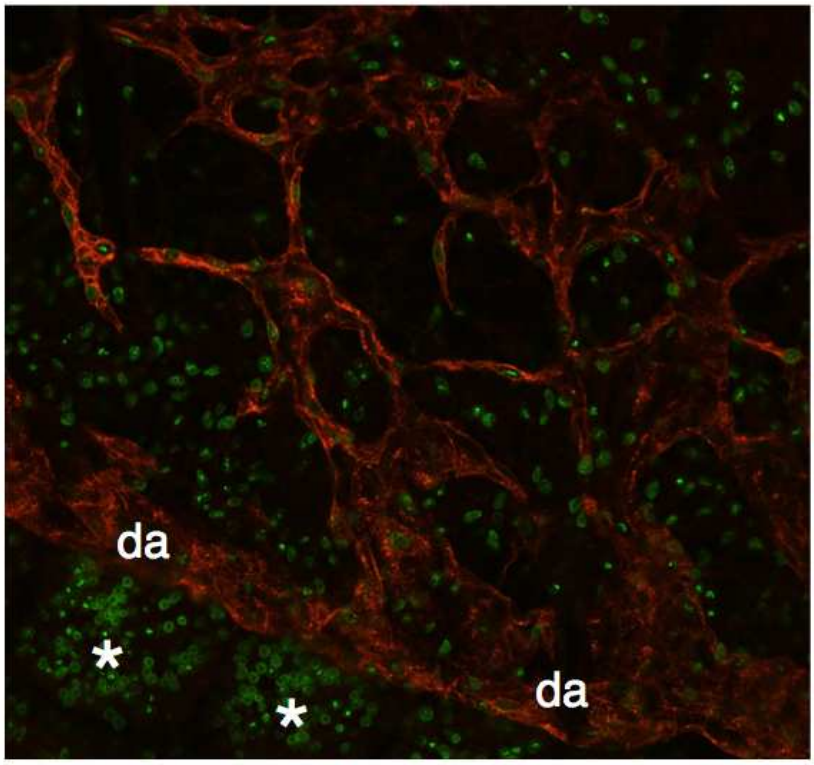

Figure 4.2: **BrdU labelling**. The developing vasculature next to the dorsal aorta (da) is shown in a quail embryo. BrdU (green) labels all nuclei in the tissue that are in the S phase of the cell cycle. QH1 (red) labels the vasculature. Every green nuclei inside the network indicates a proliferating vascular cell. Asterisks label somites.

In order to illustrate the proposed approach, a number of preliminary simulations have been run and quantified. More precisely, an extended version of the model proposed in Chapter 2 including proliferation has been used. Figure 4.3 A shows the cellular patterns generated with zero, low and high proliferation rates respectively. In those simulations the selected axis of division was as explained in Figure 4.1 and the target size was choosed constant and equal for every cell.

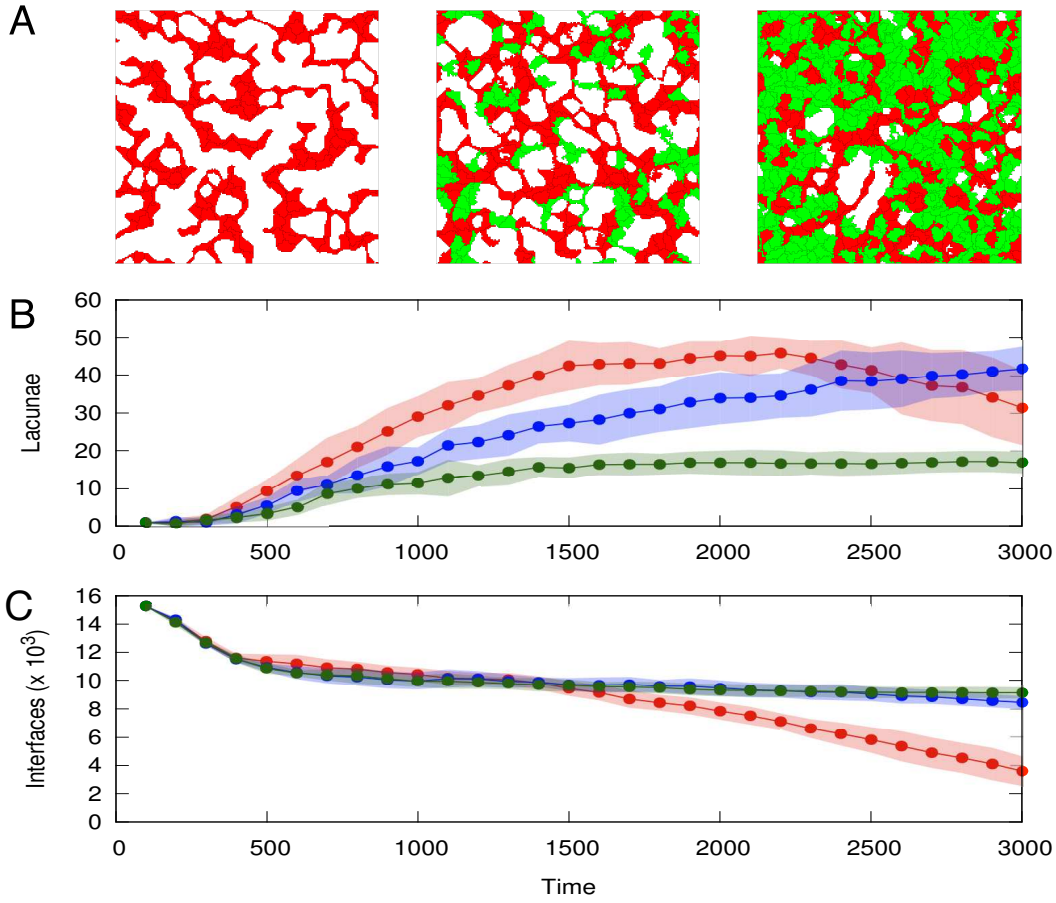

Figure 4.3: **Impact of cell proliferation in vascular patterning**. Comparison of three different simulations with different proliferation rates: no proliferation (green), low proliferation (blue) and high proliferation (red) **A.** The cellular patterns generated after 3000 MCS are shown. In all cases, the same number of cells where distributed initially in a regular mesh. Initial cells are shown in red while newly generated cells are shown in green. **B.** Time evolution of the number of lacunae. **C.** Time evolution of the total interface length between cells and extracellular medium. Lines show average values and filled areas indicate standard deviations over 10 simulations.

Figure 4.3 B and C show the time evolution of lacunae number and interface length between cells and ECM for the three cases shown in panel A. For the selected settings (initial number of cells, prolifation rates, dividing axis, etc.) Figure 4.3 shows that a network pattern can be generated with the low proliferation rate while dysmorphogenesis is achieved both for the no proliferation and high proliferation cases.

Note that in the previous example, all cells in a simulation have the same proliferation rate. An average proliferation rate of the cells in a developing vascular network can be obtained from BrdU experiments. However, it could happen

that the proliferation rates of the population under consideration are hererogeneous and dynamic. For instance, during sprouting angiogenesis cells at the tip of the sprout rarely proliferate while stalk cells behind tip cells often proliferate and those phenotypes are exchanged in a highly dynamic fashion [4]. If this is also the case during vasculogenesis, this features might have an impact in network patterning that would be hardly captured using average proliferation rates. In this case, more elaborated proliferation modes might be needed in the model. Some proliferation modes that could be explored in simulations are for instance those dependent on cell shapes, contact surface with other cells or positive or negative mitotic signals.

4.3 Role of the vasculature in liver organogenesis

It is well established that tissue-derived factors are involved in blood vessel formation. Presently, evidence is emerging that the endothelium provides crucial intructive signals to surrounding non-vascular tissue during organ development, as for instance during liver organogenesis [2]. The liver is the largest internal organ providing essential metabolic, exocrine and endocrine functions. These include production of bile, metabolism of dietary compounds, detoxification, regulation of glucose levels through glycogen storage and control of blood homeostasis by secretion of clotting factors and serum proteins. The main parenchymal cell type in the liver are hepatocytes, that account for 70 % of the mass of the adult organ. These highly polarized cells organize themselves as hepatic lobes. These are complex, regionalized histological and functional liver units in which hepatocytes produce bile to the apical membrane while the basal membrane remain in close contact with the circulation via hepatic sinusoids. Sinusoids are highly specialized vascular channels lined with fenestrated (highly permeable) endothelial cells that lack an organized basement membrane. Liver function crucially depends on the complex 3D architecture of the hepatic and sinusoidal endothelial tissues. However, little is known about the establishment of that characteristic architecture during the organogenesis of the liver.

Emerging evidence indicates that close reciprocal interactions between endothelial and hepatocytes precursor cells control crucial steps in early liver development. In particular, the feedback between the endodermal epithelium and the adjacent endothelium is crucial for normal organogenesis following hepatic specification [8], see Figure 4.4. As discussed in Chapters 1 and 2 above, endodermal tissue release differetiation and patterning signals inducing the formation of a

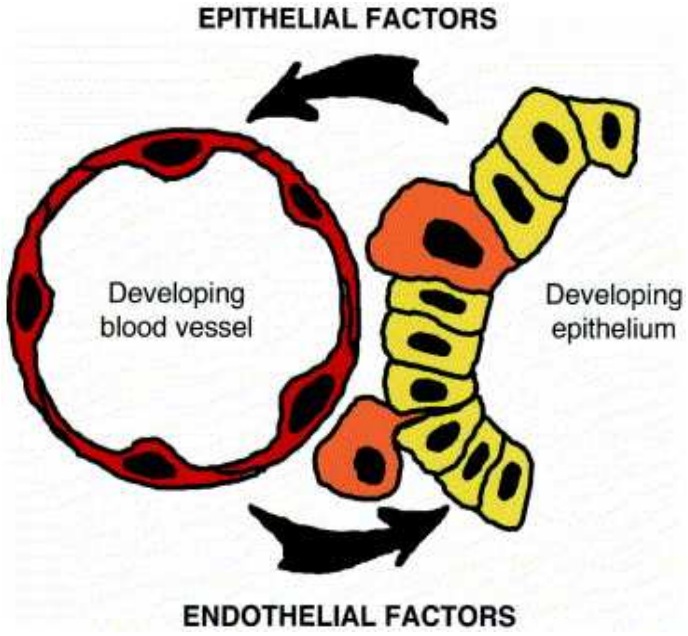

Figure 4.4: **Endothelium-endoderm feedback**. Epithelial cells from the endoderm and endothelial cells (ECs) are thought to co-develop as a result of mutual signalling events between these cell types. ECs differentiate, proliferate and form vessels as a response to epithelial factors. In turn, epithelial cells respond to endothelial signals with growth, differentiation and delamination. Image from Ref. [8].

primitive vascular plexus. Reversely, vascular cells promote endodermal hepatocytes precursors proliferation and hepatic primordium morphogenesis [10]. The primitive vascular bed covers the endodermal outgrowth that will form the liver primordium and forms the pre-existing network from which the liver sinusoids are thought to grow by a combination of angiogenesis and vasculogenesis [1, 14]. According to available data, it is natural to hypothesize that vascular growth is guided by VEGF, which is essentially produced by hepatocyte endodermal precursors. VEGF in turn, seems to upregulate production of Hepatocyte Growth Factor (HGF) in sinusoidal endothelial cells leading to hepatocyte proliferation and early liver growth [9]. Further understanding of the consequences of those and others reciprocal interactions in the spatial organization of both cell populations remain unknown.

There is a need for quantitative investigation of the dynamics of early liver development. Quantitative data on the liver architecture are scarce. Identifying spatial and temporal regularities in the establishment of the hepatocytes/sinusoids patterning requires accurate quantitative statistics of the structures along a series of morphometric descriptors that are currently unavailable. Moreover, there is

a lack of mechanistic mathematical models to describe and explain liver development and vascularization. Given the growing interest in the active role of the endothelium in organ development, it is surprising that little or no mathematical models exists that address the growth of endothelial networks during organogenesis. In particular, the role of the endothelium on the surrounding tissues has been largely neglected in models of blood vessel formation.

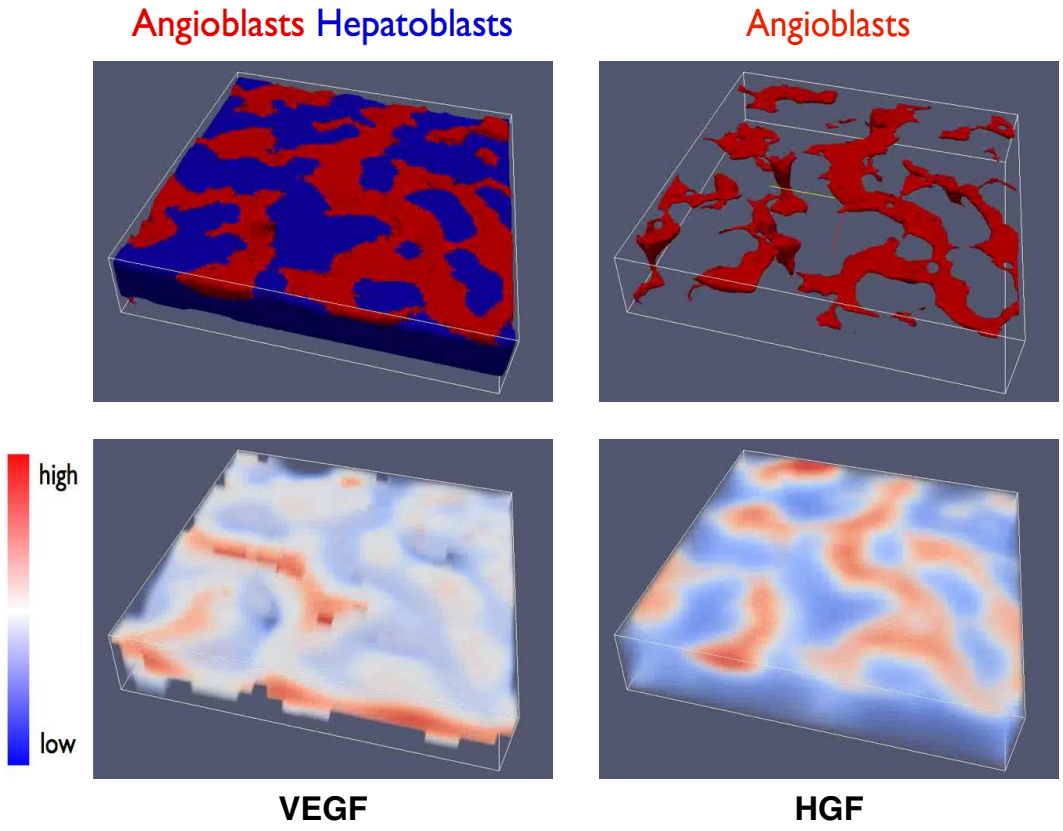

Figure 4.5: **3D simulation**. Endodermal hepatoblasts (blue) secrete VEGF. VEGF binds to ECM produced by Angioblasts (red). Bound VEGF provides patterning cues for angioblasts to organize into a network pattern. Angioblasts in turn, when stimulated by VEGF produce HGF that targets hepatoblasts. Proliferation effects caused in angioblasts and hepatoblasts by VEGF and HGF respectively are not included.

In this project, a combination of quantitative image analysis and mathematical modelling will be used to understand key mechanisms of liver morphogenesis. In particular, the emergence of 3D spatial patterning from heterotypic interactions between hepatic and vascular populations will be studied, based on confocal microscopy and dynamic imaging of *ex vivo* fetal mouse liver sections. Image analysis will be utilized to resolve the dynamics of cell populations and identify the structure of the growing vascular network. Quantification of the morphome-

tric properties will yield statistics on the spatiotemporal patterning and growth of the vascular network. To explore developmental mechanisms underlying liver morphogenesis, the model proposed in Chapter 2 will be extended. In particular, a third spatial dimension will be added to capture the complex 3D shapes originated during liver development. Also, a new cell population (hepatocyte precursors) will be included as well as key aspects of the comunication between that population and the vascular one. Quantitative morphometric comparison of results from model simulation to dynamic image data obtained from organ explants provides a platform to test theoretical predictions against biological evidence.

In order to ilustrate the proposed approach for early liver organogenesis, a preliminary 3D simulation was run (see Figure 4.5). This simulation also shows that the proposed mechanism of vascular patterning considered in this thesis works in three spatial dimensions. In this case, vascular and hepatic cell precursors together with chemical signals generated from each population, VEGF and HGF, have been included. The initial disposition of cells used in the simulation mimics the configuration of hepatic and vascular precursors prior the formation of the hepatic primordium. More precisely, hepatoblasts (in blue) were distributed in a planar layer representing the endoderm, while angioblalsts (in red) where randomly distributed on top of the hepatoblasts monolayer. The simulation in Figure 4.5 shows that angioblasts organize themselves into a connected network under the proposed mechasims. This simulation accounts just for the effect of the hepatoblasts in the vasculature but not the reciprocal effect (see Figure 4.4). In order to study how the feedback between cell populations impacts the 3D patterning of the simulated tissue, additional mechanisms are needed. In particular, it is necessary to account for the growth of each cell population, which is thought to be stimulated by the signals coming from the neighbouring one. To incorporate proliferation, a similar approach as that described in Section 4.2 will be followed independently for each particular cell population.

4.4 References

[1] S Collardeau-Frachon and J Y Scoazec. Vascular development and differentiation during human liver organogenesis. *Anat Rec (Hoboken)*, 291(6):614–627, Jun 2008.

[2] E Crivellato. The role of angiogenic growth factors in organogenesis. *Int J Dev Biol*, 55(4-5):365–375, 2011.

[3] C J Drake and C D Little. Exogenous vascular endothelial growth factor induces malformed and hyperfused vessels during embryonic neovascularizarion. *P Natl Acad Sci USA*, 92:7657–7661, 1995.

[4] H M Eilken and R H Adams. Dynamics of endothelial cell behavior in sprouting angiogenesis. *Curr Opin Cell Biol*, 22(5):617–625, Oct 2010.

[5] A Gamba, D Ambrosi, A Coniglio, A de Candia, S Di Talia, E Giraudo, G Serini, L Preziosi, and F Bussolino. Percolation, morphogenesis, and Burgers dynamics in blood vessel formation. *Phys. Rev. Lett.*, 90:118101., 2003.

[6] S F Gilbert. *Developmental Biology*. Sunderland (MA) Sinauer Associates, 2010 (9th edition).

[7] L Lai, L Bohnsack, K Niederreither, and K K Hirschi. Retinoic acid regulates endothelial cell proliferation during vasculogenesis. *Development*, 120:6465–6474, 2003.

[8] E Lammert, O Cleaver, and D Melton. Role of endothelial cells in early pancreas and liver development. *Mech Dev*, 120(1):59–64, Jan 2003.

[9] J LeCouter, D R Moritz, B Li, G L Phillips, X H Liang, H P Gerber, K J Hillan, and N Ferrara. Angiogenesis-independent endothelial protection of liver: role of vegfr-1. *Science*, 299(5608):890–893, Feb 2003.

[10] K Matsumoto, H Yoshitomi, J Rossant, and K S Zaret. Liver organogenesis promoted by endothelial cells prior to vascular function. *Science*, 294(5542):559–563, Oct 2001.

[11] R M H Merks, S A Newman, and J A Glazier. Cell oriented modelling of in vitro capillary development. *LNCS*, 3305:425–434, 2004.

[12] J C Mombach, R M Almeida, and J R Iglesias. Mitosis and growth in biological tissues. *Phys Rev E Stat Phys Plasmas Fluids Relat Interdiscip Topics*, 48(1):598–602, Jul 1993.

[13] R S Nowakowski, S B Lewin, and M W Miller. Bromodeoxyuridine immunohistochemical determination of the lengths of the cell cycle and the dna-synthetic phase for an anatomically defined population. *J Neurocytol*, 18(3):311–318, Jun 1989.

[14] J M Pérez-Pomares, R Carmona, M González-Iriarte, D Macías, J A Guadix, and R Mu noz Chápuli. Contribution of mesothelium-derived cells to liver sinusoids in avian embryos. *Dev Dyn*, 229(3):465–474, Mar 2004.

[15] E J Sanders, M Varedi, and A S French. Cell proliferation in the gastrulating chick embryo: a study using brdu incorporation and pcna localization. *Development*, 118(2):389–399, Jun 1993.

[16] M Zajac, G L Jones, and J A Glazier. Simulating convergent extension by way of anisotropic differential adhesion. *J Theor Biol*, 222(2):247–259, May 2003.

Chapter 5

Conclusions

The main conclusions from the present study are summarized below:

1) The proposed theory for early vascular patterning, based on matrix-binding of paracrine VEGF signals, suffices to generate network patterns comparable to those observed in embryos. This point of view introduces a novel answer to the question of how a homogeneous presentation of VEGF to vascular precursors can guide them to a non-homogeneous network configuration.

2) The mathematical and computational tools developed for this study provide new information and predictions, many of which are beyond the current experimental reach. For instance, simulations of the proposed hybrid model suggest that cell elongation, a characteristic feature observed in vascular structures, is an effect of the underlying patterning mechanism. Morever, simulations with different cell densities and morphometric quantitication of the generated networks highlights possible thresholds in cell density that are related with relevant properties of the generated patterns, including a percolative transition or a maximized interface between cells and surrounding tissue.

3) The morphometric methods used to quantify planar network patterns are useful to compare simulations with observed vascular networks and can also be used in future studies to detect defects in experiments in which specific process of vascular patterning are perturbed.

4) The combined theoretical and experimental analysis performed with *in vitro* Matrigel assays shows important paralelisms with the proposed theory for embryonic vasculogenesis. In particular, exogenous VEGF is key for network patterning which suggests that exogenous VEGF plays the role of paracrine VEGF in the embryo. Moreover, the accumulation of VEGF around cultivated cells seems a consequence of matrix-binding in those areas. This is supported by the localization in those regions of molecules that strongly bind to VEGF, but also by the fact that a reaction-dominant model fits the observed fluorescent recoveries

in FRAP experiments.

5) Key dynamic and kinetic properties of VEGF in Matrigel assays have been estimated.

6) Extensions of the proposed model can be used to investigate the role of proliferation in embryonic vascular patterning and the role of the vasculature in liver organogenesis.

List of Figures

List of Tables